ON THE NON-LINEAR VIBRATION AND MISTUNING IDENTIFICATION OF BLADED DISKS

A THESIS SUBMITTED TO
THE GRADUATE SCHOOL OF NATURAL AND APPLIED SCIENCES
OF
MIDDLE EAST TECHNICAL UNIVERSITY

BY

MEHMET ERSİN YÜMER

IN PARTIAL FULFILLMENT OF THE REQUIREMENTS
FOR
THE DEGREE OF MASTER OF SCIENCE
IN
MECHANICAL ENGINEERING

JANUARY 2010

Approval of the thesis:

ON THE NON-LINEAR VIBRATION AND MISTUNING IDENTIFICATION OF BLADED DISKS

submitted by **MEHMET ERSİN YÜMER** in partial fulfillment of the requirements for the degree of **Master of Science in Mechanical Engineering Department, Middle East Technical University** by,

Prof. Dr. Canan Özgen _____
Dean, Graduate School of **Natural and Applied Sciences**

Prof. Dr. Suha Oral _____
Head of Department, **Mechanical Engineering**

Prof. Dr. H. Nevzat Özgüven _____
Supervisor, **Mechanical Engineering Dept., METU**

Asst. Prof. Dr. Ender Ciğeroğlu _____
Co-Supervisor, **Mechanical Engineering Dept., METU**

Examining Committee Members:

Prof. Dr. Y. Samim Ünlüsoy _____
Mechanical Engineering Dept., METU

Prof. Dr. H. Nevzat Özgüven _____
Mechanical Engineering Dept., METU

Asst. Prof. Dr. Ender Ciğeroğlu _____
Mechanical Engineering Dept., METU

Asst. Prof. Dr. Yiğit Yazıcıoğlu _____
Mechanical Engineering Dept., METU

Asst. Prof. Dr. Demirkan Çöker _____
Aerospace Engineering Dept., METU

Date: 28 – 01 – 2010

I hereby declare that all information in this document has been obtained and presented in accordance with academic rules and ethical conduct. I also declare that, as required by these rules and conduct, I have fully cited and referenced all material and results that are not original to this work.

Name, Last name : Mehmet Ersin, YÜMER

Signature :

ABSTRACT

ON THE NON-LINEAR VIBRATION AND MISTUNING IDENTIFICATION OF BLADED DISKS

Yümer, Mehmet Ersin
M.S., Department of Mechanical Engineering
Supervisor: Prof. Dr. H. Nevzat Özgüven
Co-Supervisor: Asst. Prof. Dr. Ender Ciğeroğlu

January 2010, 140 pages

Forced response analysis of bladed disk assemblies plays a vital role in rotor blade design and has been drawing a great deal of attention both from research community and engine industry for more than half a century. However because of the phenomenon called 'mistuning', which destroys the cyclic symmetry of a rotor, there have been several difficulties related to forced response analysis ever since, two of which are addressed in this thesis: efficient non-linear forced response analysis of mistuned bladed disks and mistuning identification. On the nonlinear analysis side, a new solution approach is proposed studying the combined effect of non-linearity and mistuning, which is relatively recent in this research area and generally conducted with methods whose convergence and accuracy depend highly on the number of degrees of freedom where non-linear elements are attached. The proposed approach predicts nonlinear forced response of mistuned bladed disk assemblies considering any type of nonlinearity. In this thesis, special attention is given to the friction contact modeling of bladed disks which is the most common type of nonlinearity

found in bladed disk assemblies. In the modeling of frictional contact a friction element which enables normal load variation and separation of the contact interface in three-dimensional space is utilized. Moreover, the analysis is carried out in modal domain where the differential equations of motions are converted to a set of non-linear algebraic equations using harmonic balance method and modal superposition technique. Thus, the number of non-linear equations to be solved is independent of the number of non-linear elements used. On the mistuning identification side, a new method is enclosed herein which makes use of neural networks to assess unknown mistuning parameters of a given bladed disk assembly from its assembly modes, thus being suitable for integrally bladed disks. The method assumes that a tuned mathematical model of the rotor under consideration is readily available, which is always the case for today's realistic bladed disk assemblies. A data set of selected mode shapes and natural frequencies is created by a number of simulations performed by mistuning the tuned mathematical model randomly. A neural network created by considering the number of modes, is then trained with this data set for being used to identify mistuning of the rotor from measured data. On top of these, a new adaptive algorithm is developed for harmonic balance method, several intentional mistuning patterns are investigated via excessive Monte-Carlo simulations and a new approach to locate, classify and parametrically identify structural non-linearities is introduced.

Keywords: Non-linear Vibration, Mistuning Identification, Friction Damping, Forced Response Analysis in Modal Domain, Adaptive Harmonic Balance Method, Monte-Carlo Simulation, Non-linearity Identification, Model Identification, Neural Networks, Optimization

ÖZ

KANATÇIKLI DİSKLERİN DOĞRUSAL OLMAYAN TİTREŞİMİ VE DÜZENSİZLİK ÇÖZÜMLESİ ÜZERİNE

Yümer, Mehmet Ersin
Yüksek Lisans, Makine Mühendisliği Bölümü
Tez yöneticisi: Prof. Dr. H. Nevzat Özgüven
Yardımcı tez yöneticisi: Yrd. Doç. Dr. Ender Ciğeroğlu

Ocak 2010, 140 sayfa

Kanatçık tasarımında kritik bir rol oynayan kanatçıklı disk bütünlerinin sistem cevabı analizi yarım yüzyılı aşkın süredir hem araştırma grupları hem de türbin endüstrisi tarafından büyük ilgi görmektedir. Fakat disk-kanatçık sistemlerinde sistem cevabı çözümlerinde çevrimsel periyodikliğin kaybolmasına sebep olan 'düzensizlik'ten kaynaklanan birçok önemli problem ortaya çıkmaktadır. Bu problemlerden iki tanesi bu tezde incelenmiştir; disk-kanatçık sistemlerinin doğrusal olmayan titreşim cevabının efektif çözümü ve düzensizlik çözümlemesi. Doğrusal olmayan analiz kısmında düzensizlik ve doğrusal olmayan titreşim etkilerini birlikte inceleyen yeni bir yaklaşım geliştirilmiştir, ki bu araştırma alanında göreceli olarak yeni bir konu olmakla birlikte şimdiye kadar genellikle doğruluğu ve yakınsaklığı kullanılan doğrusal olmayan eleman sayısına doğrudan bağlı olan metodlarla gerçekleştirilmiştir. Önerilen yaklaşım düzensiz disk-kanatçık sistemlerinin doğrusal olmayan titreşim cevabını doğrusallığı bozan her kaynağa uygun şekilde tahmin etmektedir. Bu tezde özellikle disk-kanatçık yapılarında sıklıkla karşılaşılan sürtünme teması

üzerinde durulmuştur. Sürtünmenin modellenmesinde üç boyutlu uzayda değişken dikey kuvvete ve temas yüzeyinin ayrılmasına izin veren bir sürtünme elamanı kullanılmıştır. Buna ek olarak, analiz türevsel hareket denklemlerinin harmonik denge metodu ve kip çakıştırma tekniği ile doğrusal olmayan cebirsel denklemlere dönüştürüldüğü kip uzayında yapılmaktadır. Bu nedenle analizin doğruluğu ve yakınsaklığı kullanılan doğrusal olmayan elemanların sayısına bağlı olmamaktadır. Düzensizlik çözümlemesi başlığı altında ise, sinir ağları kullanılarak yeni bir çözüm yöntemi ortaya çıkarılmıştır. Bu yöntem sistem modlarını kullanarak sonuca gittiği için bütünleşik kanatçık-disk sistemlerinde kullanılmaya çok uygundur. Bahsedilen metod düzensizlik çözümlemesi yapılmak istenen disk-kanatçık sisteminin çevrimsel periyodik bir matematiksel modele sahip olduğunu varsaymaktadır, ki günümüzün bütün gerçekçi disk-kanatçık sistemleri için bu geçerlidir. Bu matematiksel modeli rastgele düzensiz hale getirerek bir grup mod şekli ve doğal frekans için belli sayıda benzetim yapılmıştır. Bu benzetim sonucu ortaya çıkan bilgi kümesi sinir ağının eğitiminde kullanılmıştır. Bahsedilenlere ek olarak, yapısal çözümlemelerde kullanılacak yeni bir "uyum sağlayan harmonik denge metodu" geliştirilmiş, birçok kasıtlı düzensizlik kalıbı Monte-Carlo benzetimleri ile incelenmiştir ve doğrusallığı bozan yapısal kaynakların yerinin, tipinin ve parametrelerinin saptanmasını sağlayan yeni bir yöntem ileri sürülmüştür.

Anahtar kelimeler: Doğrusal Olmayan Titreşimler, Düzensizlik Çözümlemesi, Kip Uzayında Titreşim Analizi, Uyum Sağlayan Harmonik Denge Metodu, Monte-Carlo Benzetimi, Doğrusal Olmayan Çözümleme, Model Çözümleme, Sinir Ağları, Optimizasyon

To my dear family,

with love and gratitude...

ACKNOWLEDGEMENTS

I am delighted to express my deepest appreciation to my supervisors Prof. Dr. H. Nevzat Özgüven and Asst. Prof. Dr. Ender Ciğeroğlu for their valuable guidance, advice, criticism and support that enabled me to produce this work successfully. Not only their technical knowledge, but also their attention to detail, concise technical writing and continuous research enthusiasm kept me running throughout this endeavor.

I would like to express my gratitude to my colleague Günay Orbay for his generous technical support during the startup of the thesis period. Without him, I would have adapted much slower.

I would also like to thank my parents for setting in me a fire of passion for education, additionally, for their understanding, support and patience. Without them I wouldn't be who I am now. I also would like to express my deepest gratefulness to Bilge Koçer for her support, which contributed appreciably to my serenity.

Contributions of TÜBİTAK-SAGE are greatly appreciated. I would especially like to thank Dr. A. Serkan Gözübüyük and Dr. Özge Şen for their support and guidance in scientific studies and M. Tuğrul Kozak for the valuable GARTEUR test data.

Finally, I would particularly like to thank my colleagues and friends for their friendship and technical support they provided throughout my life.

TABLE OF CONTENTS

LIST OF FIGURES

FIGURES

LIST OF TABLES

TABLES

LIST OF SYMBOLS

SYMBOLS

DOF : Degree of freedom

M, m : Lumped mass constant

K, k : Lumped stiffness constant

$\left[K^{cb}\right]$: Stiffness matrix of the reduced assembly

$\left[M^{cb}\right]$: Mass matrix of the reduced assembly

$\left[\widetilde{\Lambda}_d\right]$: Modal stiffness matrix of the disk

$\left[\Lambda_b\right]$: Modal stiffness matrix of the blade

$\left[\widetilde{\kappa}_{cc,d}\right]$: Reduced stiffness matrix of disk connection DOF

$\left[\widetilde{\mu}_{cc,d}\right]$: Reduced mass matrix of disk connection DOF

$\left[\kappa_{cc,b}\right]$: Reduced stiffness matrix of single blade connection DOF

$\left[\mu_{cc,b}\right]$: Reduced mass matrix of single blade connection DOF

$\left[\widetilde{\mu}_{dc}\right]$: Reduced mass matrix between disk DOF and connection DOF

$\left[\mu_{bc}\right]$: Reduced mass matrix between blade DOF and connection DOF

$[I]$: Identity matrix

$[0]$: Zero matrix

$\left[\hat{F}\right]$: Fourier expansion matrix

N : Number of blades

$\{a\}$: Contact element parameters

n : Normal force

f : Friction force

n_0 : Initial normal force

f_0 : Initial friction force

μ : Friction coefficient

v : Relative normal displacement

u : Relative tangential displacement

u_0 : Initial relative tangential displacement

k_v : Contact stiffness in normal direction

k_u : Contact stiffness in tangential direction

$[M]$: Mass matrix

$[K]$: Stiffness matrix

$[H]$: Structural damping matrix

$[C]$: Viscous damping matrix

$\{x\}$: Physical coordinate

$\{f\}$: External forcing

$\{f_{NL}\}$: Internal non-linear forcing

ω : Frequency

h : Harmonic number

p : Number of harmonics involved

$\{X\}$: Physical coordinate amplitude

$\{F\}$: External forcing amplitude

$\{F_{NL}\}$: Internal non-linear forcing amplitude

$[\Delta]$: Nonlinearity matrix

$[\Phi]$: Mass normalized modal matrix

$\{\eta\}$: Modal coefficient vector

$[\Omega]$: Diagonal matrix of squares of natural frequencies

$[\overline{C}]$: Modal viscous damping matrix

$[\overline{H}]$: Modal structural damping matrix

$\{\overline{F}_{NL}\}$: Modal internal nonlinear forcing vector

$\{\overline{F}\}$: Modal external forcing vector

s : Step length

g : Gap

MSE : Mean square error

MAC : Modal assurance constant

$\{e\}$: Error vector

$\{U\}_A$: Actual mode shape vector

$\{U\}_I$: Identified mode shape vector

A_0 : Maximum intentional mistuning amplitude

CHAPTER 1

INTRODUCTION

The structural integrity of an aircraft engine highly depends on its rotary parts. Since the ultimate goal of an engine manufacturer is to improve the efficiency and thrust-to-weight ratio, the key enhancement is to design lighter rotating equipment, which in turn requires well developed structural dynamics tools to aid designers assess accurate component life cycles driven by High-cycle fatigue (HCF).

HCF failures of rotary aero engine parts result from excessive blade vibration cycles, as thousands of these accumulate rapidly due to high engine rotation speeds. Aggravated by mistuning and aeromechanical sources, blade vibrations caused HCF is responsible for a cost of over $400 million per year [1], being a major reason for top-tier engine manufacturers' continuous interest in bladed disk assembly research.

This thesis, presenting new techniques and approaches for non-linear forced response analysis, system identification and dynamic robustness assessment, lies in the heart of structural dynamics subarea of the aforementioned research work.

1.1 Scope of the Thesis

Throughout the research conducted which lead to this work, the ultimate aim has been bringing new solutions to old problems, new ideas, and new perspectives to several aspects of the blade vibrations.

There are three main topics in which the objectives can be summarized as follows:

- Non-linear forced response analysis:
  - Developing an analysis tool which is able to analyze mistuned bladed disk assemblies in modal domain independent of the number of degrees of freedom (DOF) where non-linear elements are connected.
  - Developing efficient methods to increase solution speed without degrading accuracy.
  - Implementing efficient solution procedures to trace unstable regions.

- System identification:
  - Developing reliable approaches for mistuning identification using neural networks and optimization algorithms.
  - Identifying non-linearities present in structural systems using neural networks and optimization algorithms.

- Robustness assessment of bladed disk assemblies:

- Developing a stochastic frequency response function interpretation to numerically evaluate the magnitude amplification related to mistuning.
- Investigating the effectiveness of intentional mistuning patterns.

Although the main focus has been on the dynamics of bladed disk assemblies, any methodology developed has also been applied to other common structural dynamics problems, such as model updating, whenever possible throughout this thesis.

1.2 Outline of the Thesis

The diagram presented in Figure 1.1 overviews the contents of this work.

Chapter 2 begins with preliminary information about mistuning, its consequences, history and modeling. Then, comprehensive literature review of several sub topics are presented in the order which they appear in this thesis.

In Chapter 3, the emphasis is on mistuning modeling. The mathematical models employed in the upcoming sections, namely; lumped parameter modeling and component mode synthesis based reduced order modeling are introduced and their advantages/disadvantages are discussed in this section.

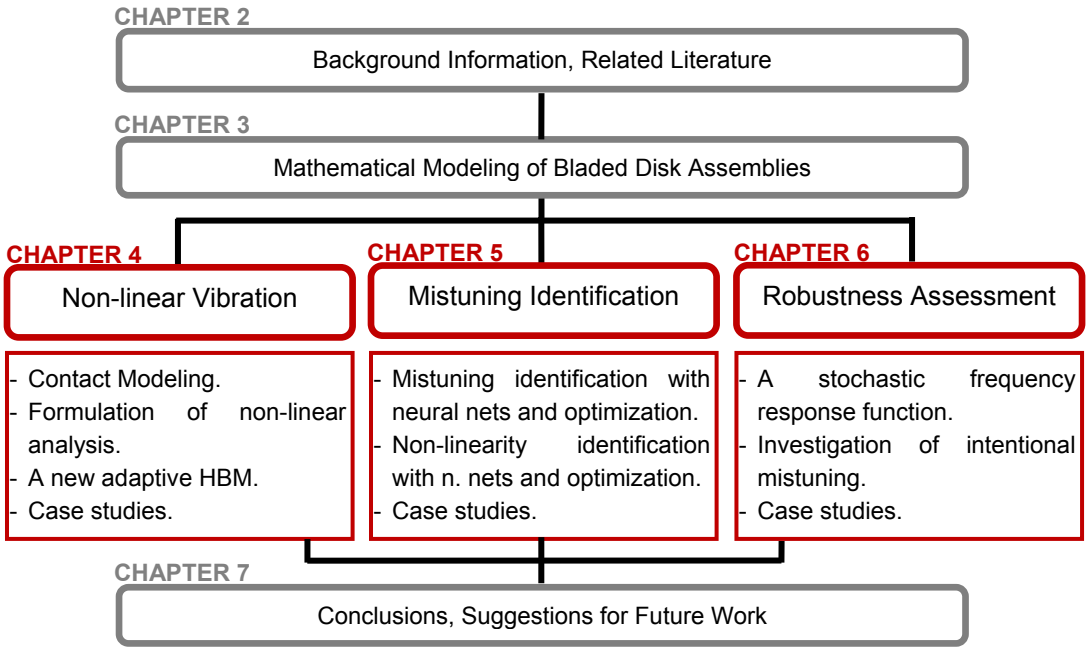

Figure 1.1 – Thesis Overview

Chapter 4 is devoted to the non-linear forced response analysis of mistuned bladed disks. For the application (demonstration) of the proposed method, friction contact nonlinearity, which is the most common type of nonlinearity in bladed disk systems, is used. Firstly, the contact model used in the analysis is presented with extensions where necessary. Secondly, the solution approach is formulated and exemplified with case studies. Thirdly, a new harmonic balance method is introduced and discussed in the light of case studies.

In Chapter 5, two methods developed for mistuning identification through use of neural networks and optimization is presented, whose efficiency is discussed throughout several case studies. These case studies investigate

the effect of noisy input data and missing modes to the effectiveness of the methods developed. Applications to model updating and non-linearity identification are also given in this chapter.

Chapter 6 is dedicated to discuss the robustness of mistuned bladed disk assemblies. A new stochastic frequency response function (FRF) representation is developed to serve as an evaluation tool. Then, the robustness of intentional mistuning patterns is evaluated and compared through intense Monte-Carlo simulations in this section.

Finally, Chapter 7 summarizes the work done throughout the above mentioned research, and evaluates the outcomes and contributions to the gas turbine industry and structural dynamics literature. In this chapter, a broad discussion is also presented accompanied by suggestions for future work.

CHAPTER 2

BACKGROUND

2.1 Mistuning Phenomenon

Throughout the history, vibration related problems of bladed disks have been extensively studied for around half a century but it is still one of the emerging areas in gas turbine design. The challenge here is mainly related to a phenomenon called mistuning, which can be defined as random deviations among the blades of a particular disk. These random deviations are primarily caused by manufacturing tolerances, uneven material properties and operational wear. Being unavoidable, mistuning cause mode localization and forced response amplification, and likely resulting in the failure of any bladed disk which is designed only considering the ideal cyclically symmetric structure.

One of the very early works on mistuning is published by Tobias and Arnold in 1957 [2]. They investigated the influence of dynamic imperfections on the vibration of rotating discs. After Whitehead's [3] and Ewins's [4] insightful work on the physics of mistuning, several researchers have documented their work on the effect of mistuning on blade vibrations since then, resulting in over 400 publications.

Rather than citing all of the mistuning related research in a chronological order, several of them are mentioned in the upcoming parts of this section considering their theme in the scope of this thesis. However the interested reader is referred to the comprehensive review published by Srinivasan [5] where he presents a substantial perception of the research issues in bladed disks and mistuning.

2.2 Non-Linear Forced Response Analysis of Bladed Disks

In order to decrease HCF failures of bladed disk assemblies, dry friction dampers are widely used by engine manufacturers. Therefore, bladed disk assemblies that feature dry friction dampers have to be analyzed via appropriate non-linear solution techniques in order to take the non-linear forcing effects resulting from frictional contacts into account. One of the efficient design features that introduce dry friction damping to the system is the shroud element. In this thesis, a new approach is proposed to predict forced response of frictionally damped mistuned bladed disk assemblies in modal domain.

2.2.1 Contact Modeling

In accurately investigating frictionally constraint structures, friction modeling is one of the key steps that require special attention since it is the friction model that assigns the non-linear forcing related to the contact points. In bladed disk designs, shrouds between the blades and under platform wedge dampers are the primary source of frictional non-linearity.

There has been extensive research for more than a couple of decades on friction contact modeling.

One of the early works is conducted by Griffin in 1980 [6], where the relative motion was restricted to the contact plane, thus resulting in constant normal load. Later Menq et al. [7-8] studied the forced response of shrouded fan stages where the authors also considered the effects of microslip [9]. They also reported a comparison with the experimental results [10]. Cameron et al. [11] presented a simplified analysis which resulted in constant normal load friction interface.

Yang et al. [12] worked on stick-slip-separation analysis and they came up with analytical rules that define transition angles. Authors also modeled normal load variation in a comprehensive way. Yang and Menq [13] also worked on normal load variation and they analyzed wedge dampers [14]. In the same year, Csaba [15] proposed a microslip friction model based on [9] where he excluded the shear layer in [9] for simplicity. Chen et al. [16] addressed the normal load variation concept and used it for three-dimensional periodic motion. Petrov and Ewins [17] analytically formulated friction elements based on similar rules defined by [12]; they also presented friction models for time domain analysis [18]. Later, Koh et al. [19] published their work on turbine blade friction dampers, where they also verified some of the friction models experimentally.

In 2006, Ciğeroğlu and Özgüven formulated a two-slope macroslip friction model which resembled microslip and still remained computationally inexpensive [20]; Ciğeroğlu et al. also developed a one-dimensional

microslip friction model in the same year [21]. Ciğeroğlu et al. [22] later developed another microslip friction model which took normal load variation into account. They analyzed a bladed disk system with wedge dampers and developed a contact stiffness prediction method [23] which is also verified experimentally [24].

2.2.2 Non-Linear Analysis in Modal Domain

Modal domain methods have been used extensively by researchers to predict forced response of mechanical structures. However, for non-linear analysis, time-domain methods are generally established which require much more computational power. In 1990, Budak and Özgüven [25] came up with the following formulation for harmonic excitation:

$$[M]\{\ddot{x}\} + [C]\{\dot{x}\} + i[H]\{x\} + [K]\{x\} + \{f_{NL}\} = \{f\} \tag{2.1}$$

$$\{f_{NL}\} = [\Delta]\{x\} \tag{2.2}$$

In (2.2), [Δ] is the response dependent non-linearity matrix. Later, Tanrıkulu et al. [26] for the first time implemented describing function method into multi-degree-of-freedom vibratory physical systems. Kuran and Özgüven [27] worked on response calculation using modal superposition and they also extended the work by Tanrıkulu et al. [26] to include multi harmonic solutions. Recently, Orbay and Özgüven [28] introduced use of reduced order models in non-linear modal domain solutions of bladed disk assemblies.

In this thesis, an approach to predict nonlinear forced response of mistuned bladed disk assemblies in modal domain employing the modal superposition method [27] is proposed. In the application of the proposed method, friction contact nonlinearity is considered. In order to assess the nonlinear force components resulting from contact, a modified version of the macroslip friction model developed by Yang et al. [12] is utilized together with the analytical transition angles for simple harmonic motion given in [22] by taking normal load variation into account. The friction model used is a simplified version of the one presented in [24], where the in-plane motion is decomposed in the two major directions. For simplicity, in this work, one friction element is utilized between contacting nodes and the direction of it is adaptively rotated according to the major direction. This friction model is employed due to the availability of analytical transition angles, which increase the speed of the solution process significantly.

Although the approach presented in this thesis is demonstrated using this friction model; it is mathematically suitable to be used with any type of friction model or non-linearity. The novel part of the approach proposed is that it enables the analysis of a non-linear mistuned bladed disk system without introducing reduced order modeling and yet leaving the number of nonlinear equations independent from the number of degrees of freedom in the model where nonlinear elements are attached.

The approach proposed in this study enables the non-linear analysis of a mistuned bladed disk system without introducing reduced order modeling. Application of reduced order modeling techniques is common in mistuned

bladed disk modeling. Sextro et al. [29] used a sub-structuring based method for nonlinear analysis of mistuned bladed disks with underplatform dampers. Petrov et al. [30] utilized a condensation method, by which, the number of degrees of freedom (DOFs) are reduced to the number of DOFs where non-linear elements are attached. For sub-structuring methods the number of non-linear equations to be solved is also at least as in the case of the mentioned condensation method. Thus, both of these methods suffer from slow non-linear solution time in the case of realistic bladed disk models. There are also other reduction techniques where direct dependency of the non-linear equations to the number of physical DOFs is eliminated. However, such models result in decreasing accuracy. For example in Ref. [31], resonant frequencies of the mistuned assembly shift considerably even for the linear response. The novel part of the approach proposed in this work is that it leaves the number of nonlinear equations independent from the number of DOFs in the mistuned bladed disk model where nonlinear elements are attached; hence, full finite element model is used which increases the accuracy compared to the reduced order models.

2.3 Identification

2.3.1 Mistuning Identification

Since mistuning is random in nature, predicting forced response of bladed disks is very complicated if mistuning is taken into consideration and it generally needs statistical approaches to be implemented if the goal is to broadly inspect the design under consideration.

Nevertheless, another aspect of the issue is to analyze a particular disk, which requires the identification of mistuning related to it. Until recently, the majority of the bladed disk assemblies were encompassing separately manufactured blades which are afterwards attached to the disk. It is relatively easy to identify the mistuning related to these individual blades since they can be cantilevered from their roots and tested [32-33]. This approach, although neglecting the mistuning caused by the connection, works to some extend for bladed disks whose blades are of detachable type.

However, for an integrally bladed disk (blisk), it is not possible to separate the blades and test for mistuning identification separately. For this type of bladed disks it is necessary to use a methodology which is capable of extracting blade mistuning parameters from system parameters available from system tests. Regarding this issue, prior work has been published by Judge et al. [34-36] where the authors present an approach which makes use of free response disk measurements to identify blade modal parameters in a reduced-order model and they validate the method experimentally. Pichot et al. [37] and Mingolet et al. [38] utilize lumped parameter modeling to identify mistuning of blisks. One of the significant studies in this scope was reported by Feiner et al. [39-40] in 2004, where the authors developed a method for mistuning identification employing their reduced order model. It is clear that increasing use of blisks in the industry pioneered several other mistuning identification works [41-48] recently.

2.3.2 Model Updating with Neural Networks

Model updating has been extensively studied and is an unavoidable tool for verifying and correcting mathematical dynamic models to have accurate and reliable representations. In recent years researchers started using neural networks as a tool in model updating.

Regarding this subject, an early work published by Levin et al. [49] showed that neural networks are working quite well with simple dynamic models and even in the presence of noise. Chang et al. [50] proposed an adaptive neural networks approach for model updating, and they developed a training sample selection methodology [51]. Yong et al. [52] proposed a two-level neural network approach which updates structural parameters in the first level and damping ratios in the second. More recently, Zapico et al. [53] reported their work on experimental validation and updating of a steel frame using neural networks.

It should be noted that in the above mentioned model updating work, neural networks are used as the stand alone tool, whereas in this thesis, it is used in conjunction with optimization methods to broaden the capability.

2.3.3 Non-Linearity Identification with Neural Networks

Non-linearity identification have been one of the most important and yet demanding subjects in structural systems. In this thesis, a new approach to

identify non-linear systems, where neural networks are playing the key role is presented.

Although the identification capabilities of neural networks have been drawing a great deal of attention from both of the control systems and structural dynamics communities, there are relatively few works done on structural non-linearity identification utilizing neural networks. One of the early works is published by Chen et al. [54] in 1992. They have employed several neural network configurations and used a one degree of freedom simulated non-linear time series process to illustrate the outcomes. In 1993, Masri et al. [55] used artificial neural networks for identification of a one degree of freedom Duffing oscillator under deterministic excitation.

Demonstrating the non-linearity identification capabilities of neural networks, the above stated works are yet restricted to relatively simple systems and are not addressing common non-linearity types, for example friction and cubic stiffness, encountered in typical structural dynamic systems. However, the methodology developed in the context of this thesis is not only capable of determining the type and location of the non-linearity involved in the structure under consideration, but also is able to identify the associated non-linearity parametrically.

A recent study whose aim is similar to the work presented here is Gondhalekar et al. [56]. They employed a previously developed methodology of Özer et al. [57-58] to locate non-linearities in the structure, and then used genetic algorithm optimization to determine the type and parameters of the related non-linearity. However, the approach presented

in [56] is short of being practical since it requires measurements taken from all of the degrees of freedom where non-linearities are assumed to be in the structure. On the other hand, the methodology presented in this thesis does not restrict measurements to be taken from any degrees of freedom where non-linearities are possibly present and yet, it is capable of locating and identifying non-linearities in a given structure.

2.4 Intentional Mistuning

As stated earlier, mistuning is inevitable for any cyclically symmetric bladed disk assembly since it is caused by manufacturing tolerances, material properties and operational wear. Since reducing the level of mistuning beyond certain limits is not possible with the current technology, the attempts are rather made to reduce or control the forced response magnification where intentional mistuning is an alternative. Intentional mistuning is referred as the methodically controlled introduction of variations in blade properties to obtain a preferred intensity of forced response.

The advantageous effects of a prearranged deviation from the tuned system, namely 'detuning', was demonstrated by Ewins [59]. Ewins [60] also demonstrated the benefits of selecting the right packing configuration of blades for response level reduction. Griffin et al. [61] investigated an 'alternate mistuning' where low and high frequency blades are alternated on the circumference of the rotor. With a lumped parameter model, Castanier et al. [62] illustrated the maximum forced response reduction that can be obtained by implementing a pseudo-harmonic intentional pattern.

Castanier et al. [63] also investigated the combined effects of intentional and random mistuning for the so-called sinusoidal pattern. Ayers et al. [64] proposed that for the same intentional mistuning amplitudes, changing the order of the blades around the rotor can reduce the magnification factor. Nicolic et al. [65] developed large random mistuning tactics to reduce the response amplification but the main drawback of this strategy is a widened speed avoidance zone for the engine caused by the random spreading of natural frequencies of the rotor.

Since some uncontrolled variation is still unavoidable although intentional mistuning is applied on a particular rotor design, it is vital to evaluate any intentional mistuning pattern together with a certain amount of random mistuning. The aim of the analysis carried out in this thesis is to statistically compare the robustness of intentional mistuning patterns such as harmonic, linear and pseudo harmonic, with different levels of random mistuning applied on top. Monte Carlo simulations with selected intentional and random mistuning pairs are performed under different engine order excitations to compare the performance of the intentional mistuning patterns applied. This study differs from the previous ones with its deep investigation in model, random mistuning and forcing dependency of intentional mistuning patterns.

CHAPTER 3

MATHEMATICAL MODELING

Other than standard 3D Finite Element Modeling (FEM), two types of reduced order mathematical models are used in some of the case studies throughout this thesis. In this chapter, a brief description of the models used in thesis is provided.

Since modeling is not in the scope of the present work, additional attention will not be paid on it; however, an inclusive survey on modeling issues in bladed disk assemblies is presented by Castanier et al. [66]. He refers to several lumped parameter and reduced order models (ROM) in the literature.

In this thesis two models, other than standard finite element modeling, which have different levels of complexity, are employed. The first one is a relatively simple lumped parameter model with two different configurations which enables non-linear and linear modeling. The second one is a component mode synthesis [67] based reduced order model.

3.1 Lumped Parameter Modeling

The lumped parameter model used in this work is a modified version of the model of Dye et al. [68].

3.1.1 Model for Non-Linear Analysis

The schematic view of the lumped parameter model used in this work for non-linear analysis is as depicted in Figure 3.1.

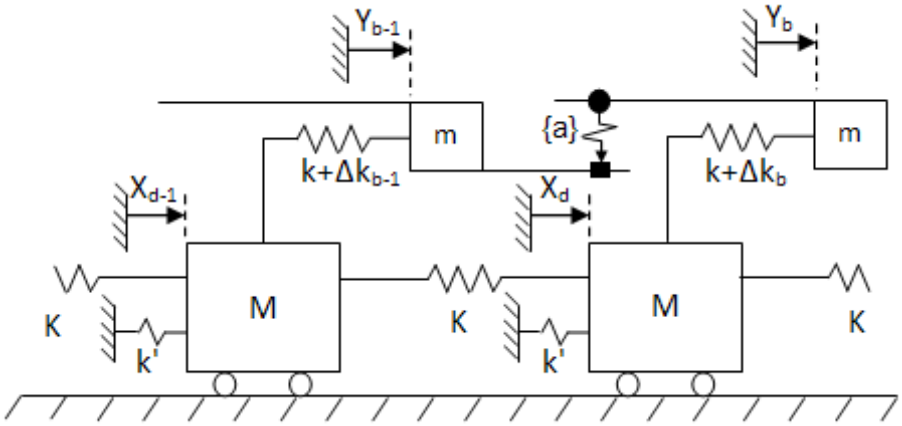

Figure 3.1 – Non-Linear Lumped Parameter Model

In this model, m is the lumped mass representing the blade, M stands for disk sector mass, K is the stiffness coupling between sectors, k' is the stiffness connecting the disk to the ground and k is the stiffness connecting the blade to the disk. $\{a\}$ is the vector denoting contact element parameters.

Theoretically, this modified version of the lumped parameter model is available to be used with any point contact model.

For blade alone mistuning perturbation positive and negative Δk values are used. This simple lumped parameter model is appropriate for the purpose of investigating the applicability of the proposed method since it is based on a cyclically symmetric nominal structure.

3.1.2 Model for Identification and Intentional Mistuning

The schematic view of the lumped parameter model used in this work for mistuning identification and intentional mistuning is as shown in Figure 3.2. Note that it is the linear version of Figure 3.1, where non-linear contact elements are omitted.

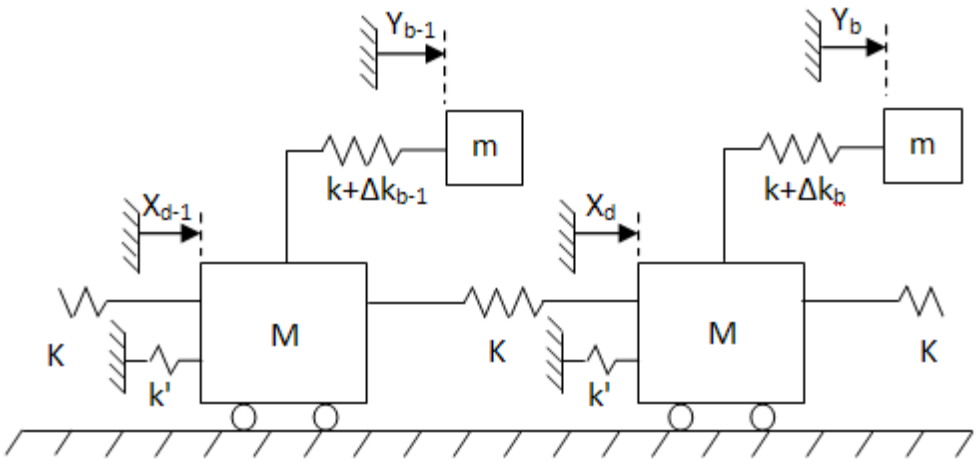

Figure 3.2 – Linear Lumped Parameter Model

In this model, parameters m, M, K, k', k, and Δk have the same definition as given in section 3.1.1.

This simple lumped parameter model is appropriate for the purpose of investigating robustness of intentional mistuning patterns and usefulness of neural networks mistuning identification since its nominal base includes basic features of a cyclically symmetric bladed disk structure.

3.2 Reduced Order Modeling (Craig-Bampton)

The reduced order model used in this study is formulated by Bladh et al. [69] and utilized by Orbay and Özgüven [28] for non-linear forced response analysis of bladed disks.

This reduced order model is based on component mode synthesis [67] which is modified by Bladh et al. [69] making blade cantilever frequency mistuning possible. The formulation of the stiffness and mass matrices for this reduced order model is given below as derived in [69].

$$\left[K^{cb}\right]=\begin{bmatrix} \left[\widetilde{\Lambda}_d\right] & [0] & [0] \\ [0] & \left[\widetilde{\kappa}_{cc,d}\right]+[I]\otimes\left[\kappa_{cc,b}\right] & [0] \\ [0] & [0] & \underset{n=1\ldots N}{Bdiag}\left[\underset{m=1\ldots m_b}{diag}\,(1+\delta_n^k)\left[\Lambda_b\right]\right] \end{bmatrix} \tag{3.1}$$

$$\left[M^{cb}\right]=\begin{bmatrix} [I] & \left[\widetilde{\mu}_{dc}\right] & [0] \\ \left[\widetilde{\mu}_{dc}\right]^T & \left[\widetilde{\mu}_{cc,d}\right]+[I]\otimes\left[\mu_{cc,b}\right] & \left[\hat{F}\right]^T\left[[I]\otimes\left[\mu_{bc}\right]^T\right] \\ [0] & \left[[I]\otimes\left[\mu_{bc}\right]\right]\left[\hat{F}\right] & [I] \end{bmatrix} \tag{3.2}$$

In this formulation, where $\otimes$ denotes the Kronecker product, $\left[K^{cb}\right]$ and $\left[M^{cb}\right]$ are the stiffness and mass matrices of the reduced assembly, $\left[\tilde{\Lambda}_d\right]$ is the modal stiffness matrix of the disk, $\left[\Lambda_b\right]$ is the modal stiffness matrix of one blade, $\left[\tilde{\kappa}_{cc,d}\right]$ and $\left[\tilde{\mu}_{cc,d}\right]$ are the reduced stiffness and mass matrices of connection degrees of freedom (DOF) on the disk, $\left[\kappa_{cc,b}\right]$ and $\left[\mu_{cc,b}\right]$ are the reduced stiffness and mass matrices of connection DOF on one blade, $\left[\tilde{\mu}_{dc}\right]$ and $\left[\mu_{bc}\right]$ are the reduced mass matrices between disk DOF and connection DOF; and blade DOF and connection DOF, respectively. Moreover, $\left[I\right]$ is the identity matrix, $\left[0\right]$ is the zero matrix, $\left[\hat{F}\right]$ is the Fourier expansion matrix, $Bdiag[\ ]$ and $diag()$ are the block-diagonal and diagonal matrices respectively, δ_n^k denotes the n^{th} blade's mistuning perturbation, N is the number of blades and m_b is the number of modes retained per blade.

The detailed description and derivation, which is not the subject of this study, is available in [69]. It should be noted that this reduced order model will speed up the training data generation step in mistuning identification with neural networks and Monte-Carlo simulations in intentional mistuning analysis since it allows easy manipulation of the blade alone natural frequencies.

CHAPTER 4

NON-LINEAR VIBRATION ANALYSIS

4.1 Contact Model

The friction model used to calculate contact forces in this thesis is a modified version of the friction model developed by Yang et al. [12]. In Figure 4.1, three-dimensional contact of two bodies is shown. The contact surface on each body is represented by a number of contacting points. Each of the red points in the figure represents a contact pair. The distributed contact model is plotted for the i^{th} contact pair as shown in Figure 4.1.

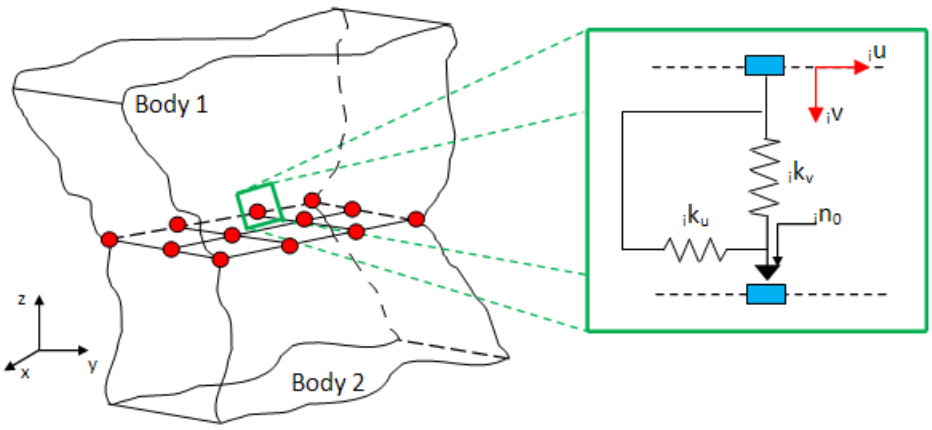

Figure 4.1 – 3D Contact and Distributed Contact Model

Every contact pair in such a distribution will have its separate local coordinates such that the normal direction is perpendicular to the contact surfaces in the vicinity of the pair under consideration. For example, for the i^{th} pair represented in Figure 4.1, ${}_iu$ and ${}_iv$ are the tangential and normal directions of the i^{th} local coordinate axis. ${}_in_0$, ${}_ik_u$ and ${}_ik_v$ are the normal force and the contact stiffness values in tangential and normal directions, respectively. For such a configuration, contact forces will be calculated for each pair separately and then transformed to the global coordinates to be included in the system solution.

$$n(\theta) = \begin{cases} n_0 + k_v v(\theta) & (Slip - Stick) \\ 0 & (Separation) \end{cases} \tag{4.1}$$

$$f(\theta) = \begin{cases} 0 & (Separation) \\ \pm \mu n(\theta) & (Slip) \\ k_u[u(\theta) - u_0] + f_0 & (Stick) \end{cases} \tag{4.2}$$

For harmonic motion, relative normal displacement, v, relative tangential displacement, u, normal force, n, and friction force, f will be functions of an angular variable in equations (4.1) and (4.2), say $\theta = \omega t$ [22]. Normal force will be either zero, which is the separation case where friction force is also zero, or it will be a non-zero value calculated according to (4.1). Friction force will be calculated according to (4.2) considering stick, slip, and separation states. While formulating the contact model for this study, analytical stick-slip-separation transition angles are taken from [22]. In non-linear contact dynamics where periodic forcing and response is assumed, transition angles refer to those angles where the relative motion between the contacting points change state. For more detail on this subject see Ref.

[22]. For the separation case these angles yield the well defined 10 possible sequences reported by Yang et al. [12].

The modification made over the formulation of Yang et al. [12] is the introduction of adaptive determination of the friction coordinate axis at each solution step according to the relative displacements between the two nodes associated with the friction element.

In a 3D contact model, projection of the relative motion of contacting nodes on to the contact plane will not necessarily lie on a straight line; in fact for simple harmonic motion it will be an elliptic trajectory as depicted in Figure 4.2. For such a trajectory, generally a static axis is defined for the contact element where the forcing of the relatively lower magnitude axis is ignored [12].

Ciğeroğlu et al. [24] utilized two orthogonal friction elements between the same nodes to account for the motion of the ignored axis, in order to capture the relative motion in the minor axis also. However, since there is no floating contact body such as a wedge damper in the case of shroud contacts, the relative motion will generally be larger in one direction. Therefore, in this study, one friction element is adaptively positioned at each solution step so that the tangential direction of the element is on the major axis of the friction path in the contact plane.

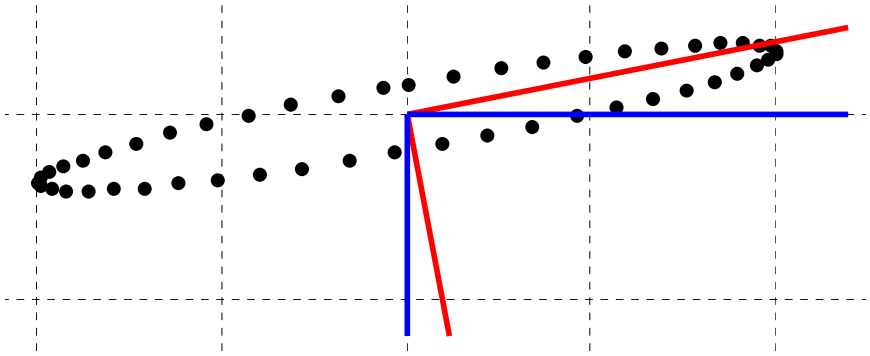

Figure 4.2 – Relative Motion Path (. . . .), Static Coordinate Axis (▬) and Adapted Coordinate Axis (▬) in the Contact Plane

In Figure 4.3, examples of full-stick, stick-slip, and stick-slip-separation cases calculated by the model proposed are presented with their corresponding hysteresis curves. Note that, the analytically calculated single harmonic representation of normal, $n_f(\theta)$, and friction, $f_f(\theta)$, forces are also included. It is clear from Figure 4.3 that the proposed contact model is able to represent the classical stick and stick-slip motions as well as the possible separation of contacting points in the normal direction.

In Figure 4.3-(c), four transition angles are evident; stick-to-positive slip (~0.5 rad), positive slip-to-stick (~1.8 rad), stick-to-negative slip (~3.0 rad) and negative slip-to-stick (~4.4 rad). Also in Figure 4.3-(e), transition from positive slip-to-separation (~1.4 rad) and separation-to-negative slip (~3.9 rad) are clearly exemplified.

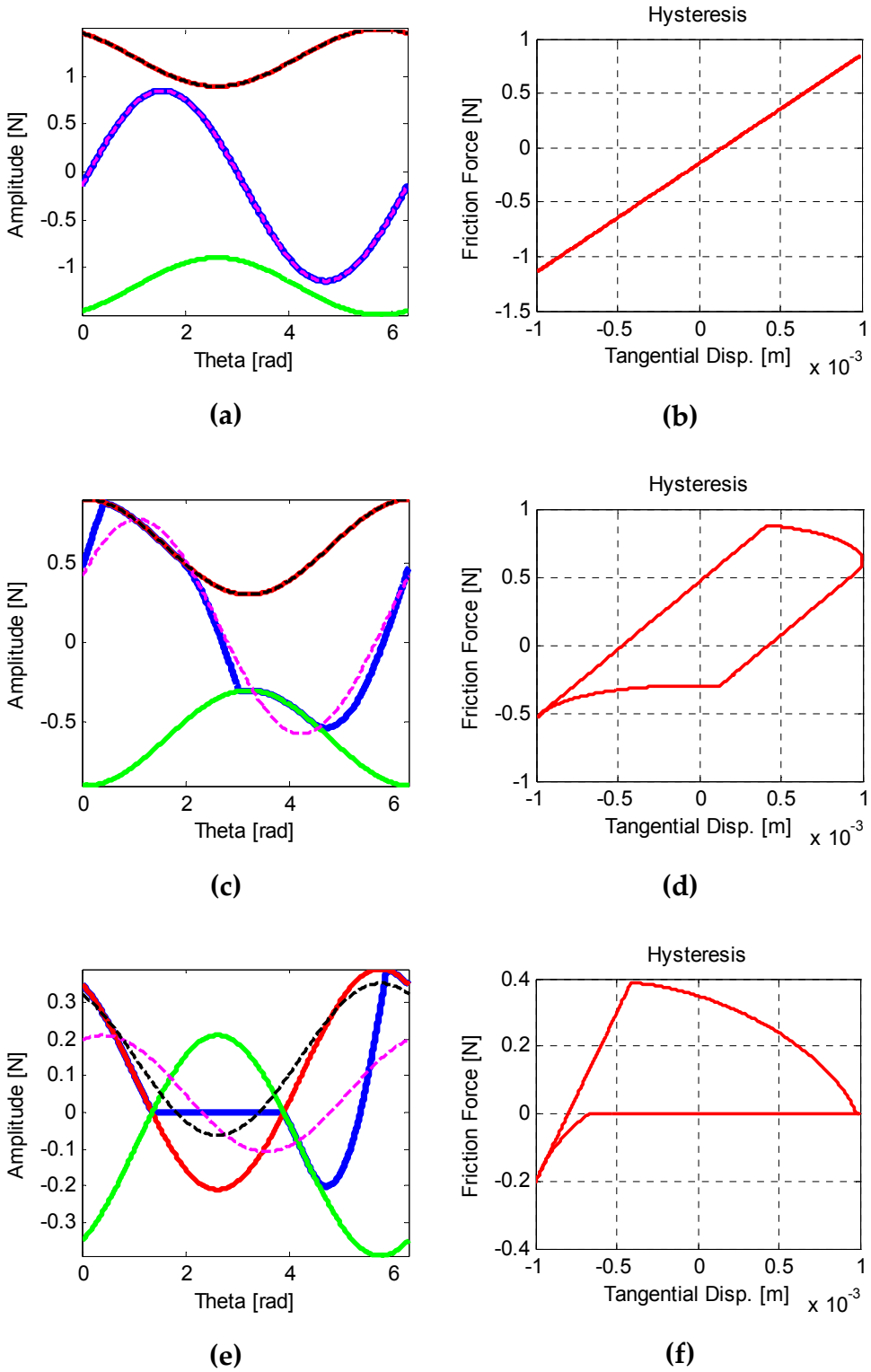

Figure 4.3 – Friction Force and Hysteresis Plots of Full-Stick (a, b), Stick-Slip (c, d) and Stick-Slip-Separation (e, f). In (a, c, e); $f(\theta)$ (—), $\mu n(\theta)$ (—), -$\mu n(\theta)$ (—), $f_f(\theta)$ (– –), $\mu n_f(\theta)$ (– –)

4.2 Non-Linear Forced Response

4.2.1 Formulation

The equation of motion for a linear multi degree of freedom system, under harmonic forcing, in time domain is

$$[M]\{\ddot{x}\} + [C]\{\dot{x}\} + i[H]\{x\} + [K]\{x\} = \{f\}. \tag{4.3}$$

In equation (4.3), [*M*], [*C*], [*H*], and [*K*] represent the mass, viscous damping, structural damping and stiffness matrices respectively; whereas {*x*} and {*f*} are the response and external forcing vectors in time domain. If any non-linearity is introduced, it can be represented as a non-linear forcing vector, $\{f_{NL}\}$, which can be added to the left-hand side of equation (4.3), representing the inter-structural forcing. The resulting non-linear equation of motion is

$$[M]\{\ddot{x}\} + [C]\{\dot{x}\} + i[H]\{x\} + [K]\{x\} + \{f_{NL}\} = \{f\}. \tag{4.4}$$

If the external forcing is harmonic and the response is assumed to be harmonic, {*x*} and {*f*} in (4.4) can be replaced by (4.5) and (4.6) respectively where *h* is the harmonic-number.

$$\{x(t)\} = \mathrm{Im}\left(\sum_{h=0}^{\infty} \{X\}_h e^{ih\omega t}\right) \tag{4.5}$$

$$\{f(t)\} = \mathrm{Im}\left(\sum_{h=0}^{\infty} \{F\}_h e^{ih\omega t}\right) \tag{4.6}$$

Moreover, since the response is assumed to be harmonic, the internal non-linear forcing vector can also be assumed to be harmonic as stated by Kuran and Özgüven [27], which can be expressed as follows:

$$\{f_{NL}(t)\} = \mathrm{Im}\left(\sum_{h=0}^{\infty} \{F_{NL}\}_h e^{ih\omega t}\right). \tag{4.7}$$

Substituting equations (4.5), (4.6) and (4.7) into equation (4.4), differential equation of motion of the nonlinear system can be converted into a set of algebraic equations as follows:

$$[-(h\omega)^2[M] + i(h\omega)[C] + i[H] + [K]]\{X\}_h + \{F_{NL}\}_h = \{F\}_h, \tag{4.8}$$

$$[K]\{X\}_0 + \{F_{NL}\}_0 = \{F\}_0. \tag{4.9}$$

In equation (4.8), ω and h are corresponding to frequency and harmonic number, respectively; whereas 0 in (4.9) stands for the bias component. Using the formulation of non-linear forcing as stated by Budak and Özgüven [25] nonlinear forcing vector in (4.8) and (4.9) can be written as

$$\{F_{NL}\} = [\Delta]\{X\}. \tag{4.10}$$

This representation allows (4.8) and (4.9) to be transformed via (4.11), where n is the number of degrees of freedom, m is the number of modes employed, [Φ] is the mass normalized modal matrix and $\{\eta\}$ is the modal coefficient vector, resulting in (4.12) and (4.13).

$$\{X\}_{n\times 1} = [\Phi]_{n\times m}\{\eta\}_{m\times 1} \tag{4.11}$$

$$\left([\Omega]-(h\omega)^2[I]+i(h\omega)\left[\overline{C}\right]+i\left[\overline{H}\right]\right)\{\eta\}_h+\{\overline{F}_{NL}\}_h=\{\overline{F}\}_h \tag{4.12}$$

$$[\Omega]\{\eta\}_0+\{\overline{F}_{NL}\}_0=\{\overline{F}\}_0 \tag{4.13}$$

In (4.12) and (4.13), [Ω] is the diagonal matrix of squares of natural frequencies, [*I*] is the identity matrix, $\left[\overline{C}\right]$, $\left[\overline{H}\right]$, $\left[\overline{F}_{NL}\right]$, and $\{\overline{F}\}$ are the modal viscous damping matrix, modal structural damping matrix, modal nonlinear forcing vector and modal forcing vector respectively and are given as follows:

$$\left[\overline{C}\right]=[\Phi]^T[C][\Phi], \tag{4.14}$$

$$\left[\overline{H}\right]=[\Phi]^T[H][\Phi], \tag{4.15}$$

$$\{\overline{F}_{NL}\}=[\Phi]^T\{F_{NL}\}, \tag{4.16}$$

$$\{\overline{F}\}=[\Phi]^T\{F\}. \tag{4.17}$$

It should be noted that the number of modes, *m*, in equation (4.11) can be selected accordingly to represent the dynamic response of the mistuned bladed disk assembly considering the frequency range in which the solution is sought. For a realistic finite element model the resulting number of non-linear equations defined by (4.12) and (4.13) is a function of the number of modes, *m,* and the number of harmonics used in the solution process, and it is much less than the number of nonlinear equations defined by equations (4.8) and (4.9).

A residual vector combining equations (4.12) and (4.13) for all harmonics, can be defined as follows:

$$\{R(\{\eta\},\omega)\}=\begin{Bmatrix} [\Omega]\{\eta\}_0+\{\overline{F}_{NL}\}_0-\{\overline{F}\}_0 \\ [-\omega^2[I]+i\omega[\overline{C}]+i[\overline{H}]+[\Omega]]\{\eta\}_1+\{\overline{F}_{NL}\}_1-\{\overline{F}\}_1 \\ \vdots \\ [-(p\omega)^2[I]+i(p\omega)[\overline{C}]+i[\overline{H}]+[\Omega]]\{\eta\}_p+\{\overline{F}_{NL}\}_p-\{\overline{F}\}_p \end{Bmatrix}. \quad (4.18)$$

where p is the total number of harmonics involved. For the iterative solution of this system of equations, Newton's method can be employed. Then the solution will be sought at $\{R(\{\eta\},\omega)\}=0$, and iteration on modal coefficients can be performed as;

$$\{\eta\}_{j+1}=\{\eta\}_j+\left[\frac{\partial\{R(\{\eta\},\omega)\}}{\partial\{\eta\}}\right]^{-1}\{R(\{\eta\}_j,\omega)\}. \quad (4.19)$$

Defining $[\overline{b}(\omega)]$ and $[\overline{a}(\omega)]^{-1}$ as follows:

$$[\overline{b}(\omega)]=[\Phi]^T[\Delta][\Phi]+[\Phi]^T\frac{\partial([\Delta])}{\partial\{\eta\}}[\Phi]\{\eta\}, \quad (4.20)$$

$$[\overline{a}(\omega)]^{-1}=\begin{bmatrix} [\Omega] & [0] & [0] & [0] \\ [0] & [\overline{\alpha}(\omega)]_1^{-1} & [0] & \vdots \\ [0] & [0] & \ddots & [0] \\ [0] & \cdots & [0] & [\overline{\alpha}(\omega)]_p^{-1} \end{bmatrix}, \quad (4.21)$$

where:

$$[\overline{\alpha}(\omega)]_h^{-1}=[-(p\omega)^2[I]+i(p\omega)[\overline{C}]+i[\overline{H}]+[\Omega]]. \quad (4.22)$$

Then the Jacobean in equation (4.19) can be represented as follows if external forcing is independent of modal displacements:

$$\left[\frac{\partial\{R(\{\eta\},\omega)\}}{\partial\{\eta\}}\right]^{-1} = \left[[\bar{a}(\omega)]^{-1} + \left[\bar{b}(\omega)\right]\right]^{-1}. \tag{4.23}$$

Note that in equation (4.23), $\left[\bar{a}(\omega)\right]^{-1}$ term is constant at each frequency step so it has to be calculated once at the beginning of the iteration. To increase calculation speed, $\left[\bar{b}(\omega)\right]$ is considered as a modification to $\left[\bar{a}(\omega)\right]^{-1}$ by utilizing Özgüven's matrix inversion method [70]. The author originally developed the method for structural modifications but mathematically it is available for being employed to any matrix inverse calculation that involves summation of a constant and a modifying matrix.

Moreover, for numerical calculations of (4.23), the accuracy of $\left[\bar{b}(\omega)\right]$ is increased by employing Romberg's method [71] which is based on Richardson's extrapolation methodology [72]. Details of this technique are not presented herein, although a summary is presented in Appendix A, but the interested reader is referred to Bauer et al. [73] for a survey which also presents other similar methods and to Mysovskikh [74] for elementary information on Romberg's method. For the proposed approach, since the non-linear forcing vector is calculated analytically as described in section 3, only the derivative of non-linear forcing is calculated numerically.

To further enhance the capability of Newton-Raphson iteration approach explained above, path-following [75] is implemented for unstable region tracing and faster convergence. To be able to do so, the dependent variable vector is changed from $\{\eta\}$ to $\{q\} = \left\{\{\eta\}^T \quad \omega\right\}^T$, and a new independent

variable s is defined as arc-length. The solution is then sought on the multi dimensional sphere defined by $s^2 = \{\Delta q\}_k^T \{\Delta q\}_k$ at k^{th} solution point by introducing a new residual equation as follows:

$$g(\{\eta\}_k, \omega_k) = \{\Delta q\}_k^T \{\Delta q\}_k - s^2 = 0. \tag{4.24}$$

In equation (4.24), $\{\Delta q\}_k$ is given by;

$$\{\Delta q\}_k = \{\{q\}_k - \{q\}_{k-1}\}, \tag{4.25}$$

where $\{q\}_{k-1}$ correspond to the last converged solution. Adding the additional residual equation defined by (4.24) to the residual vector previously defined by (4.18), the new residual vector is defined as $\left\{\{R(\{\eta\}_k^j, \omega_k^j)\}^T \quad g(\{\eta\}_k^j, \omega_k^j)\right\}^T$ and iterating on the dependent vector $\{q\} = \left\{\{\eta\}^T \quad \omega\right\}^T$ as follows:

$$\{q\}_k^{j+1} = \{q\}_k^j - \left[\begin{array}{cc} \dfrac{\partial R(\{\eta\},\omega)}{\partial\{\eta\}} & \dfrac{\partial R(\{\eta\},\omega)}{\partial\omega} \\ \dfrac{\partial g(\{\eta\},\omega)}{\partial\{\eta\}} & \dfrac{\partial g(\{\eta\},\omega)}{\partial\omega} \end{array}\right]^{-1} \Bigg|_{\{\eta\}_k^j, \omega_k^j} \begin{Bmatrix} R(\{\eta\}_k^j, \omega_k^j) \\ g(\{\eta\}_k^j, \omega_k^j) \end{Bmatrix}. \tag{4.26}$$

Note that by adding ω to the vector of dependant variables and defining a new independent variable, s, the continuation parameter for solution curve becomes the arc-length, s, rather than the frequency, ω, and thus will trace the unstable regions.

4.2.2 Case Studies

In this section 4 case studies are presented to verify and demonstrate the capabilities of the method proposed.

4.2.2.1 Case Study I – Time Verification

To verify the solution methodology presented in section 4.2.1, a 6-bladed Lumped Parameter bladed disk model is created as described in section 3.1.1. The model is mistuned with a random set of numbers which fit a normal distribution with zero mean and 2% standard deviation. The natural frequencies of the resulting mistuned assembly are given in Table 4.1.

Table 4.1 – Mistuned Assembly Natural Frequencies

Mode	Frequency	Mode	Frequency
1	25 Hz	7	7400 Hz
2	6280 Hz	8	15200 Hz
3	6345 Hz	9	15225 Hz
4	6425 Hz	10	25100 Hz
5	6500 Hz	11	25150 Hz
6	6555 Hz	12	30050 Hz

The analysis is carried out in the frequency range starting from 6000 Hz to 7000 Hz considering the high density of modes in that region.

To emphasize the effect of the modes used in the analysis on the results, two different models are prepared: the first one with the first 6 modes of the assembly and the second one with the first 7 modes. Forced responses of the tuned case with no frictional contact (free)are presented in Figure 4.4.

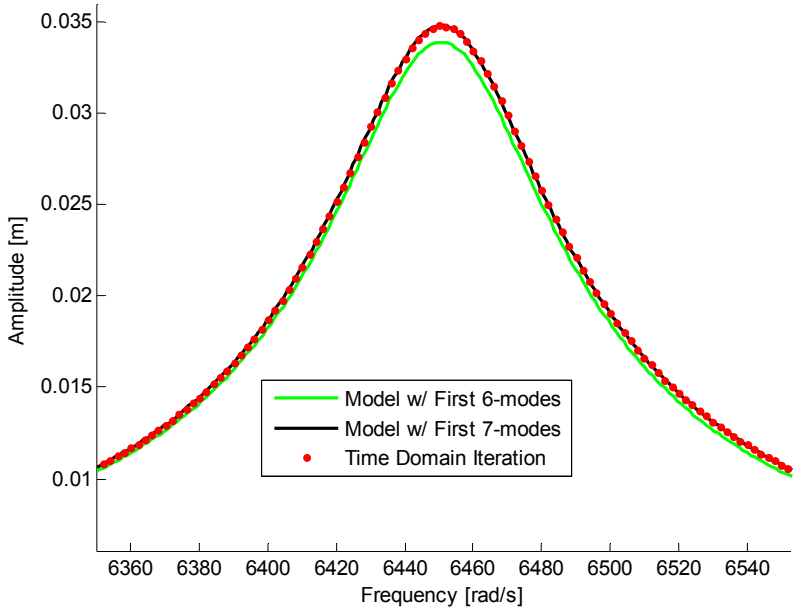

Figure 4.4 – Free Response of Tuned Assembly

Free response of the mistuned assembly is given in Figure 4.5 and Figure 4.6. Whereas the fully stick forced response solution for it is plotted in Figure 4.7 and Figure 4.8.

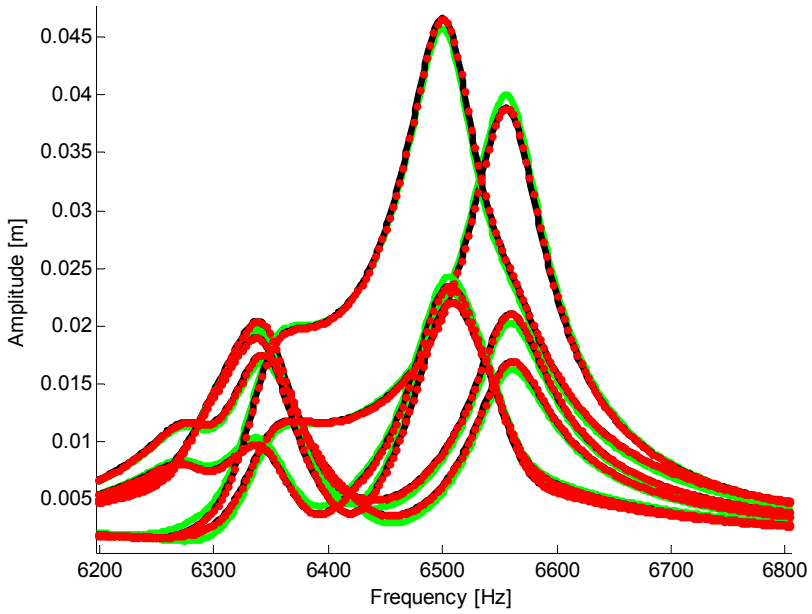

Figure 4.5 – Free Response of Mistuned Assembly – Model with 6 Modes (____), Model with 7 Modes (____), Time Integration (. . . .)

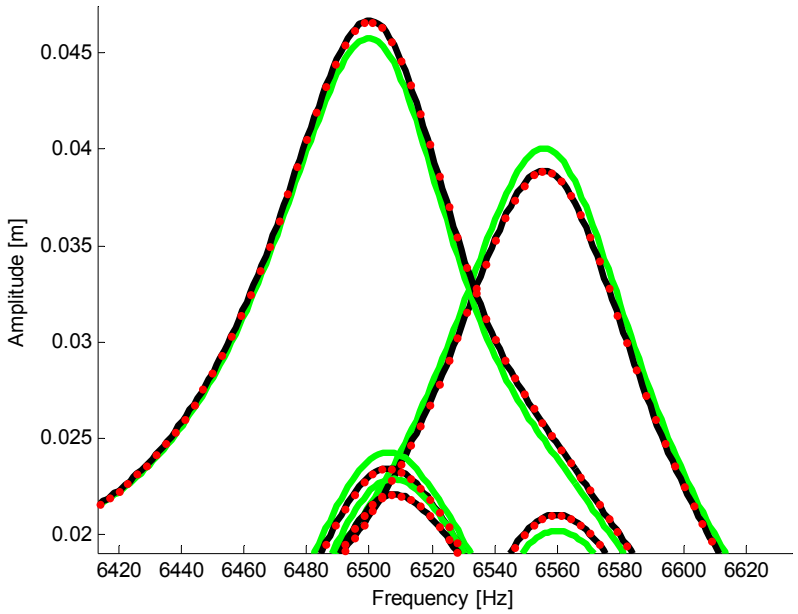

Figure 4.6 – Free Response of Mistuned Assembly (Close-Up) – Model with 6 Modes (____), Model with 7 Modes (____), Time Integration (. . . .)

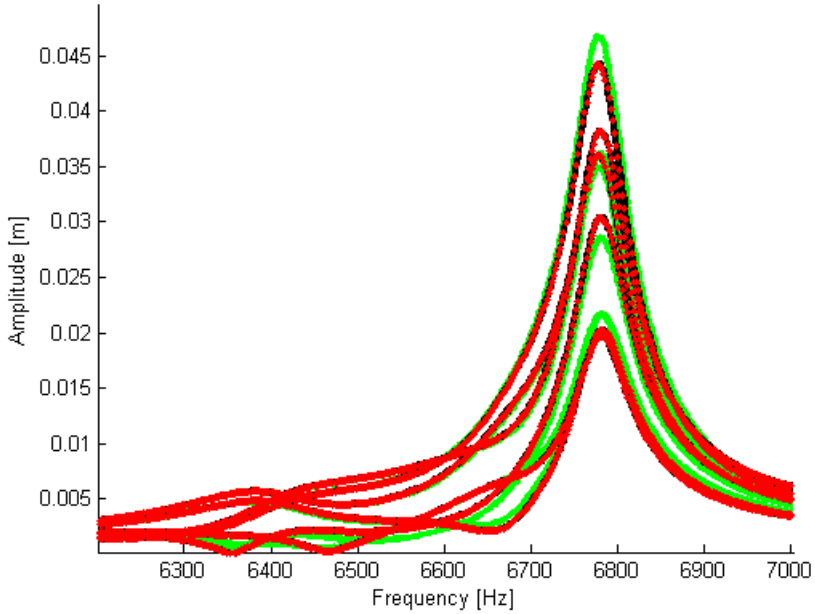

Figure 4.7 – Forced Response of Mistuned Assembly: Fully Stuck – Model with 6 Modes (____), Model with 7 Modes (____), Time Integration (. . . .)

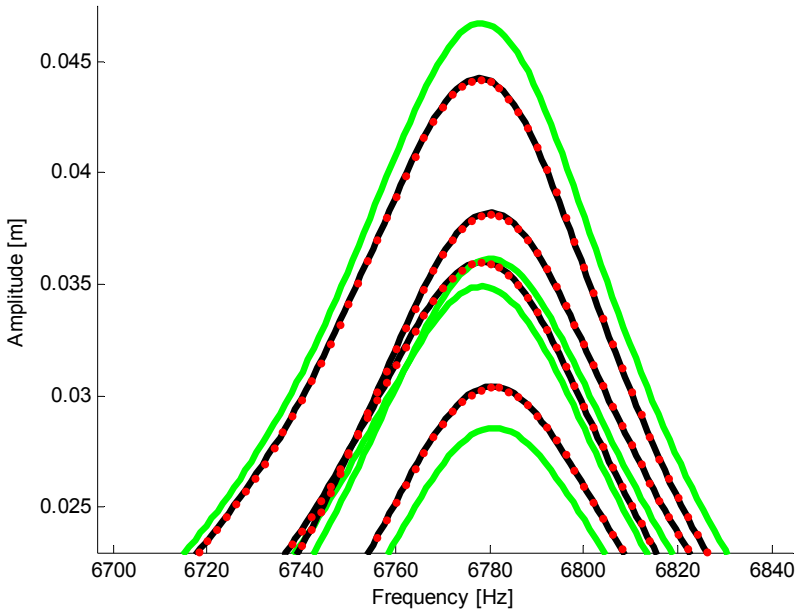

Figure 4.8 – Forced Response of Mistuned Assembly (Close-Up): Fully Stuck – Model with 6 Modes (____), Model with 7 Modes (____), Time Integration (. . . .)

It is clearly seen from Figure 4.6 and Figure 4.8 that including the seventh mode in the frequency domain model increased the accuracy of the response significantly. Note that it is an expected result since the 7th mode is close to the frequency range of interest.

In Figure 4.9 and Figure 4.10 non-linear forced response with a 1000 N normal force is given.

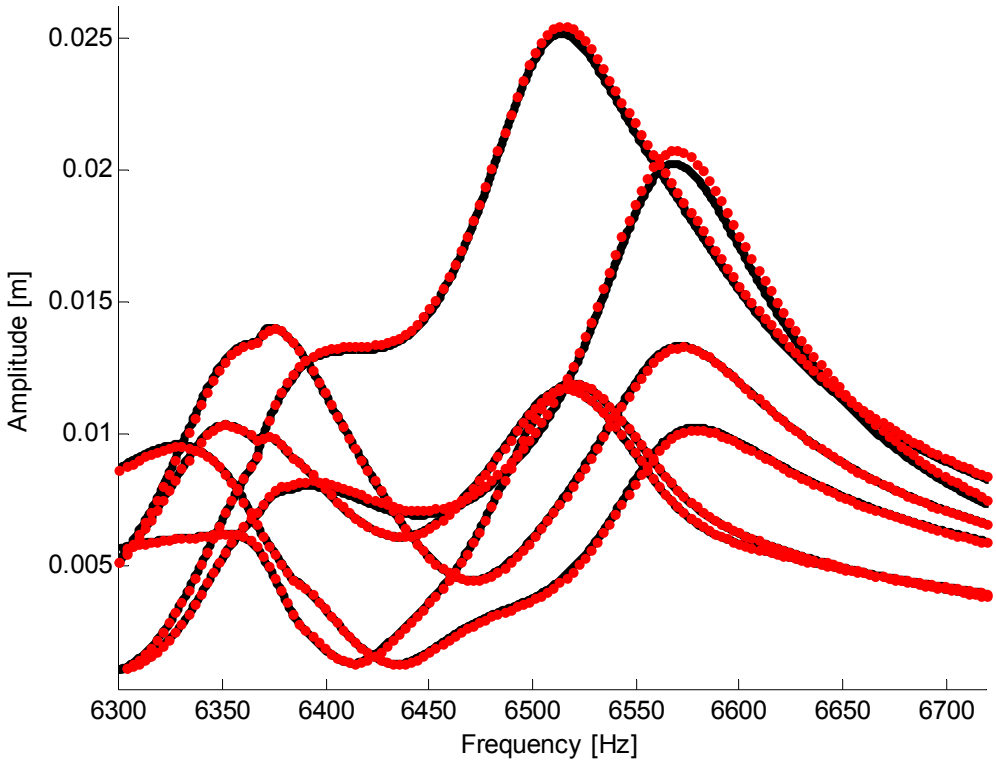

Figure 4.9 – Non-Linear Forced Response of Mistuned Assembly with n_0 = 1000 N –Model with 7 Modes (___), Time Integration (. . . .)

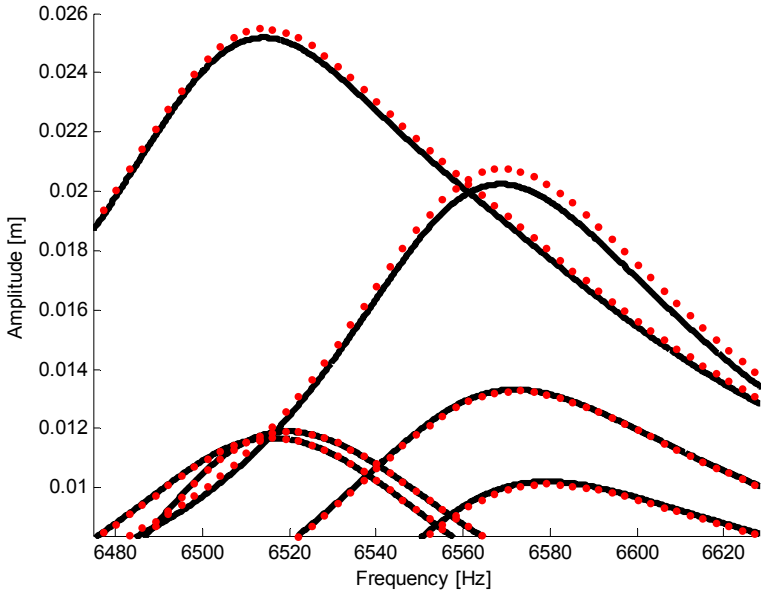

Figure 4.10 – Non-Linear Forced Response of Mistuned Assembly with n_0 = 1000 N (Close-Up) –Model with 7 Modes (___), Time Integration (. . . .)

Comparing the forced response of the mistuned assembly for Free (Figure 4.6), Stick (Figure 4.8), and n0=1000 N (Figure 4.10), one can state that the error in free and stick cases, there is no error as expected. The reason of this discrepancy is the single harmonic representation of the nonlinear forces. Nevertheless, results obtained from HBM are still in very good agreement with the time integration solution; hence, single harmonic representation of the nonlinear contact forces is acceptable. Forced responses for free, n0=1000 N, and stick cases for the 7-mode model calculated in frequency domain and in time domain are given in Figure 4.11 and Figure 4.12, respectively. Both of these solutions are performed on the same computer and for the nonlinear case for n0=1000 N, frequency domain solution noted to be more than 100 times faster, compared to the same solutions in time domain.

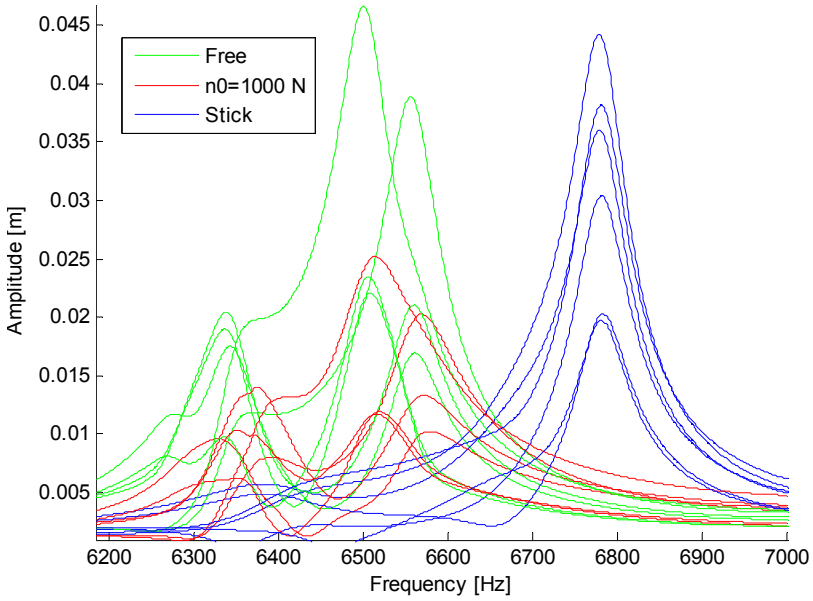

Figure 4.11 – Forced Response of Mistuned Assembly of Frequency Domain Model Constructed with 7-modes

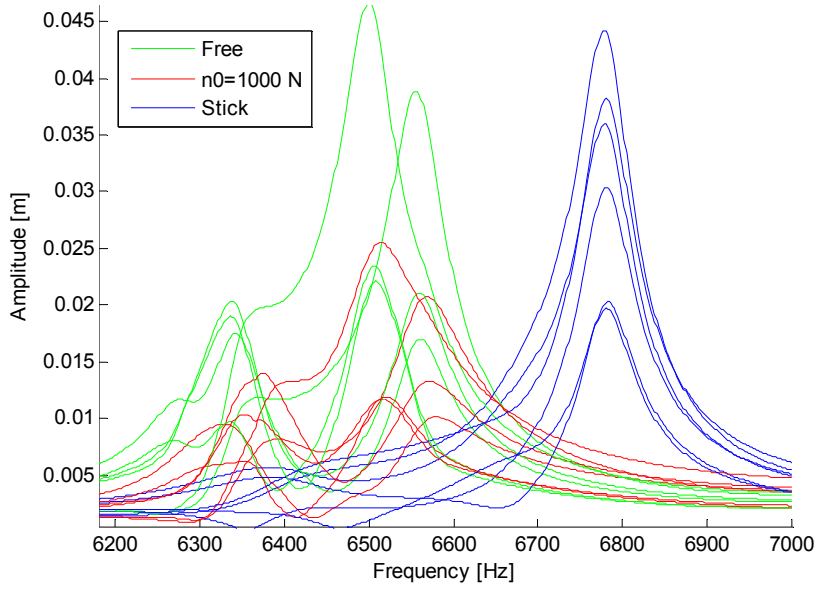

Figure 4.12 – Forced Response of Mistuned Assembly – Time Integration

4.2.2.2 Case Study II – 12 Bladed Lumped Parameter Model

In this section the proposed approach is demonstrated with a 12-bladed Lumped Parameter bladed disk model constructed as described in section 3.1.1. The model is mistuned with a random set of numbers generated to fit a normal distribution with zero mean and 2% standard deviation on the first cantilevered blade modes by altering Δk values. The contact model presented in section 3 is used between the blades and the solution is carried out with the solution procedure proposed in section 4.2.1. Forced response solutions for both of the tuned and mistuned systems are performed with different normal load values in order to observe the effect under 6^{th} engine order excitation.

In Table 4.2, magnification of the mistuned forced response with respect to tuned free (linear) response in the frequency range of interest is tabulated for all contact conditions considered in the solution.

Table 4.2 – Magnification Factor

Contact Condition	Factor
Free	1.27
n0 = 100N	1.19
n0 = 500N	0.98
n0 = 1000N	0.83
n0 = 2500N	0.94
Stick	1.22

It is seen from Table 4.2 that among the different contact conditions where normal force is altered, most efficient damping is obtained by n_0=1000N. If further attention is paid on the tuned and mistuned forced response solutions presented in Figure 4.13 and Figure 4.14, respectively, this fact will be much clearly observed.

Furthermore, solution for all blades of tuned and mistuned systems are given in Figure 4.15, Figure 4.16, and Figure 4.17 corresponding to the free, stick and n_0=1000N cases, respectively. It should be noted that for different normal load values, the blade that has the maximum response is also different in each case.

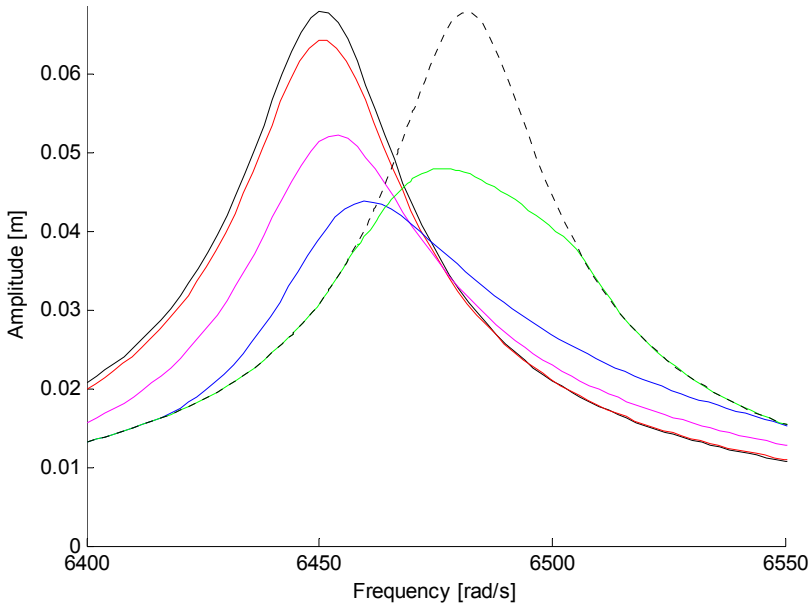

Figure 4.13 – Tuned Response - Free (__), n_0=100N (__), n_0= 500N (__), n_0=1000N (__), n_0=2500N (__), Stick (_ _)

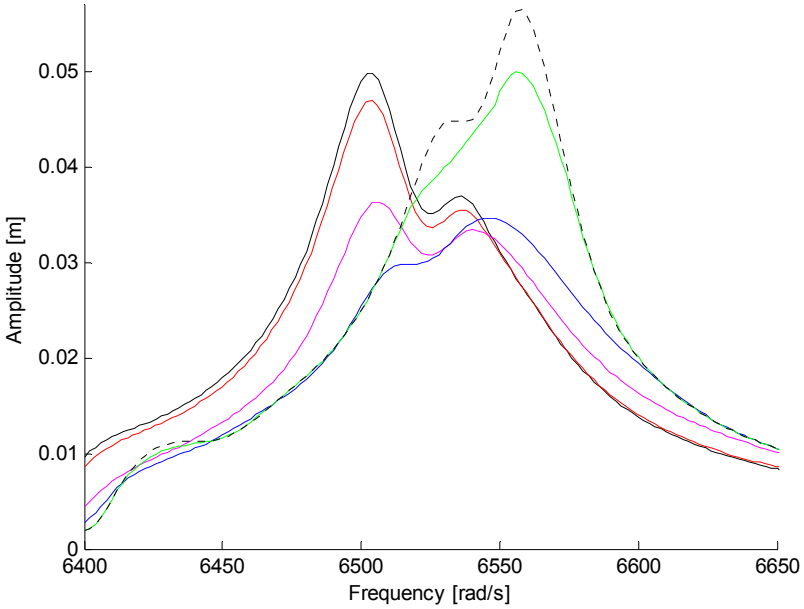

Figure 4.14 – Mistuned Response - Free (—), n_0=100N (—), n_0= 500N (—), n_0=1000N (—), n_0=2500N (—), Stick (– –)

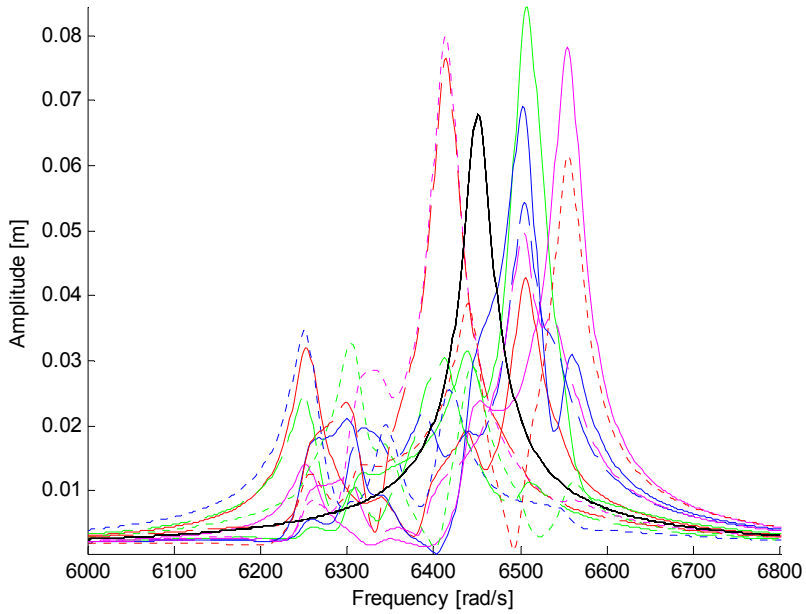

Figure 4.15 – Forced Response - Free - Tuned (—), Mistuned (Colored)

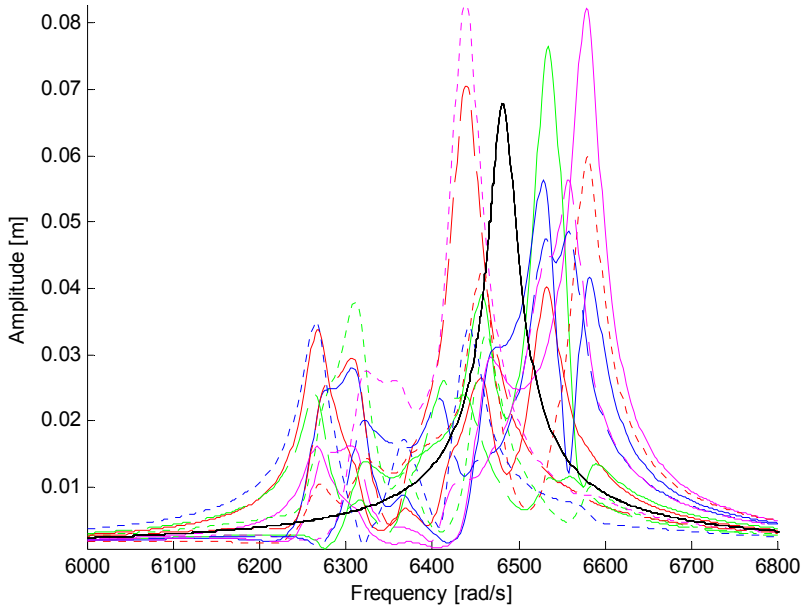

Figure 4.16 – Forced Response - Stick - Tuned (__), Mistuned (Colored)

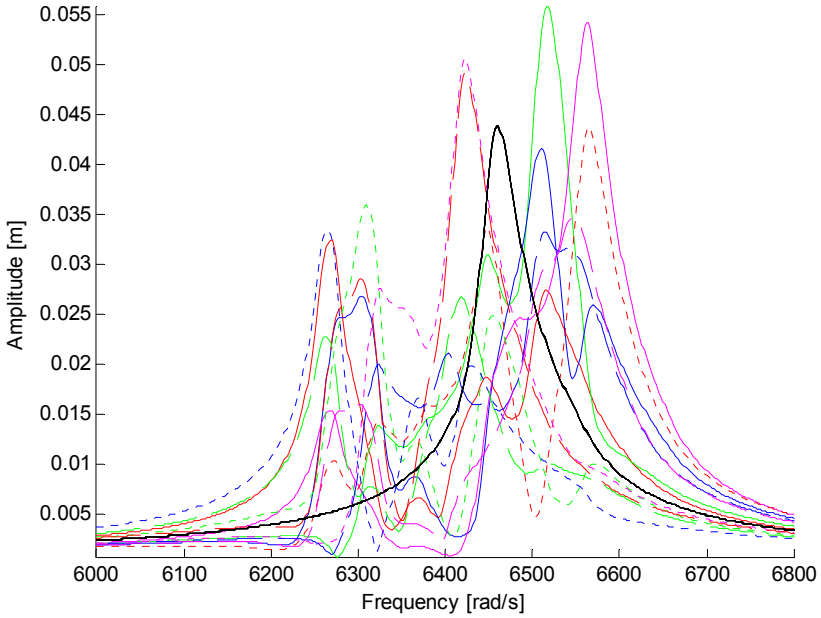

Figure 4.17 – Forced Response - n_0 = 1000N - Tuned (__), Mistuned (Colored)

4.2.2.3 Case Study III – 24 Bladed FEM I

In this case study, to address a relatively more realistic problem, finite element model (Figure 4.19) of a 24 bladed disk assembly (Figure 4.18) with shrouds is created. A sector mesh of the assembly is depicted in Figure 4.20. The full finite element model has 12672 degrees of freedom. Finite element modeling is carried out with the commercial software package ANSYS.

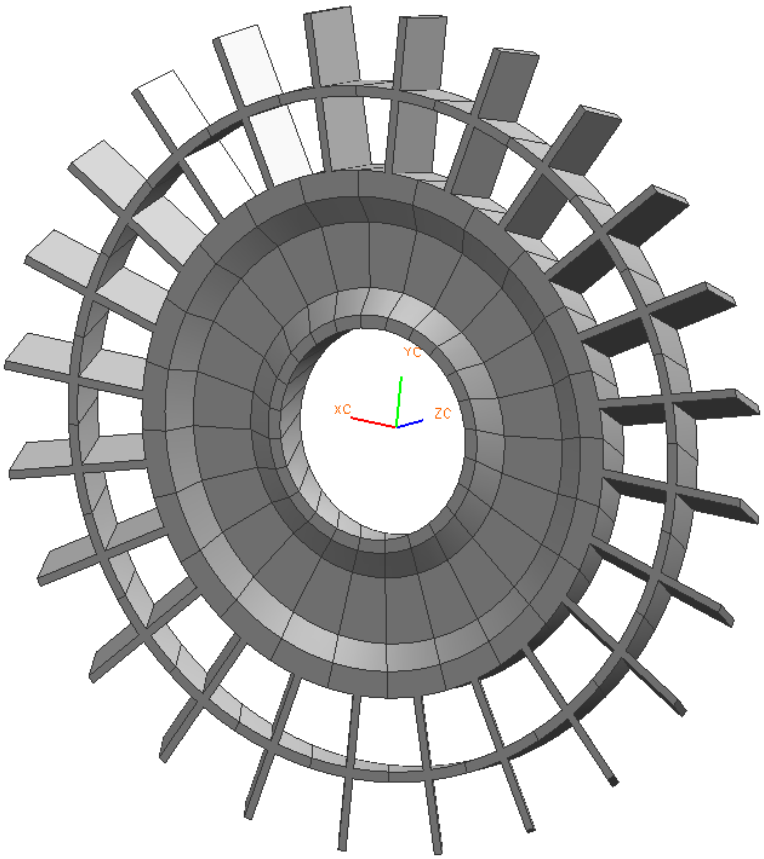

Figure 4.18 – 24-Bladed Disk Assembly

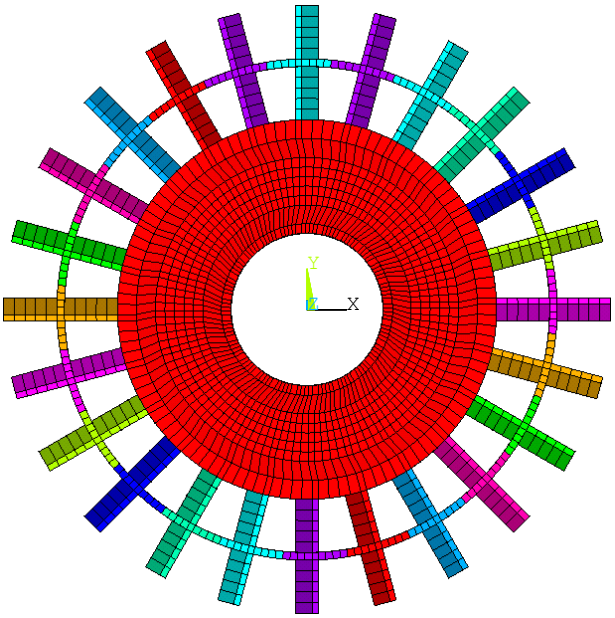

Figure 4.19 – 24-Bladed Disk Assembly Mesh

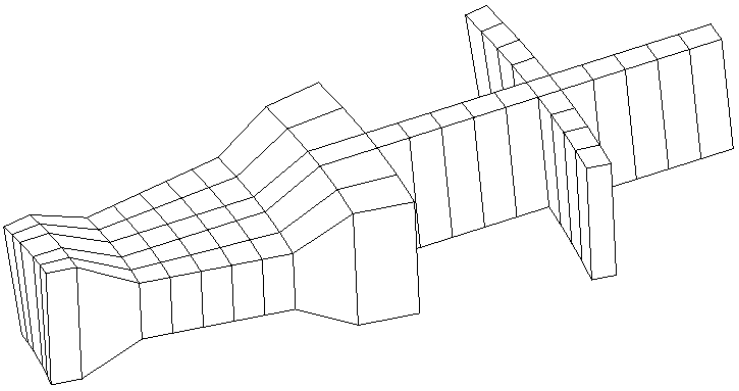

Figure 4.20 – 24-Bladed Disk Sector Mesh

Mistuning is applied through altering the elastic modulus of the blades with a normal distribution of zero mean and 1.5% standard deviation on cantilevered blade modes. In Figure 4.21, comparison of finite element

model solution with the method proposed here is shown for the free case with EO 12. In the analysis, 24 modes of the full finite element model are used and it is clearly seen that the number of modes involved in the analysis is sufficient to represent the system in the frequency range of interest for the free contact mode.

Nonlinear analysis of the mistuned system is performed by introducing contact elements between all nodes that intersect through the contact planes defined by the neighboring shrouds. In this analysis contact parameters are taken as identical for all contact surfaces.

In Figure 4.22 and Figure 4.23, results for all blades are depicted for different normal loads.

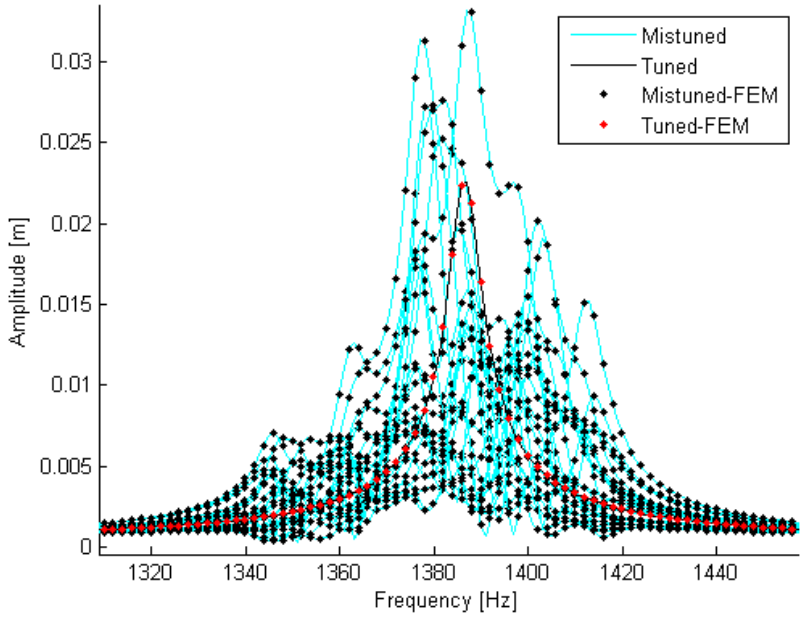

Figure 4.21 – FEM Comparison

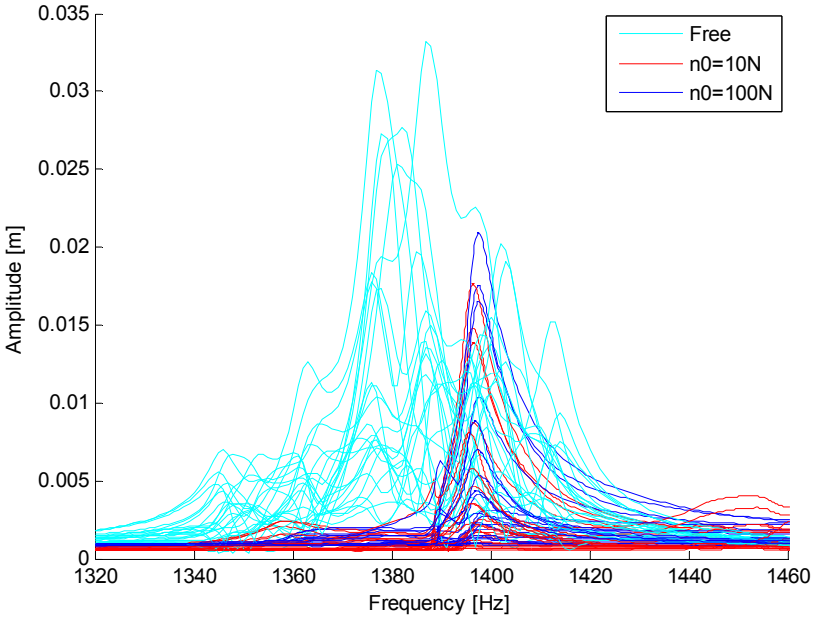

Figure 4.22 – Mistuned Assembly Response 1

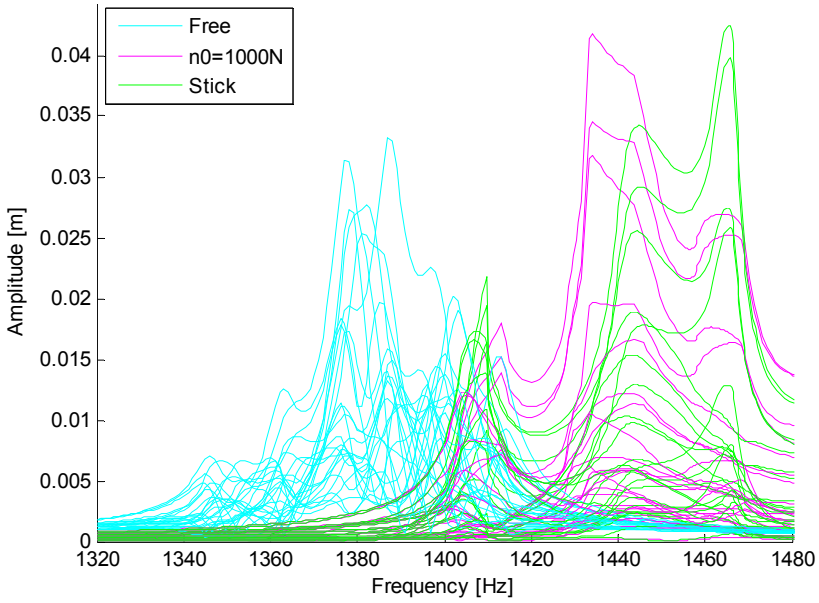

Figure 4.23 – Mistuned Assembly Response 2

From the assembly response, Figure 4.22 and Figure 4.23, it is seen that although n_0=10N and n0=100N normal loads decrease the maximum amplification, for n_0=1000N, system response is higher than the maximum amplitude of free response. Amplification factors of the response compared to the free tuned case are 1.47, 0.78, 0.93, 1.85 and 1.88 for free, n_0=10N, n_0=100N, n_0=1000N and stick cases respectively.

For two of the blades from the assembly, all normal load cases are plotted in Figure 4.24 and Figure 4.25. Note that for Blade B, n_0=10N and n_0=100N suppress the vibratory response very efficiently but a higher normal load or stick condition the maximum vibration amplitude rapidly increases.

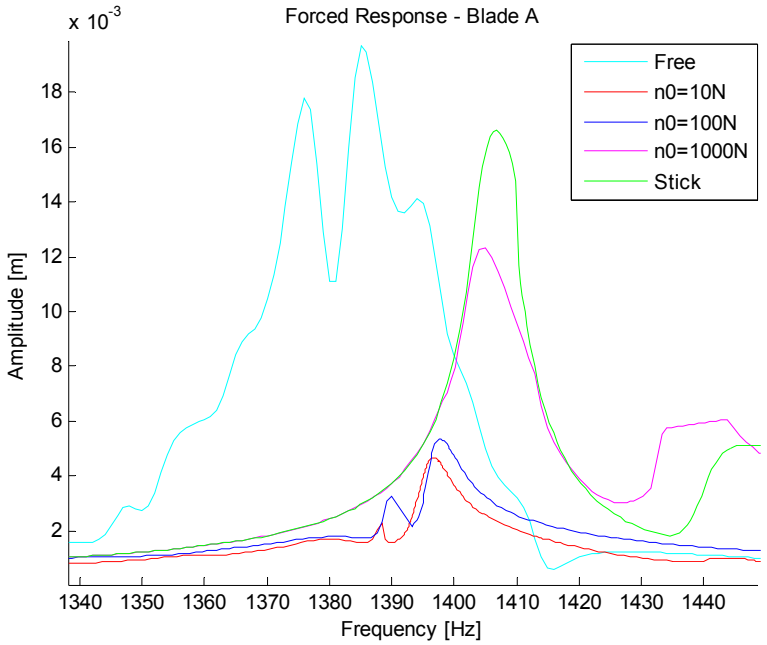

Figure 4.24 – Forced Response – Blade A

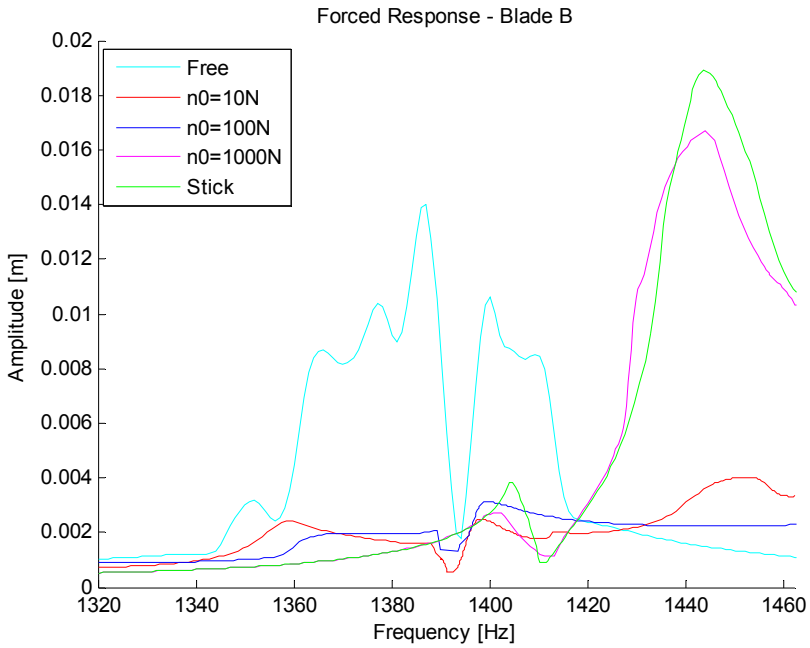

Figure 4.25 – Forced Response – Blade B

4.3 A New Adaptive Harmonic Balance Method

In structural dynamics, harmonic balance method (HBM) is employed to represent time dependent non-linear phenomena with several pure harmonic oscillations [27] for obtaining steady-state response. As stated earlier, Budak and Özgüven [25] made the representation of harmonic balance method applicable in modal domain by introducing the non-linearity matrix representation.

One of the major difficulties in the use of HBM is the determination of the number of harmonics to be used in the analysis. The non-linear phenomena under consideration should be examined carefully for the solution to yield acceptable accuracy. In some cases, not only the non-linearity associated,

but also the structure may demand more than single harmonic representation. This is generally an iterative and case dependent process, which can only be avoided by using an excessive number of harmonics thus disregarding the needs of the problem in hand. However, the computational power needed will increase with more than a linear slope, degrading the efficiency and speed of the solution remarkably. In fact, solving a large problem may even be impossible in an average work station. Referring to equation (4.23), where $[\bar{b}(\omega)]$ and $[\bar{a}(\omega)]^{-1}$ are represented by equations (4.20) and (4.21) respectively, which are reprinted below as (4.27) and (4.28) for the sake of completeness, will support the discussion mathematically.

$$[\bar{b}(\omega)] = [\Phi]^T [\Delta][\Phi] + [\Phi]^T \frac{\partial([\Delta])}{\partial\{\eta\}}[\Phi]\{\eta\} \tag{4.27}$$

$$[\bar{a}(\omega)]^{-1} = \begin{bmatrix} [\Omega] & [0] & [0] & [0] \\ [0] & [\bar{\alpha}(\omega)]_1^{-1} & [0] & \vdots \\ [0] & [0] & \ddots & [0] \\ [0] & \cdots & [0] & [\bar{\alpha}(\omega)]_p^{-1} \end{bmatrix} \tag{4.28}$$

Note that, the number of equations, n_E, and the number of cells, n_C, in the matrices defined by (4.27) and (4.28) can be represented by (4.29) and (4.30) respectively.

$$n_E = n(1+p) \tag{4.29}$$

$$n_C = \left(n(1+p)\right)^2 \tag{4.30}$$

where *n* is the number of modal coefficients used to model the system and *p* is the number of harmonics involved.

From (4.29) and (4.30), it is evident that the number of additional equations to be solved will increase by n for each harmonic added to the solution space. Moreover, operations carried out on the elements of matrices, for example matrix inversion, will result in larger performance degradation.

A new adaptive harmonic balance method (AHBM) approach is introduced in order to overcome the difficulties in the determination of the number of harmonics required for the analysis and the computation time spent.

4.3.1 Methodology

The term 'Adaptive Harmonic Balance Method' is previously used by both fluid dynamics and circuit analysis communities. Maple et al. [76] determined the number of harmonics required in each cell of a CFD mesh based on the spectral power associated with the harmonics to solve a supersonic/subsonic diverging nozzle which is subjected to unsteady periodic flows. Whereas Zhu et al. [77] employed a similar approach to separately resolve the number of harmonics required to force convergence of the solution of a bipolar oscillator. Both of these approaches are formulated for computational methods where element based harmonics optimization is carried out. The method proposed here, on the contrary, focuses on the accuracy of the solution based on the whole system response. This will ensure that the response related with a higher harmonic force component acting on a point to be captured at all points in the structure.

At each solution step, the non-linear forcing vector associated with each nonlinear element is monitored. To guarantee automatic switching between lower and higher number of harmonics, the following criterion is set:

$$|f_{0c}|+|f_{0s}|+|f_{1c}|+|f_{1s}|+\cdots+|f_{kc}|+|f_{ks}| \geq a\cdot\left(|f_{(k+1)c}|+|f_{(k+1)s}|+\cdots+|f_{rc}|+|f_{rs}|\right) \quad (4.31)$$

In (4.31), *c* and *s* stands for the cosine and sine components of the non-linear forcing vector respectively, *k* is the number of harmonics required for the representation of the nonlinear forcing vector at the current solution step, and *r* is the maximum number of harmonics allowed. Accuracy of the solution is pre-defined by setting the accuracy constant *a*. A higher accuracy constant will result in a relatively more accurate solution because the solver will be forced to include more harmonics to the analysis, and vice versa.

After determining the number of harmonics, *k*, required for each non-linear element of nonlinear forcing vector, the highest one is selected as the global number of harmonics for the current solution step of the system.

4.3.2 Case Studies

Two case studies are presented to demonstrate the capabilities of the proposed system; a single degree of freedom oscillatory point mass, and a 12 bladed lumped parameter bladed disk model.

4.3.2.1 Single Degree of Freedom Oscillator

The schematic view of the SDOF system employed in this case study is presented in Figure 4.26.

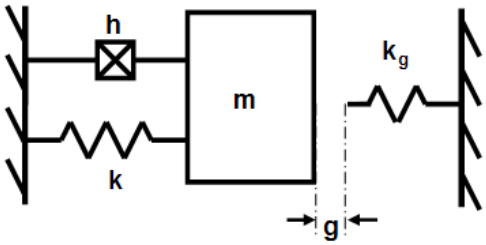

Figure 4.26 – SDOF Oscillator with Gap Non-linearity

The gap element shown schematically in Figure 4.26 is formulated with the following equation:

$$F_g(x) = \begin{cases} k_g(x-g) & (x > g) \\ 0 & (Otherwise) \end{cases} \tag{4.32}$$

where g , h, and k_g are the gap length, structural damping constant, and gap stiffness, respectively. Multi-harmonic representation of the gap element under consideration has been derived by many researchers and is not included here. Interested readers are referred to Orbay [78], where he not only derives HBM representation of gap element but also other non-linear elements like macro-slip friction and cubic stiffness.

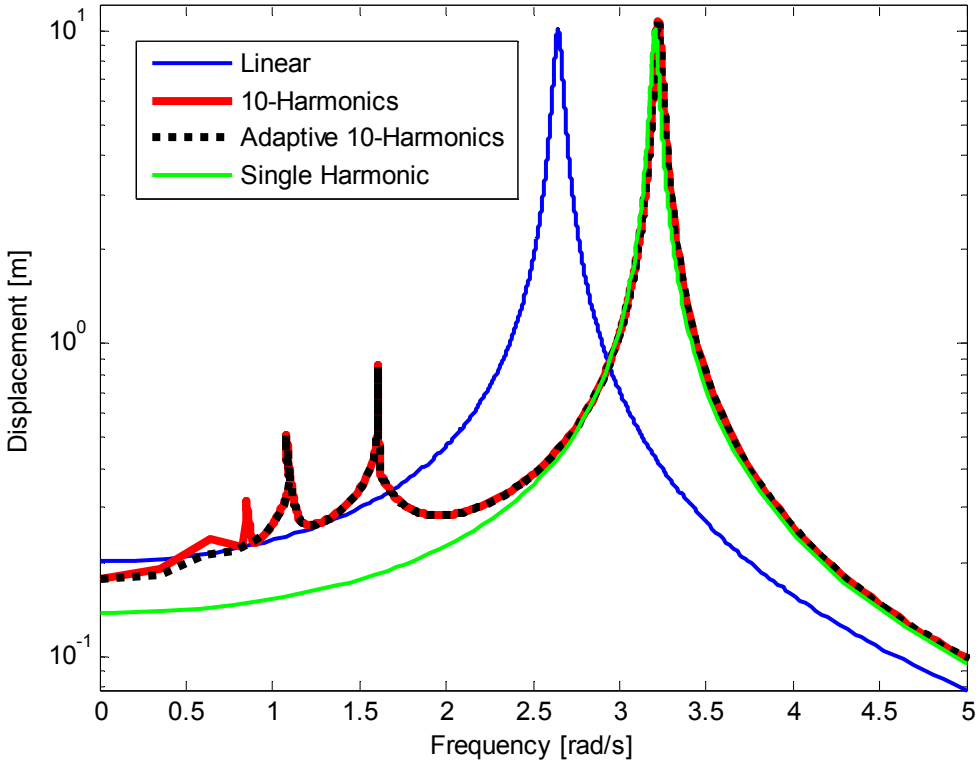

Figure 4.27 – SDOF Oscillator Free and Non-linear Response

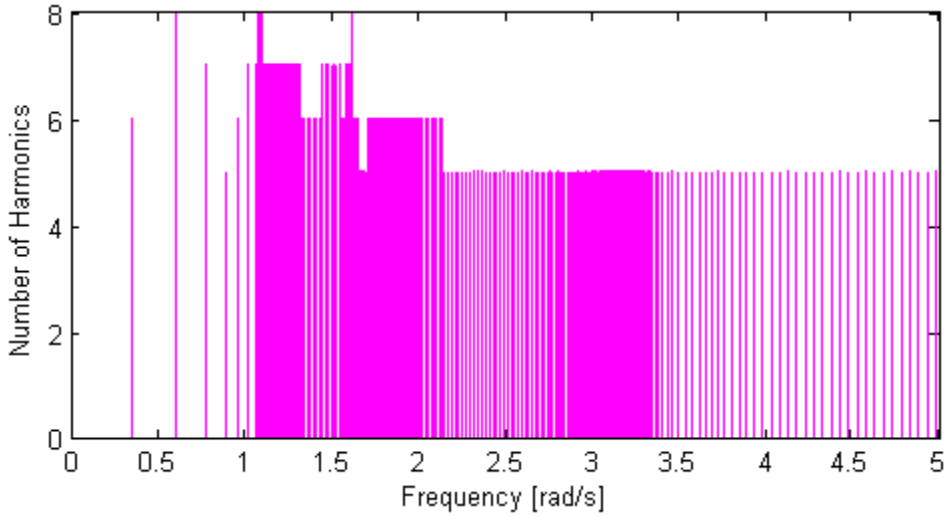

Figure 4.28 – SDOF Oscillator – Number of Harmonics used in AHBM

The results (Figure 4.27) clearly show that AHBM captures the sub-harmonic effects to an acceptable degree. The AHBM used for the solution of this problem is limited to a maximum harmonic number of 10. In Figure 4.28, the number of harmonics used at each solution step is depicted. Note that, the step size is not constant and gets relatively smaller near resonant frequencies, which is achieved by the path-following solution technique. AHBM solution has been 2.3 times faster than the 10 harmonics HBM solution.

4.3.2.2 12-Bladed Lumped Parameter Model

In this section the proposed AHBM approach is demonstrated with a 12-bladed Lumped Parameter bladed disk model constructed as described in section 3.1.2, where a gap element is introduced between the two neighboring blades representing a manufacturing imperfection.

The model is mistuned with a random set of numbers generated to fit a normal distribution with zero mean and 2% standard deviation on the first cantilevered blade modes by altering Δk values.

The solution is carried out with the solution procedure proposed in section 4.2.1.

In Figure 4.29 linear responses of the tuned and mistuned models are depicted. The maximum amplification in this frequency range is recorded as 1.74.

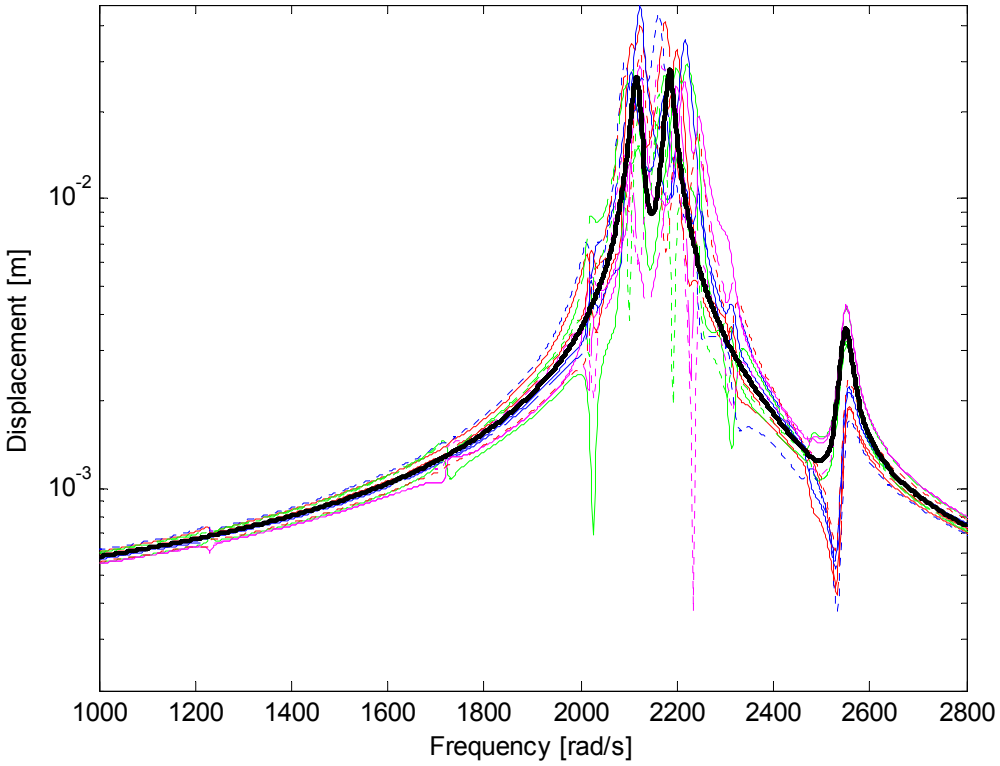

Figure 4.29 – Free Response – Tuned (—), Mistuned (Colored)

For comparison purposes, solutions with single harmonic HBM, 11-harmonics HBM, and Adaptive HBM with maximum harmonics of 11 are performed.

Overall error between the 11-harmonics HBM and Adaptive HBM is noted to be less than 0.01% on the magnitude of displacement for all blades. For one of the two blades where the gap element was connected, the results are as shown in Figure 4.30 and Figure 4.31. For this analysis, AHBM solution has been 2.7 times faster than the 11-harmonics HBM solution.

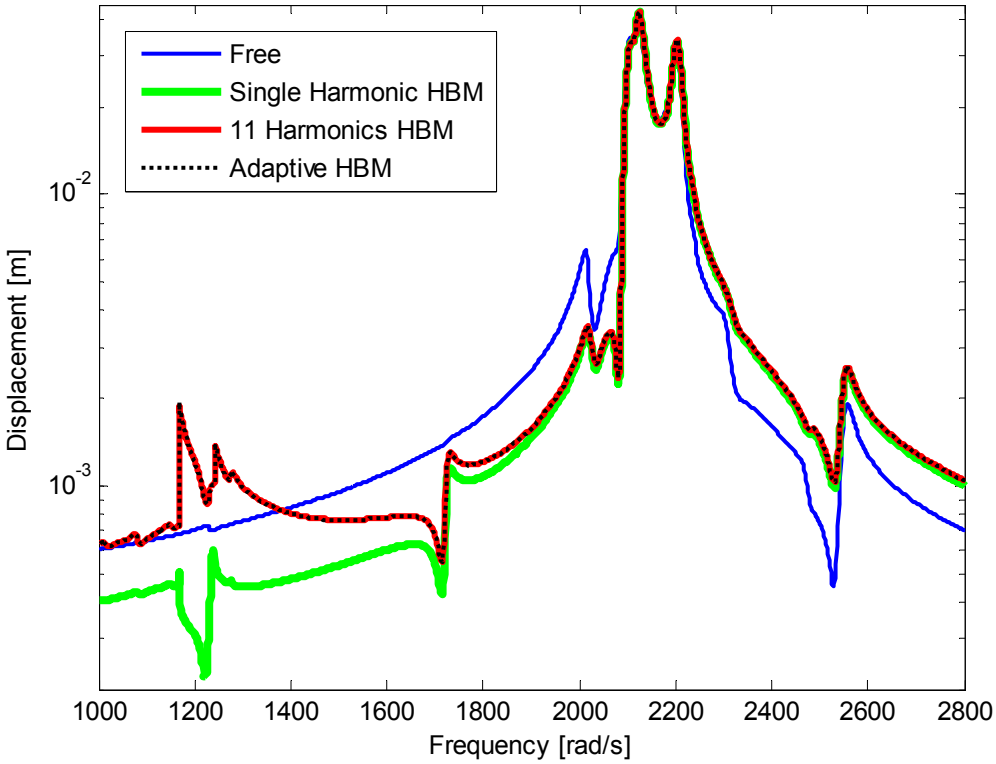

Figure 4.30 – 12-Bladed Disk – Free and Non-linear Response

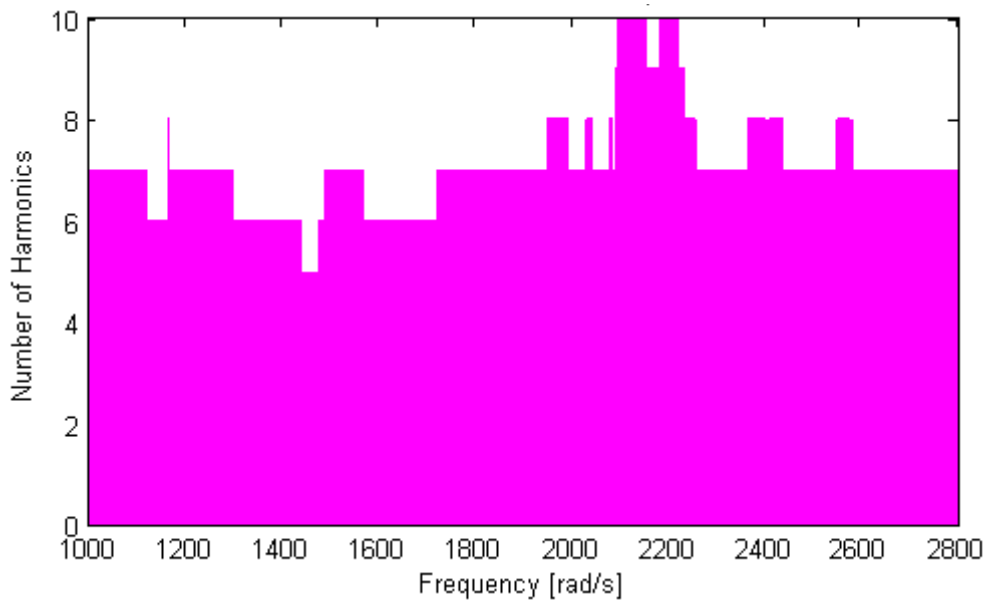

Figure 4.31 – 12-Bladed Disk – Number of Harmonics used in AHBM

CHAPTER 5

MISTUNING IDENTIFICATION

From the mathematical point of view, mistuning identification problem is the same as model updating problem and any model updating method should fit the mistuning identification problem. However, this is not the case in real applications. The difference primarily arises from the relatively small deviations seen in mistuning and cyclic symmetry of a gas turbine rotor. These two differences sum up and result in high modal density regions in the frequency response of bladed disk assemblies, such that several closely spaced modes block others from being observed in test results. Moreover, the small deviations causing the mistuning phenomenon are generally at levels that would be considered as noise by most of the model updating methods.

In this chapter, to identify mistuning, neural networks are utilized. Moreover, the performance of the proposed approach is enhanced by post-neural networks optimization. It is believed that the study encompassed herein will enrich the literature of not only mistuning identification but also model updating since it proposes a means of improving the neural networks usage in system identification. To prove so, the methodology developed here is also applied to model updating and non-linearity identification.

5.1 Neural Networks Identification (NetID)

In this section, the methodology to identify mistuning of bladed disk assemblies from system response by employing neural networks is explained. The proposed approach is also tested with a lumped parameter model.

5.1.1 The Network

The pattern of the neural network used in this study is a two layer feed-forward back-propagation configuration given in Figure 5.1.

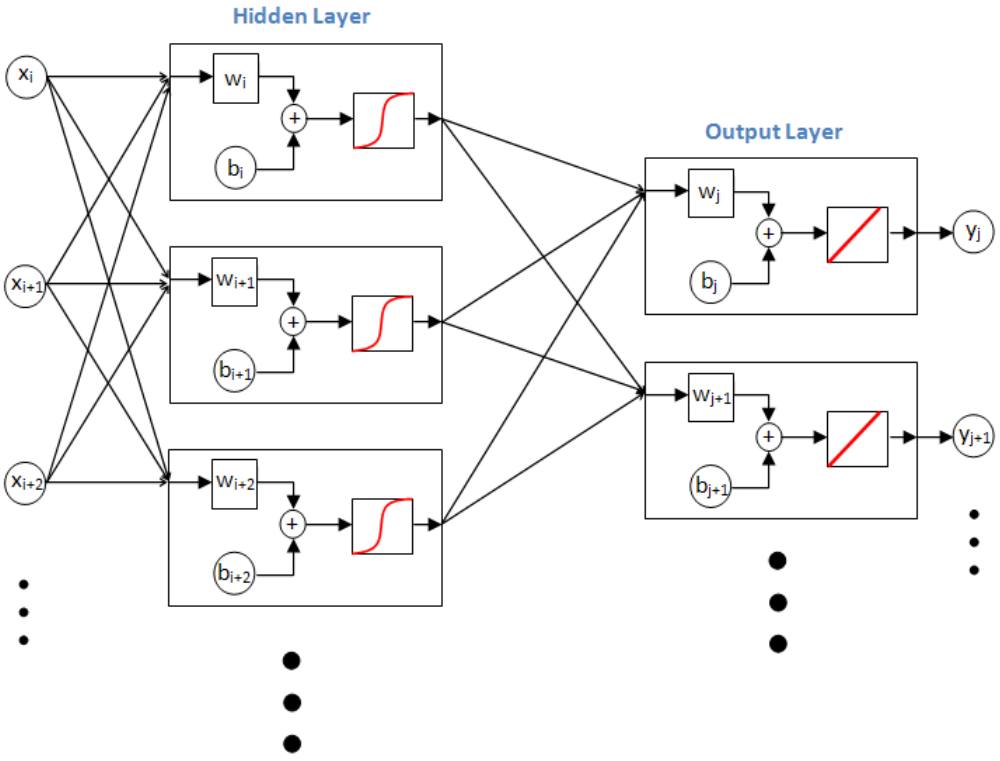

Figure 5.1 – Neural Network Configuration

In this network a hidden layer of neurons, where a nonlinear function and bias components are utilized, is receiving information from the input parameters. The second layer, which is named as output layer, receives information from the hidden layer, then via a linear function and bias components calculate the outputs. In Figure 5.1, w_i is the weighting factor vector and b_i is the bias component of i^{th} neuron. With this type of neural networks, the number of neurons in the output layer is fixed by the number of outputs. However, the number of neurons employed in the hidden layer depends on the needs of the problem since with increasing number of neurons utilized in the hidden layer enhances the capability of the network to some extend [79].

A neural network has to be fitted to the problem by a process called 'training'. In the training process, the network is fed by a data set of inputs and corresponding outputs and with back propagation; fitting of the network is accomplished. During the network fitting process, weights and bias components of each of the neurons are adjusted in order to fit the training data. In this study, Levenberg-Marquardt (L-M) algorithm is used for training purposes, whereas the error function utilized is the mean square error (MSE).

5.1.2 Methodology and Data Selection

In any identification problem, the known parameters are generally the outputs of the system and the unknown factors are some physical parameters that are used to formulate the system under consideration. In this work, the system is a blisk, the known parameters are some

combination of results coming from a modal test, and the unknown parameters are the blade cantilever natural frequency mistuning percentages. In other words, the aim is to obtain the mistuning parameters from system response. To serve this requirement, the input $\{x\}$ and output $\{y\}$ vectors in (5.1) are used in the training step.

$$\{x\} = \begin{Bmatrix} \begin{Bmatrix} \vdots \\ \omega_i \\ \omega_{i+1} \\ \vdots \end{Bmatrix} \\ \begin{Bmatrix} \vdots \\ \{u\}_i \\ \{u\}_{i+1} \\ \vdots \end{Bmatrix} \end{Bmatrix} \qquad \{y\} = \begin{Bmatrix} \vdots \\ p_j \\ p_{j+1} \\ \vdots \end{Bmatrix} \tag{5.1}$$

In (5.1), ω_i and $\{u\}_i$ are the natural frequency and mode shape of i^{th} mode of the blisk respectively, and p_j are the blade cantilever natural frequency mistuning of the j^{th} blade. The mode shapes considered are formed by the blade tip displacements in the dominant direction of the mode family considered.

5.2 Neural Networks and Optimization Identification (OptID)

In this section, the methodology to identify mistuning of bladed disk assemblies from system response by employing neural networks and optimization is explained. The proposed approach is also tested with a component synthesis based reduced order model (ROM).

5.2.1 Methodology

NetID provides efficient means of mistuning identification, which will be adequate for many applications, but there may be demanding situations where more accurate results are needed. Moreover, the input from test results may be limited (i.e. incomplete mode families and/or mode shapes) which may decrease the performance of the pure neural networks approach, namely NetID.

For such situations, an optimization routine is proposed which takes the result of NetID as an initial point and seeks the optimum solution within the domain specified. NetID not only provides the starting point of the optimization problem, but also supplies information to narrow the lower and upper bounds of optimization parameters, which are the blade cantilever frequency mistuning percentages for the case of this study.

In Figure 5.2, the flowchart of NetID and OptID is depicted where a specific optimization function is not employed because theoretically any optimization routine which allows setting parameter bounds would fit in OptID. One can decide on which optimization function to use according to the lower and upper bounds of the optimization parameters set by considering the performance of the trained network. An example illustrating this process is provided in one of the case studies later in this section.

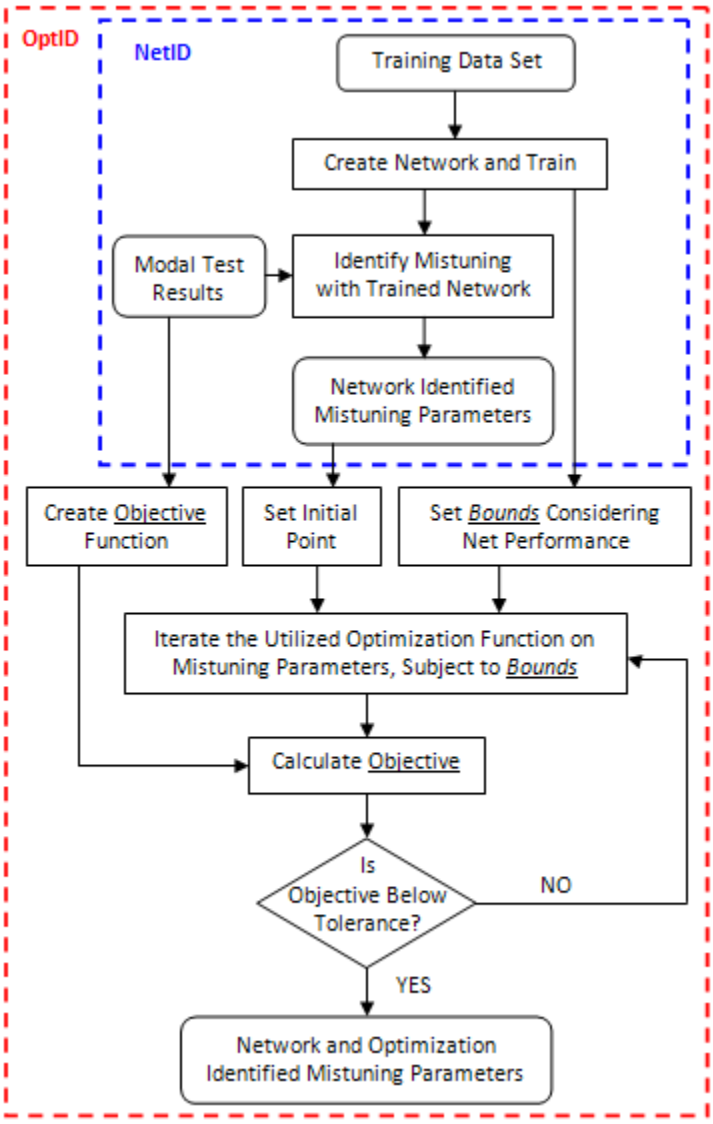

Figure 5.2 – Flowchart of NetID and OptID

It should be noted that there is no restriction which requires the actual results to lie within the lower and upper bounds selected. Several optimization routines can be applied in an iterative way where the gradient of the objective function is monitored. If although the objective function gradient reaches to a specified tolerance but the objective function tolerance

is not reached yet, then the next optimization routine shall start for which the lower and upper boundaries are set again according to the last step of the previous optimization routine.

5.3 Case Studies

Three case studies are presented herein to illustrate the efficiency, applicability and robustness of NetID and OptID for mistuning identification.

5.3.1 NetID – Standard Training

In this section the performance of NetID is demonstrated with a training procedure where a data set of noise free input-output pairs are used. A 12-bladed lumped parameter model constructed according to the model presented in section 3.1.2. The model is mistuned with a random set of numbers generated to fit a normal distribution with zero mean and 1.5% standard deviation on the first cantilever mode of each blade altering Δk values. A fleet of 15000 mistuned assemblies are formed accordingly and solved for the first 12 modes where only natural frequencies and blade tip mode shapes are recorded. The recorded mode vectors are used as the input vector set, and the mistuning parameter vectors are used as the output vector set according to (5.1).

A network is created according to Figure 5.1 with 12 neurons in the output layer and 24 neurons in the hidden layer. Afterwards, it is trained with the data set created as explained above.

The data set is divided between training, validation and test sets as 75%, 15%, 10% respectively. The validation set is used to monitor the network performance during the training iterations and to stop training accordingly. The test set is used to check the overall performance of the network when the training process is finished. The resulting linear regression between actual mistuning parameters and network outputs (identification values) are 0.945 for training set, 0.944 for validation set, and 0.942 for test set; which shows very high correlation on a 0 to 1 scale. In Figure 5.3, the mean squared error (MSE) progress during network epochs (iterations) is plotted.

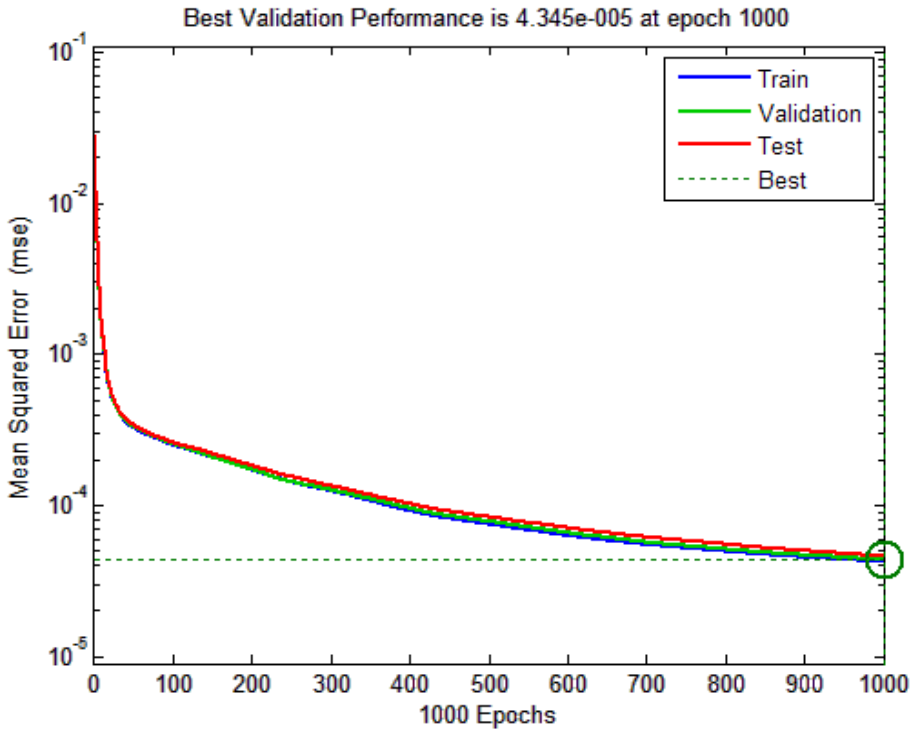

Figure 5.3 – Mean Square Error Progress

MSE is a way of quantifying the difference between estimation and the actual value which is being estimated. MSE is the second moment of error, which is defined as follows:

$$MSE = \frac{1}{n}\sum_{i=1}^{n} e_i^2, \tag{5.2}$$

where

$$\{e\} = \{x\}_{ACTUAL} - \{x\}_{IDENTIFIED}, \tag{5.3}$$

where $\{x\}_{ACTUAL}$ is the vector of actual mistuning parameters and $\{x\}_{IDENTIFIED}$ is the identified mistuning parameters written in a vector form. Note that, since the square of each of the elements in the error vector is utilized in (5.2), MSE accounts for both variance and bias of the error [80]. The best performance attained in this case study at epoch 1000, 4.345×10^{-5}, clearly shows that the network training process was successful.

A typical identification performed with the trained network results in the identified mistuning and mode shapes shown in Figure 5.4, and Figure 5.5 respectively. The trained network is first fed with a noise free natural frequency and mode shape vector and the resulting identification is recorded. Then the same natural frequency and mode shape vector is polluted with random noise having normal distribution with zero mean and 2.5% standard deviation for each element of the mode shapes.

The mode shapes are also compared via Modal Assurance Constant (MAC) which is a quantitative way of comparing two vectors of same length [81].

MAC takes a value between 0 and 1 where 1 denotes that the compared vectors are identical. Considering $\{U\}_A$ and $\{U\}_I$ as the actual and identified mode shape vectors, respectively, for a particular mode MAC value is calculated as follows:

$$MAC = \frac{\left|\{U\}_A^T \{U\}_I\right|^2}{\left(\{U\}_A^T \{U\}_A\right)\left(\{U\}_I^T \{U\}_I\right)}. \tag{5.4}$$

The MAC value comparison for this case study is given in Table 5.1. As clearly seen, NetID is able to identify the mistuning to an acceptable degree for both cases.

Table 5.1 – MAC Comparison for Mode Shapes

Mode No	MAC between Actual and Noise Free Identified Model	MAC between Actual and Noisy Identified Model
1	1.00	1.00
2	1.00	0.99
3	1.00	0.99
4	0.99	0.99
5	0.99	0.98
6	0.98	0.93
7	0.98	0.84
8	0.99	0.93
9	1.00	0.90
10	1.00	0.97
11	1.00	0.99
12	1.00	1.00

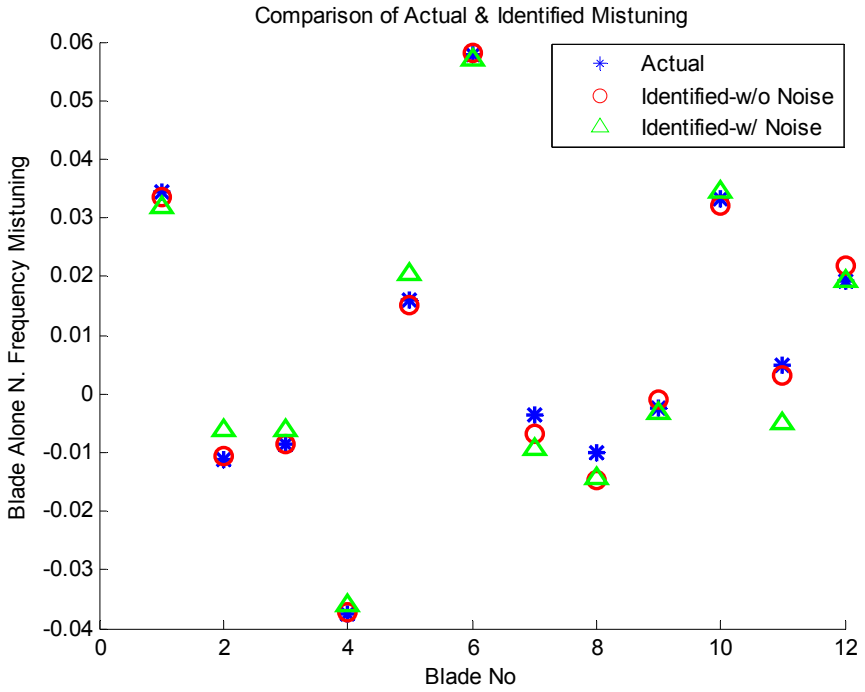

Figure 5.4 – Comparison of Actual and Identified Mistuning

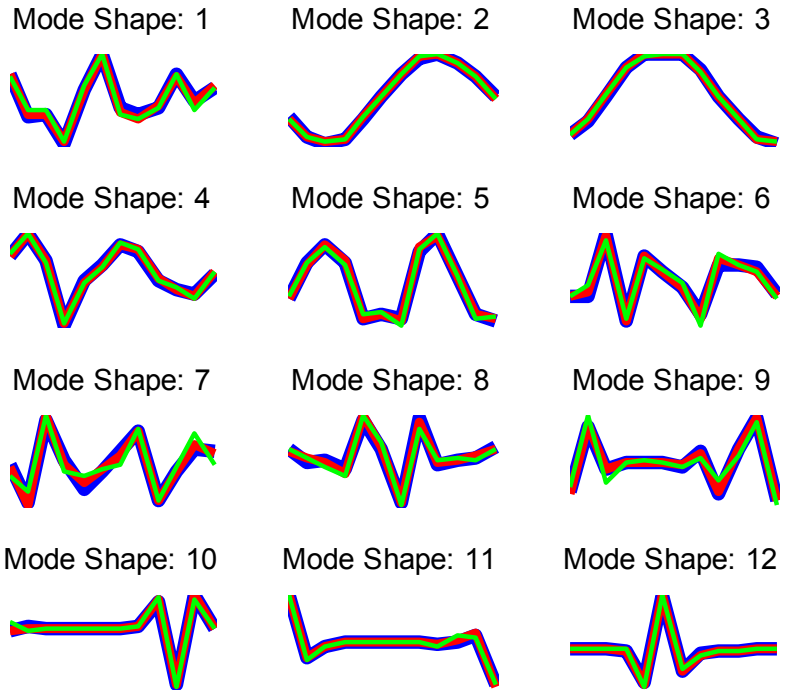

Figure 5.5 – Actual (▬), identified from noise free data (▬), identified from noisy data (▬) mode shapes

5.3.2 NetID – Injection Training

To increase the robustness of NetID with noisy inputs, a training methodology named 'Noise Injection' is applied in the training step. The input data of the network (which is the output of simulations as natural frequencies and mode shapes), is polluted with error but the corresponding network output (mistuning parameters) is not changed. With this procedure, a network formed again according to the same structure and neurons explained in section 5.3.1, is trained with input data polluted with random noise having normal distribution with zero mean and 2.5% standard deviation for each element of the mode shapes.

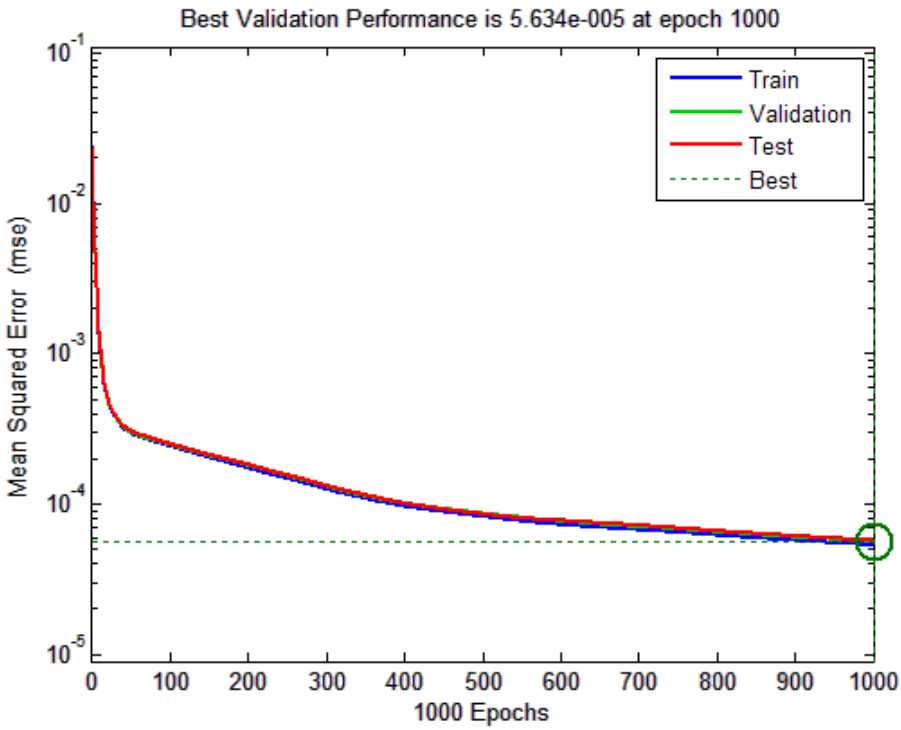

Figure 5.6 – Mean Square Error Progress

The resulting linear regression between actual mistuning parameters and network outputs are 0.931 for the training set, 0.926 for the validation set, and 0.927 for the test set; which again shows very high correlation on a 0 to 1 scale. In Figure 5.6, the MSE progress during network epochs is plotted. The best performance attained at epoch 1000, 5.634×10^{-5}. A comparison of the identification performance of the network trained with noise injected data (Network-INJ) and the network trained in section 5.3.1 (Network-STD) under noisy input data is done. Both of the networks are fed with a particular set of input vector which is polluted randomly having normal distribution with zero mean and 5% standard deviation. The resulting mistuning identification performance is as shown in Figure 5.7 and Figure 5.8. MAC value comparison for the mode shapes is given in Table 5.2.

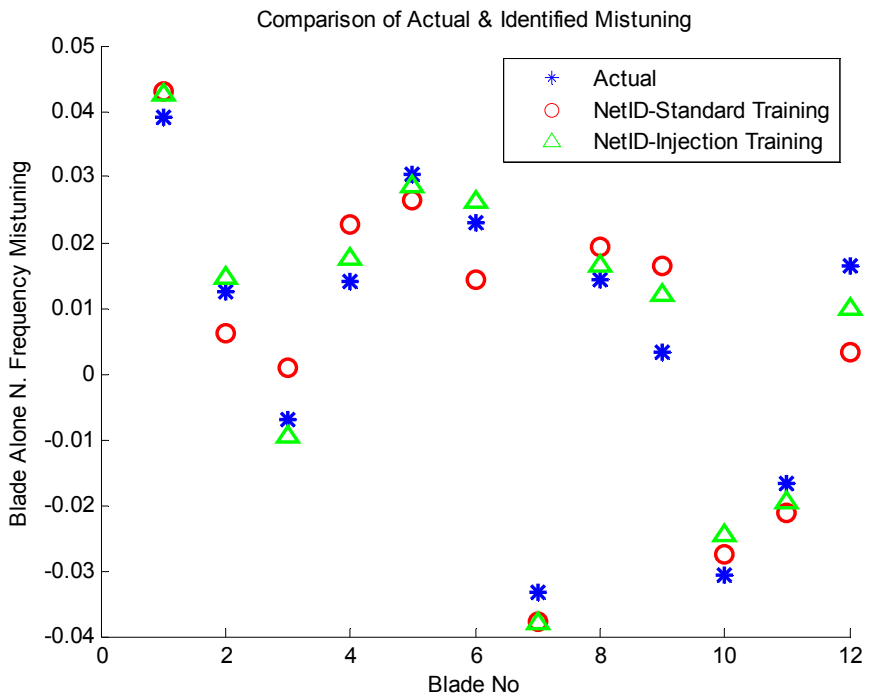

Figure 5.7 – Comparison of Actual and Identified Mistuning

Considering these results, NetID performs better if the training data is modified with noise injection under noisy input. Since we assume that the network input is coming from modal tests, it is very likely that mode shapes will be noisy to some extend even if the natural frequencies are more accurate. Moreover, the network created with Noise injection training is also tested with a noise free data set formed by simulating a fleet of 3000 disks with the same random parameters for mistuning, and the resulting regression between actual and identified values was 0.938, which also shows that for noise free data NetID performs equally well with both standard training and noise injection training.

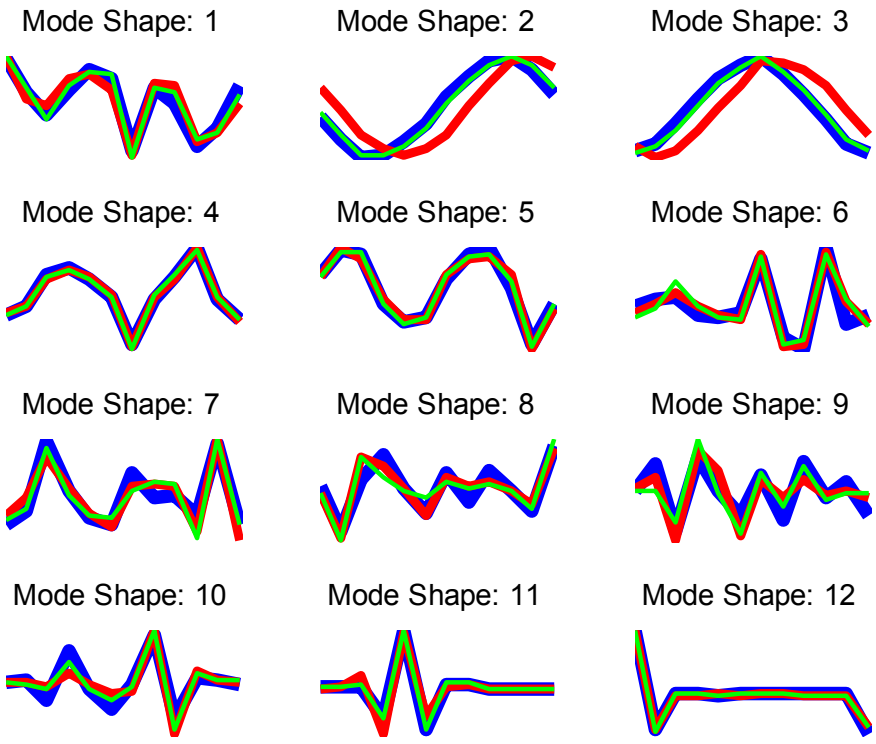

Figure 5.8 – Actual (▬), identified with Network-STD (▬), identified with Network-INJ (▬) mode shapes

Table 5.2 – MAC Comparison for Mode Shapes

Mode No	MAC between Actual and Identified Model (NetID-STD)	MAC between Actual and Identified Model (NetID-INJ)
1	1.00	1.00
2	0.59	0.99
3	0.59	0.99
4	0.98	0.99
5	0.96	0.99
6	0.89	0.86
7	0.86	0.87
8	0.85	0.75
9	0.68	0.69
10	0.79	0.92
11	0.91	1.00
12	0.99	0.99

5.3.3 OptID – Genetic Optimization

In this case study, to address a relatively more realistic problem, a 24 bladed blisk finite element model is created, a sector of which is given in Figure 5.9, and its ROM is structured according to the component mode synthesis presented in section 3.2. 10 modes for each blade and for each nodal diameter of the disk for the first mode-family are involved in the ROM. The resulting number of degrees of freedom is 658 in the ROM; whereas for the full finite element model it is 10368.

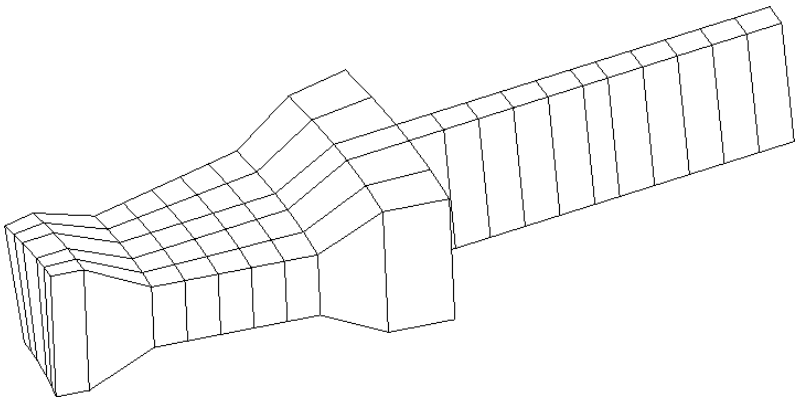

Figure 5.9 – Sector Mesh of the 24-bladed Blisk

Mistuning is applied through blade cantilever natural frequency perturbations, δ_n^k in section 3.2, and a fleet of 45000 disks are simulated with random mistuning using normal distribution with zero mean and 1.5% standard deviation. The simulation output was the first 24 natural frequencies and corresponding blade tip mode shapes. Only 23 modes are assumed to be measured in the test, resulting in a largely incomplete set of modes considering 658 degrees of freedom in the reduced order model.

First, a network created according to Figure 5.1, in which hidden layer and output layer consist of 24 neurons. The network is then trained over 1000 epochs with the dataset created, after polluting it by noise injection as explained in section 3.4. The dataset is divided between training, validation and test sets with 75%, 15% and 10% respectively. The resulting regression between identified and actual values for training, validation and test sets were 0.802, 0.794 and 0.787 which may be sufficient for many applications but is considered unsatisfactory for the scope of this work.

Afterwards, the neurons in the hidden layer are increased to 120 and the network is trained with the same data set again. The resulting regression for training, validation and test sets are 0.923, 0.905, and 0.908. Best validation MSE is 7.2793×10^{-5}, the progress of which through 1000 epochs is plotted in Figure 5.10. Error is calculated as the difference of actual and identified values of blade cantilever percentage mistuning from the 45000 simulated disks for each blade. The cumulative probability density function (CDF) of the absolute error, is given in Figure 5.11. As it is clearly seen, more than 90% of the blades have an error between actual and identified frequency percentage mistuning less than 1.25%. This value is used for setting the lower and upper bounds of the optimization process as -0.0125 and +0.0125 respectively. To illustrate, for a disk, for which the actual values are calculated with the full scale finite element model, network identification and the set bounds are plotted in Figure 5.12.

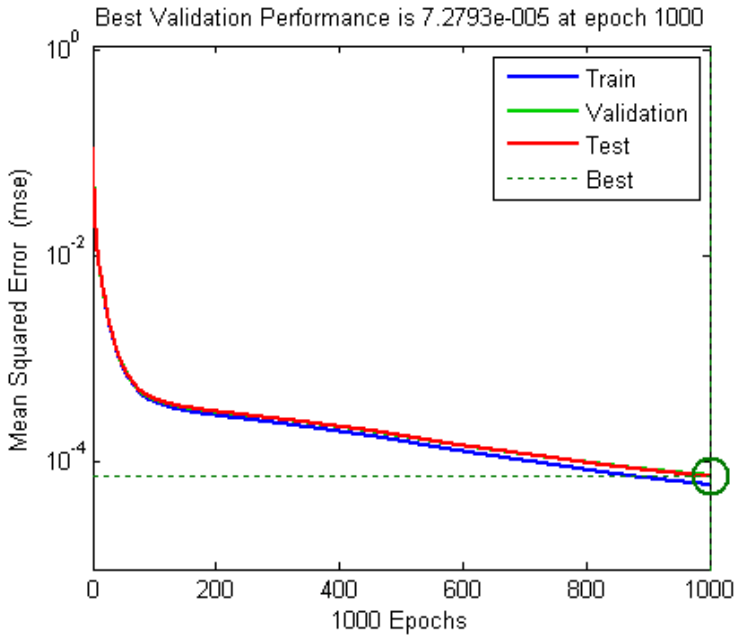

Figure 5.10 – Mean Square Error Progress

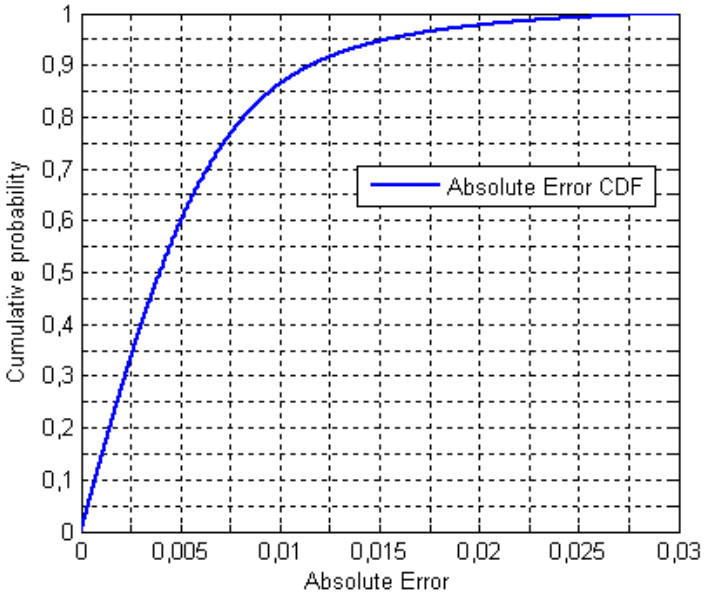

Figure 5.11 – CDF of Absolute Error

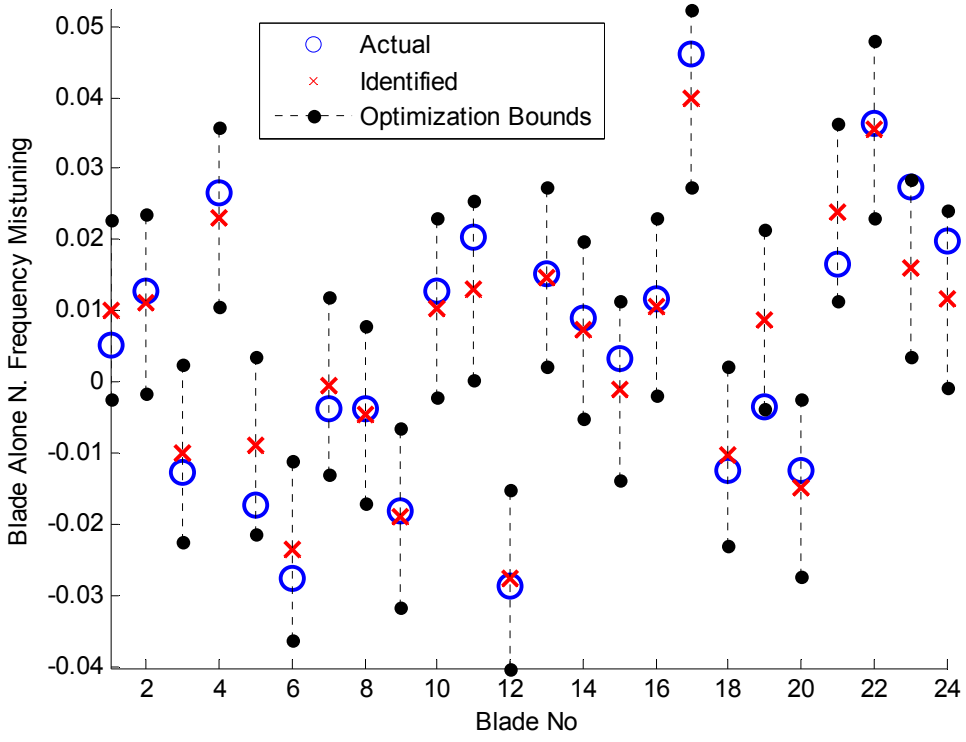

Figure 5.12 – Actual and network identified mistuning with optimization bounds

Since the selected lower and upper bounds are not quite narrow, in the optimization routine multi objective genetic algorithm is used. As the objective functions, MSE on each of the mode shapes are utilized. Multiobjective genetic algorithm is programmed according to the parameters given in Table 5.3, via MATLAB's optimization toolbox.

Neither the terminology of genetic algorithms nor the selection of these parameters is included here since it is out of the scope of this work. However, interested readers are referred to the works of Fonseca et al. [82-83] and the Optimization Toolbox User's Guide of MATLAB [84] for further information about multiobjective optimization, genetic algorithms, related terminology and parameter selection.

Table 5.3 – Genetic Optimization Parameters

Population Size	480
Tournament Size	20
Crossover Function	0.85
Mutation Function	Adaptive feasible
Crossover Function	Random
Migration Direction	Forward
Migration Fraction	0.15
Migration Interval	15
Pareto Front Pop. Fraction	0.3

The optimization routine is run starting from the initial point set by the network identification subject to upper and lower bounds presented in Figure 5.12, with the above specified parameters. After around 7000 iterations the relative error tolerance is reached. The resulting natural frequency mistuning percentages identified are given in Figure 5.13, with the corresponding mode shapes in Figure 5.14. Mode shapes are compared with Modal Assurance Constant (MAC) in Table 5.4.

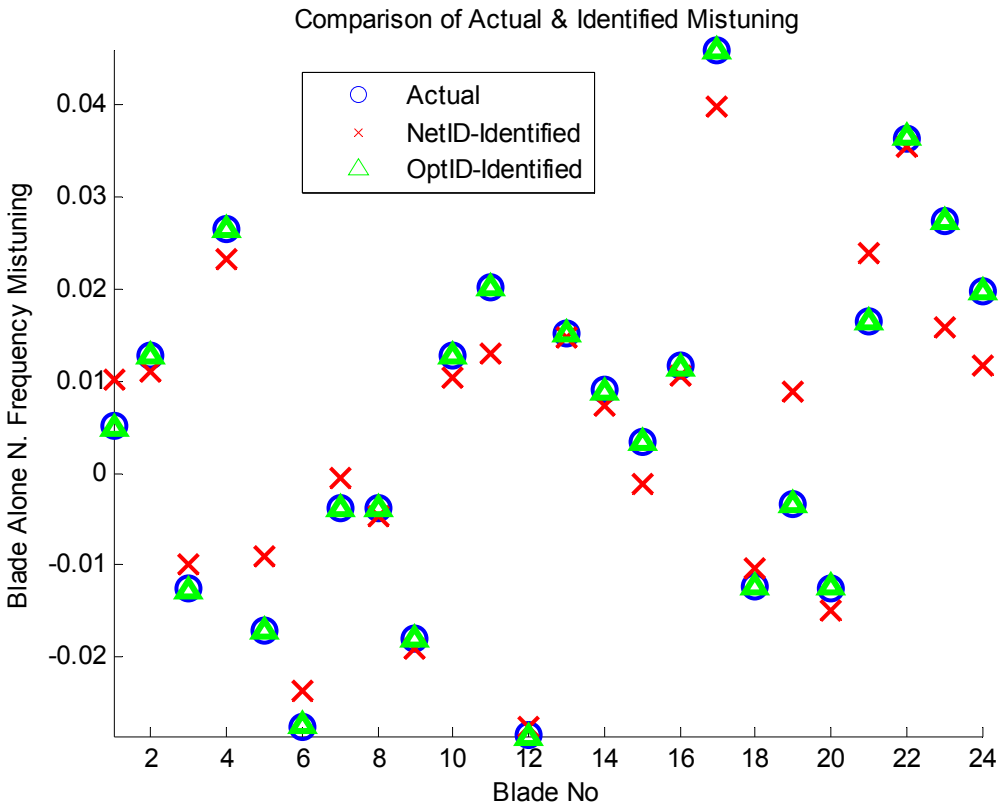

Figure 5.13 – Comparison of NetID and OptID Identification

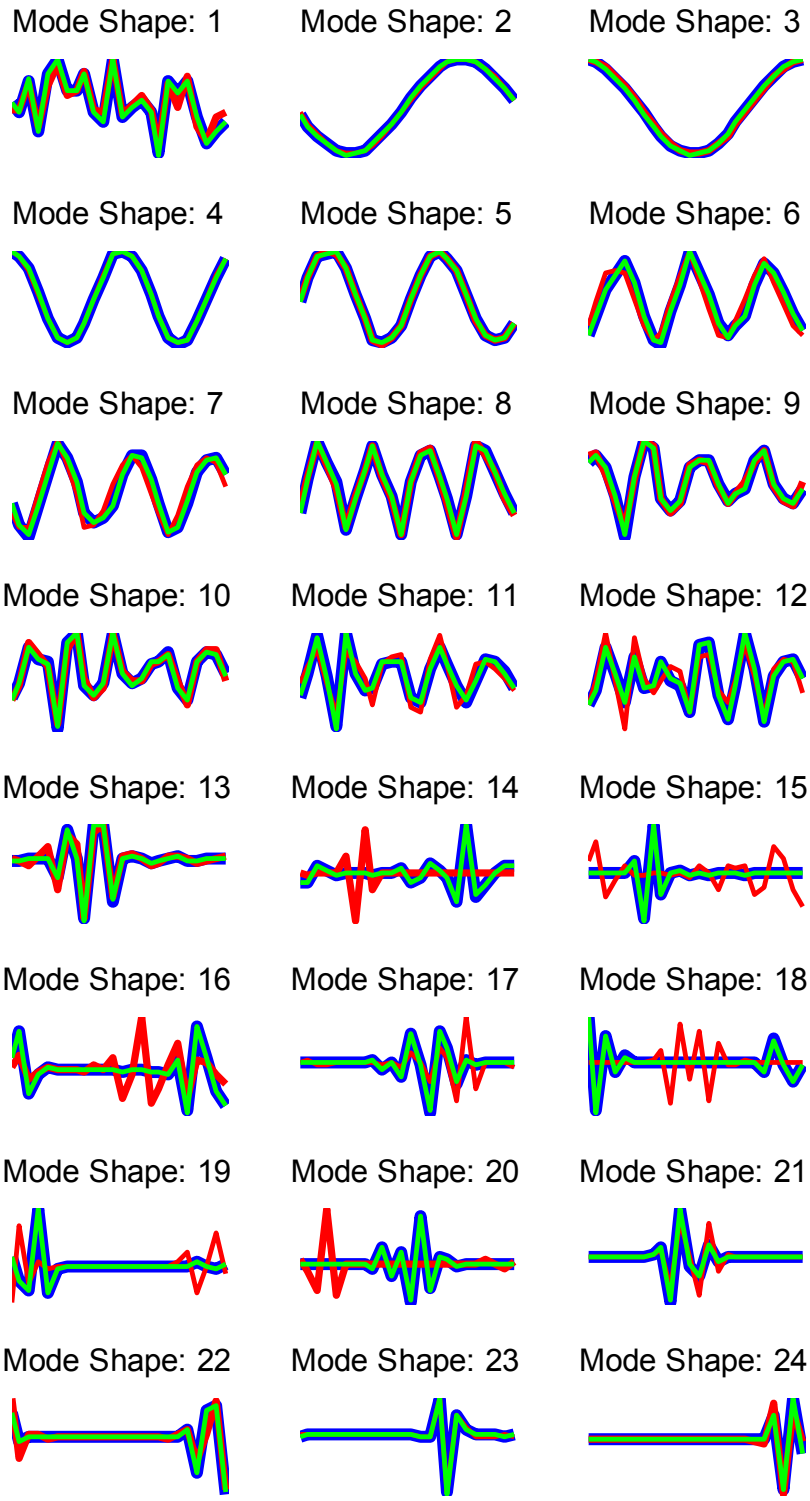

Figure 5.14 – Actual (▬), identified with NetID (▬), identified with OptID (▬) mode shapes

Table 5.4 – MAC Comparison for Mode Shapes

Mode No	MAC between Actual and NetID-Identified	MAC between Actual and OptID-Identified
1	1.00	1.00
2	0.99	1.00
3	0.99	1.00
4	1.00	1.00
5	1.00	1.00
6	0.86	1.00
7	0.86	1.00
8	0.98	1.00
9	0.97	1.00
10	0.96	0.99
11	0.75	0.99
12	0.77	0.99
13	0.93	0.99
14	0.00	0.99
15	0.01	0.99
16	0.21	1.00
17	0.28	0.99
18	0.00	1.00
19	0.01	1.00
20	0.00	0.99
21	0.74	1.00
22	0.83	1.00
23	1.00	1.00
24	0.90	1.00

The results of this case study show that OptID is very effective in identifying mistuning of a realistic blisk design for which only incomplete and noisy data is available from assembly modal tests.

5.4 OptID – Application to Model Updating Problems

In this section, the capability of OptID is explored in the area of model updating. For this purpose, real test data taken from a benchmark structure designed to simulate the dynamics of an aircraft structure, namely GARTEUR SM-AG 19, is used. For the test bed employed in this study (Figure 5.15); the wing-fuselage, fuselage-vertical stabilizer and vertical stabilizer-horizontal stabilizer are joined by welding, instead of bolts which are used in the original GARTEUR model [85-87]. The test data taken from this test-bed has also been used by Kozak et al. [88].

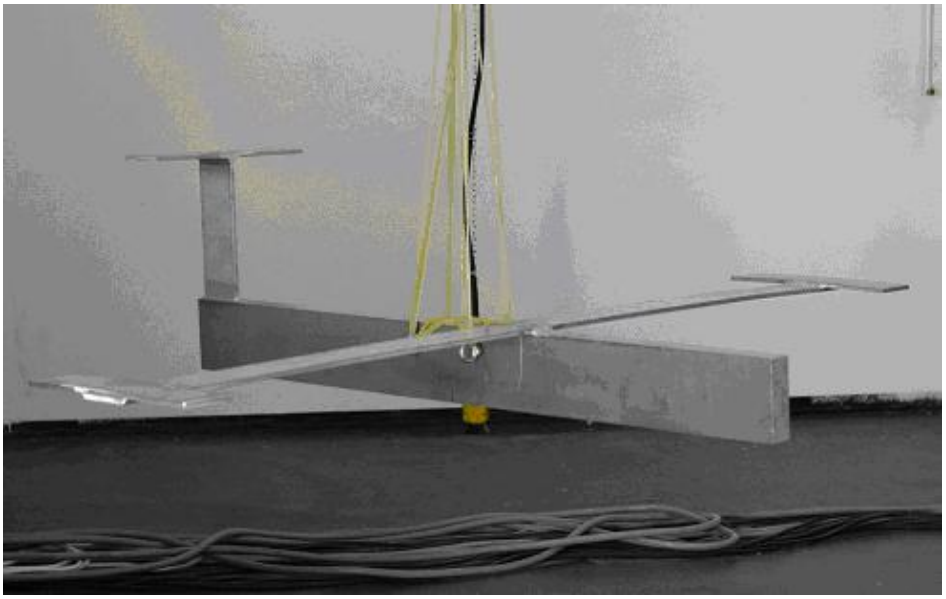

Figure 5.15 – GARTEUR Test Bed

The modal tests were conducted by using accelerometers, a modal hammer and a modal sledge hammer. A total of 12 accelerometers, 36 impact points and 66 impact degrees of freedom were used throughout the tests.

A Finite Element (FE) model, which is shown in Figure 5.16, is constructed by using 6-DOF beam, 2-DOF spring and rigid elements. To overcome the discontinuities in the mating junctions of the model, which is caused by the differences in the positions of the neutral axes of the beam elements, rigid multi point constraints (MPC) are used. The first 10 natural frequencies of this initial FE model and the experimental results are given in Table 5.5.

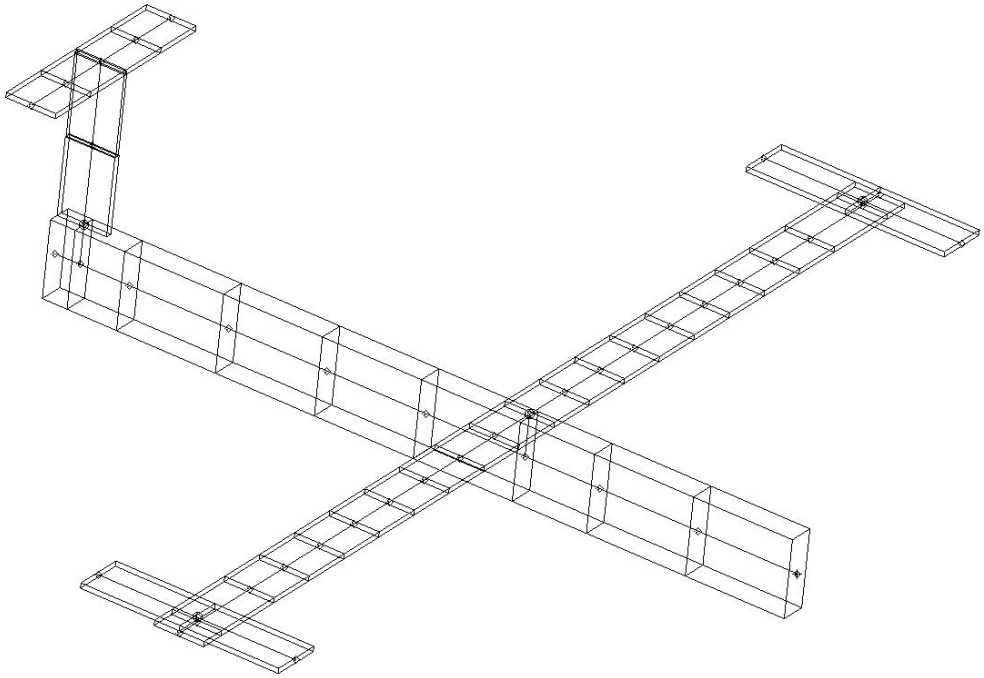

Figure 5.16 – GARTEUR Beam Model

Table 5.5 – Natural Frequencies from Test and Initial FE Model

Test Mode No	Test Nat. Freq. (Hz)	Initial FEM Mode No	Initial FEM Nat. Freq. (Hz)	Error in Natural Frequency (%)
1	5.65	1	5.66	0.2
2	15.73	2	16.52	5.0
3	36.79	5	37.02	0.6
4	37.51	3	30.82	-17.8
5	37.65	4	30.91	-17.9
6	43.73	6	43.21	-1.2
7	50.32	7	50.25	-0.1
8	55.00	8	54.68	-0.6
9	60.66	10	72.41	19.4
10	68.23	9	63.97	-6.2

As it is clear from Table 5.5, 4^{th}, 5^{th}, 9^{th}, and 10^{th} modes are most poorly represented ones by the initial FE model. An investigation of the test mode shapes reveal that 4^{th} and 5^{th} modes are dominated by the torsional movement of the wings, where as 9^{th} and 10^{th} are controlled by the torsional and bending movements of the vertical stabilizer. As a result, to achieve a minimum parameter updating model, 4 parameters are selected. The thicknesses of the two elements which model the vertical stabilizer, a torsional stiffness (modeling two torsional springs each between the fuselage-wing joint and a wing end), and another torsional stiffness which models a torsional spring placed between the fuselage-vertical stabilizer joint and vertical stabilizer-horizontal stabilizer joint.

A data set of 20000 samples is generated where the 4 updating parameters are modeled with random numbers taken from 4 different uniform random distributions. First two distributions, used for the thickness parameters, have minimum and maximum bounds as 5 mm and 20 mm. Bounds of the third distribution corresponding to the vertical stabilizer are 50 Nm/rad and 4000 Nm/rad. The last distribution which is used for the torsional stiffness of wings has bounds of 50 Nm/rad and 2000 Nm/rad. Samples of the data set is solved for modal response and the recorded mode shape vectors (corresponding to test DOFs) and natural frequencies of the modes corresponding to the ones in the test results are used as the input vector set for the network, where the updating parameter vectors are used as the output vector set according to (5.1).

A network is created according to Figure 5.1 with 4 neurons (Corresponding to the updating parameters) in the output layer and 76 neurons in the hidden layer. Afterwards, it is trained with the data set created as explained above but the input vectors are polluted with random noise picked from a pool of uniform random distribution with bounds -5% and 5%. The data set is divided between training, validation and test sets as 75%, 15%, 10% respectively.

The resulting linear regression between actual updating parameters and network outputs are 0.931 for training set, 0.932 for validation set, and 0.928 for test set; which shows very high correlation on a 0 to 1 scale. The network is then used to update the initial FE model with real test data. A second updating starting with the network updated FE model is performed with genetic optimization where the parameters are set according to Table

5.3. The boundaries are not limited in the optimization problem. After 1652 iterations the relative error tolerance is reached and the optimization is stopped. The resulting natural frequencies are given in Table 5.6, with the corresponding mode shapes in Figure 5.17.

Note that the order of the modes is corrected and the error associated is reduced remarkably compared to the initial FE model. Moreover the mode shapes are consistent with the test results.

Table 5.6 – Natural Frequencies from Test and Final Updated FE Model

Test Mode No	Test Nat. Freq. (Hz)	Final FEM Mode No	Final FEM Nat. Freq. (Hz)	Error in Natural Frequency (%)
1	5.65	1	5.66	0.2
2	15.73	2	16.86	7.2
3	36.79	3	36.43	-0.9
4	37.51	4	37.57	0.2
5	37.65	5	37.65	0
6	43.73	6	43.22	-1.2
7	50.32	7	49.81	-1.0
8	55.00	8	54.71	-0.5
9	60.66	9	60.96	0.5
10	68.23	10	68.30	0.1

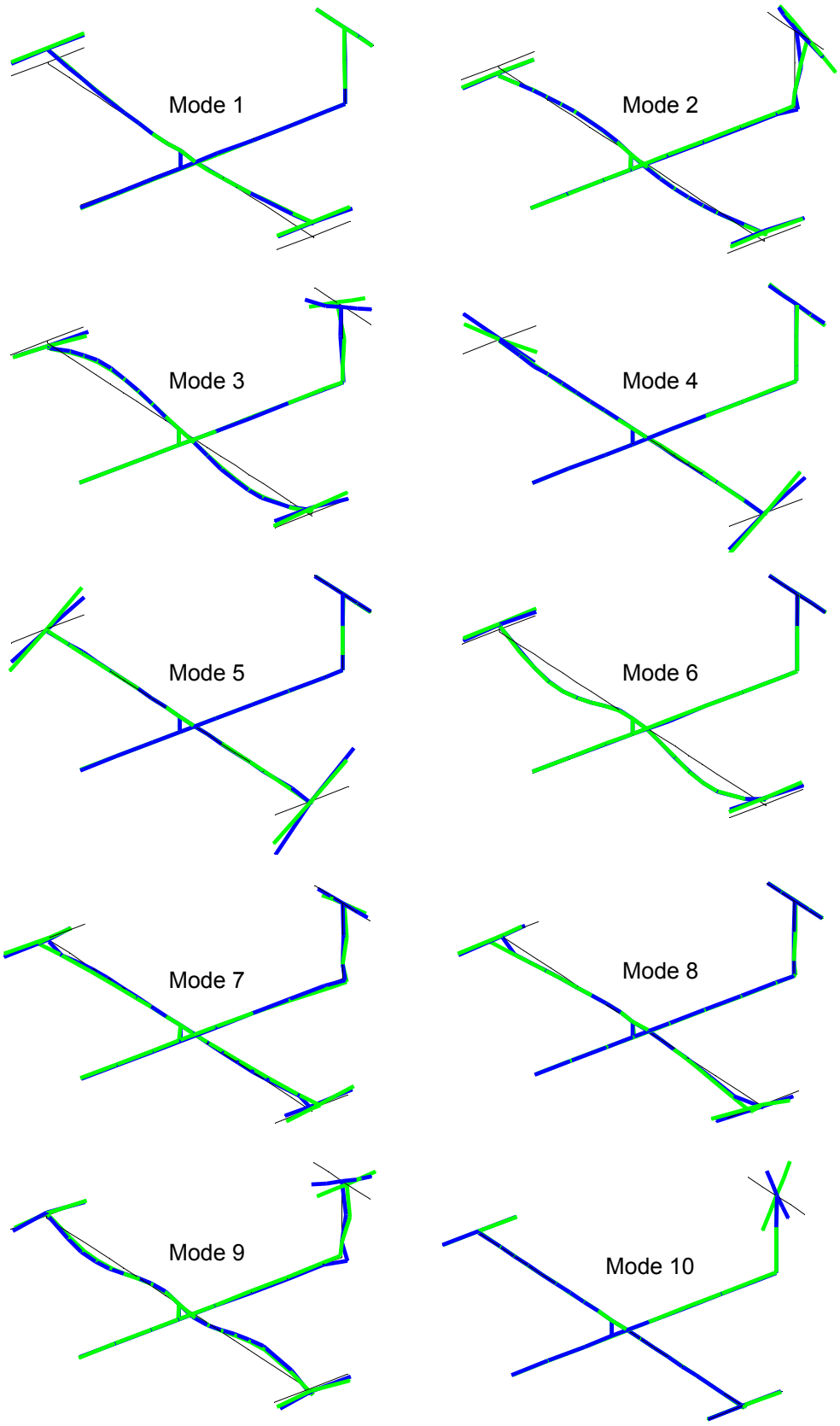

Figure 5.17 – Test (▬), and Updated FE Model (▬) Mode Shapes

Finally, to quantitatively analyze the improvement from the initial FE model to the network updated FE model and from the network updated FE model to the optimization updated (final) FE model, error on the natural frequencies of the first 10 modes are plotted in Figure 5.18.

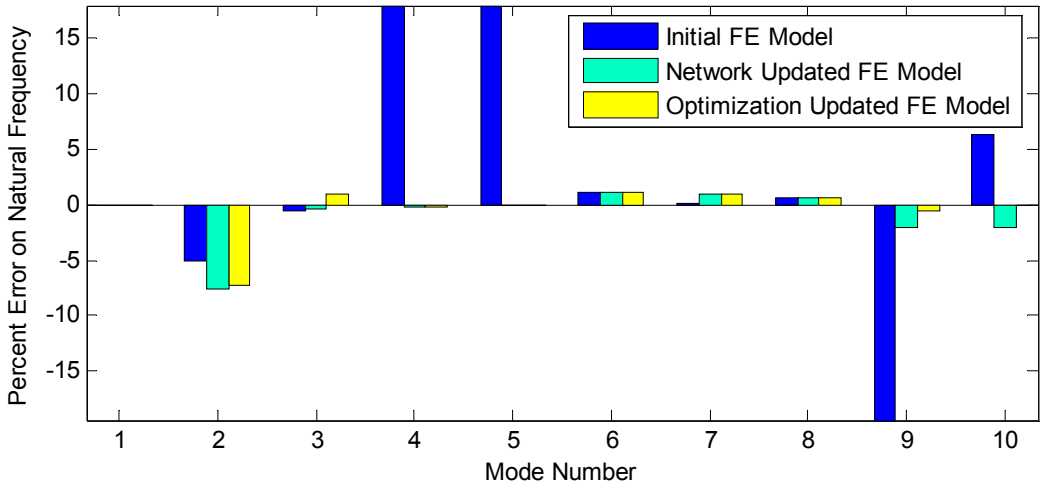

Figure 5.18 – Percent Error on Natural Frequencies

5.5 Non-linearity Classification and Identification with Neural Nets

Modeling non-linearities such as dry friction, cubic stiffness, and gap-interface in structural dynamics is generally a cumbersome and fictitious process if it is not accompanied with identification of real test data. Because, it is the micro-level surface and/or interface conditions which drive the dry friction contact conditions and without test data, having a

well representative non-linear model is not easy. Likewise, materials modeled with cubic stiffness should be tested for accurate modeling.

In some certain cases, even the non-linearity type associated with a structure is not obvious and moreover, the exact location of the non-linearity within the structure can be undetermined.

In this section, a new approach which employs neural networks and optimization algorithms to locate, classify and parametrically identify any non-linearity in a given structure via means of dynamic response of the structure is enclosed.

5.5.1 The Approach

In this study, two different types of neural networks are used in a sequence. The first one is a parametric identification configuration constructed according to the network introduced in section 5.1.1. The second one is a classification network formed by modifying the first such that rather than a linear function, tangent function is used in the output layer. As an optional third step, to improve the performance of the method in complex systems, optimization routine can be used. This procedure is explained schematically in Figure 5.19.

Note that, any optimization algorithm is applicable with the method sketched by the flowchart given in Figure 5.19.

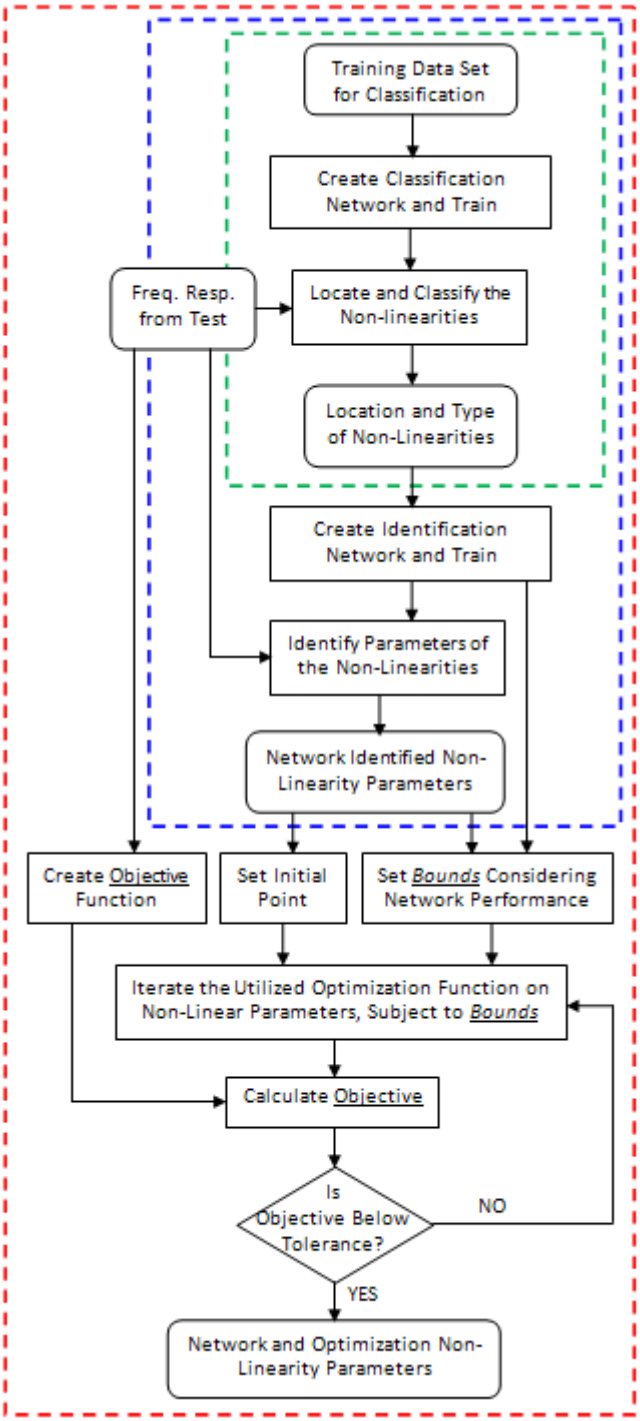

Figure 5.19 – Flowchart of Non-Linear Classification (_ _) and Identification with Neural Networks (_ _) and Improvement with Optimization Algorithms (_ _)

5.5.2 Case Studies

Two case studies are presented here to demonstrate the approach presented in section 5.5.1. Throughout the case studies, two different non-linearities are considered; macro-slip dry friction and cubic stiffness.

Assuming a sinusoidal displacement expression as follows:

$$x(\theta) = X\cos(\theta) \tag{5.5}$$

Then, for a macroslip friction element, the force-displacement relationship is shown in Figure 5.20, where k_x is the tangential contact stiffness, X is the response amplitude and F_{max} is the maximum friction force that can occur.

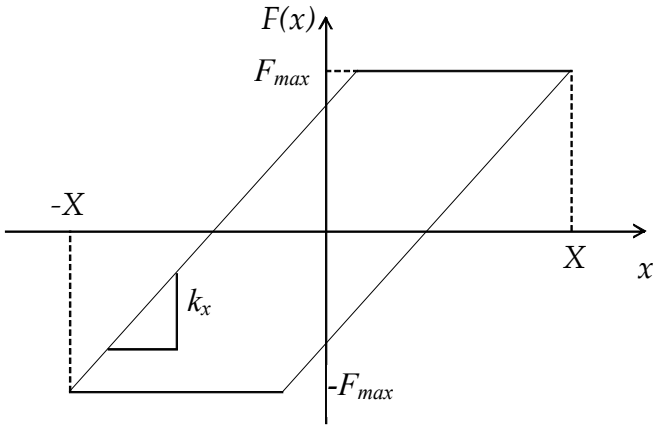

Figure 5.20 – Macro-slip Friction Model

The force expression for this macro-slip friction element is then written as follows:

$$F_{fr}(\theta)=\begin{cases} k_x X\cos(\theta)+F_{\max}-k_x X & (0\le\theta<\alpha) \\ -F_{\max} & (\alpha\le\theta<\pi) \\ k_x X\cos(\theta)-F_{\max}+k_x X & (\pi\le\theta<\pi+\alpha) \\ F_{\max} & (\pi+\alpha\le\theta<2\pi) \end{cases} \tag{5.6}$$

where

$$\alpha=\arccos\left(\frac{X-2(F_{\max}/k)}{X}\right) \tag{5.7}$$

$$F_{\max}=\mu\cdot n_0 \tag{5.8}$$

In (5.8), μ is the friction coefficient and n_0 is the normal force between the contacting surfaces.

To model the cubic stiffness element, which creates a force proportional to its extension to the third power, following force expression can be employed:

$$F_{cs}=k_c x^3 \tag{5.9}$$

where k_c is the coefficient of cubic stiffness and x is the extension of the cubic stiffness element.

Since it is not in the scope of this work, for harmonic inputs, Fourier representations of these non-linearities, namely macro-slip friction and cubic stiffness, can be found in Orbay [78].

5.5.2.1 Case Study I – SDOF Non-Linear System

In this case study, a single degree of freedom system with an unknown non-linearity is identified. First, a classification network is trained to determine the type of the non-linearity, where two possible types are implemented: macro-slip dry friction and cubic stiffness (Figure 5.21), which are modeled with the formulations given before in this section. In Figure 5.21, h, k, m and k_c are the structural damping, stiffness, mass, and cubic stiffness constants respectively. It is assumed that the normal force parameter of the macro-slip friction element and stiffness constant of the cubic stiffness element are the selected unknowns.

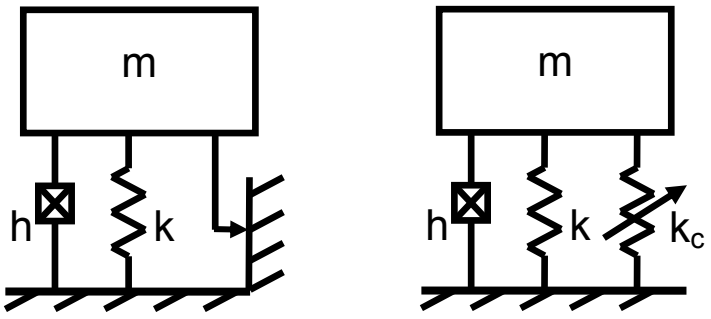

Figure 5.21 – SDOF Non-Linear System: Macro-Slip Configuration (Left), Cubic Stiffness Configuration (Right)

To detect the type of the non-linearity associated with the SDOF system, a classification network formed according section 5.5.1, in which the hidden and output layers are constructed by 41 and 2 neurons respectively. Network input is the frequency response of the system under a constant amplitude force formed as a vector corresponding to a predefined frequency interval. On the other side, the output is a vector of two binary variables where $\{1, 0\}^T$ represents a cubic-stiffness non-linearity and $\{0, 1\}^T$ represents a macro-slip friction non-linearity.

In the training step, a set of 2000 samples are used, half of which is constituted by systems with cubic-stiffness and the other half being systems with macro-slip friction element (Figure 5.22). 70% of the samples are used for training, 15% used for validation and the rest are used for testing. Figure 5.23 presents the confusion matrix after 9 iterations, which clearly shows that classification performance of the network is 100%.

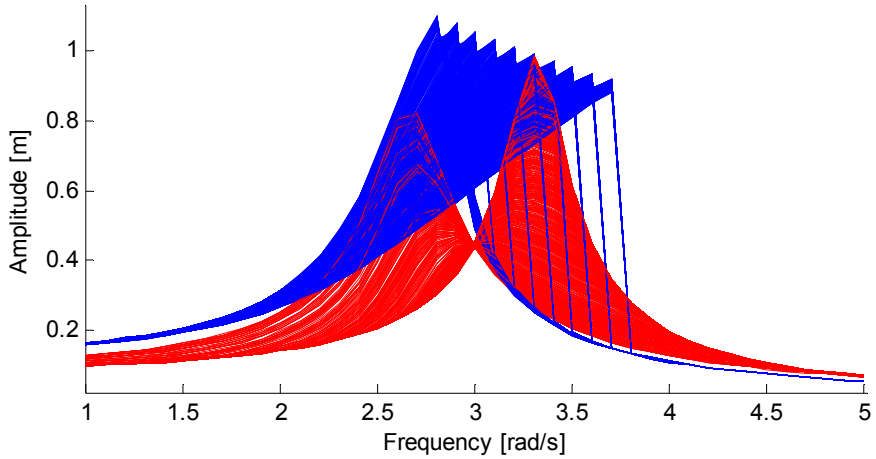

Figure 5.22 – Cubic Stiffness (▬), and Macro-Slip (▬) Training Samples

Figure 5.23 – Classification Network Confusion Matrices

Afterwards, two different identification networks are created according to section 5.1.1, in both of which the hidden and output layers are formed by 41 and 1 neurons respectively. One of the networks is trained to identify cubic stiffness systems, so the input vector set is composed of the 1000 samples (Figure 5.22) corresponding to the cubic stiffness non-linear systems and the output is the stiffness constant. The other network is trained to identify macro-slip systems, so the input vector set is composed of the 1000 samples (Figure 5.22) corresponding to the macro-slip non-linear systems and the output is the normal force.

For both of the identification networks, training, validation and test set regressions between actual parameter value and network output are 1, which imply that the networks are able to identify unknown cubic stiffness constant or macro-slip normal force, which are the assumed unknowns. Typical re-constructed forced responses of cubic stiffness and macro-slip systems identified with the proposed methodology is given in Figure 5.24.

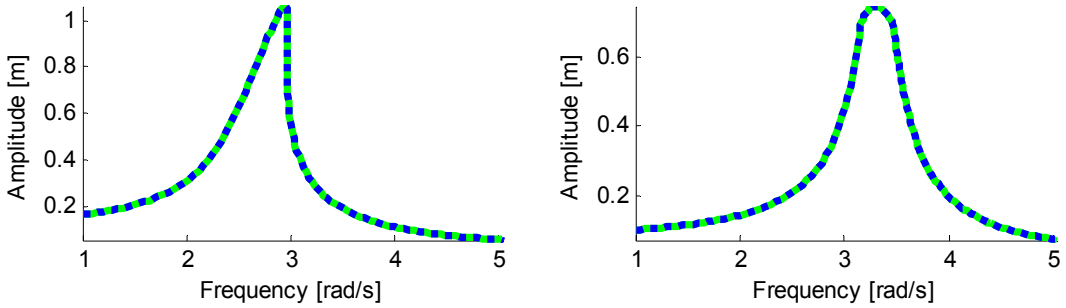

Figure 5.24 – Actual (——), and Identified (. . . .) Cubic Stiffness (Left), and Macro-Slip (Right) System Response

5.5.2.2 Case Study II – MDOF Non-Linear System

In this case study, it is aimed to demonstrate the capabilities of the proposed system which can be listed as; the ability to locate non-linear degrees of freedom, classify the non-linearity found, and identify the parameters associated with it in a multi degree of freedom system. The most remarkable feature of the proposed method, which is the ability of determining non-linearities in a system without taking measurements from the non-linear degrees of freedom, is also exhibited herein.

The system used here for non-linear identification purposes is a 3 degree of freedom oscillatory mass-spring system. It is known that the first degree of freedom does not have any non-linearity associated with it. However, there is no information about the linearity state of the second and third degrees of freedom (Figure 5.25).

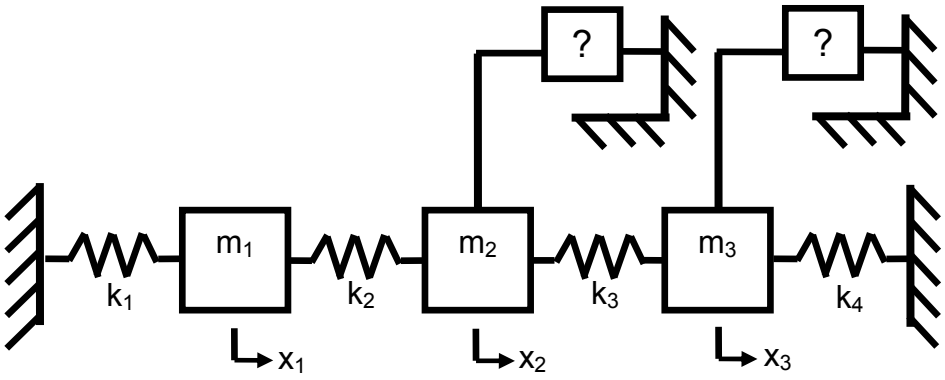

Figure 5.25 – 3-DOF Non-Linear System Schematic View

It is assumed that each one of second and third degrees of freedom either does not have a non-linear element associated with it, or there is friction or cubic stiffness non-linearity related to that degree of freedom. In such a setting, there will be 8 possible system configurations as given in Table 5.7 with their corresponding classification network outputs. The fully linear case is not included in the identification process since its determination is easier via applying several different amplitude forcing vectors.

Table 5.7 – Possible 3-DOF System Configurations and Corresponding Classification Network Outputs

Conf. No	D.O.F. 2	D.O.F. 3	Binary Network Output
1	Cubic Stiff.	Linear	$\{1, 0, 0, 0, 0, 0, 0, 0\}^T$
2	Linear	Cubic Stiff.	$\{0, 1, 0, 0, 0, 0, 0, 0\}^T$
3	Macro-Slip	Linear	$\{0, 0, 1, 0, 0, 0, 0, 0\}^T$
4	Linear	Macro-Slip	$\{0, 0, 0, 1, 0, 0, 0, 0\}^T$
5	Cubic Stiff.	Cubic Stiff.	$\{0, 0, 0, 0, 1, 0, 0, 0\}^T$
6	Macro-Slip	Macro-Slip	$\{0, 0, 0, 0, 0, 1, 0, 0\}^T$
7	Cubic Stiff.	Macro-Slip	$\{0, 0, 0, 0, 0, 0, 1, 0\}^T$
8	Macro-Slip	Cubic Stiff.	$\{0, 0, 0, 0, 0, 0, 0, 1\}^T$

A classification network, whose output and hidden layer are constructed by 8 and 142 neurons respectively. The output of the network is a binary vector of 8 elements which yields the 8 possible configurations given in Table 5.7. Data sets with around 1500 samples corresponding to each of the configurations are created where the stiffness constant and normal force is considered as unknowns. Stiffness constant sets are created by a uniform random distribution with minimum and maximum bounds of 100 N/m and 30000 N/m. Normal force sets are created by a uniform random distribution with bounds of 1 N and 40 N. The input vector of the network is constructed as the frequency response of the 1st degree of freedom under constant amplitude loading applied to the 1st degree of freedom only, in a pre-defined frequency range. This means that, no measurements taken from the "possible" non-linear degrees of freedom are used in the classification and identification process.

The eight data sets created in this manner are then used together to train the classification network in which 70% of the samples are separated for training, 15% for validation and the rest for testing the network. Figure 5.26 presents the confusion matrix after 72 iterations, which clearly shows that classification performance of the network is 100%. This concludes that the trained network is capable of locating and classifying any non-linearity in the system under consideration without using measurements taken from the non-linear degrees of freedom.

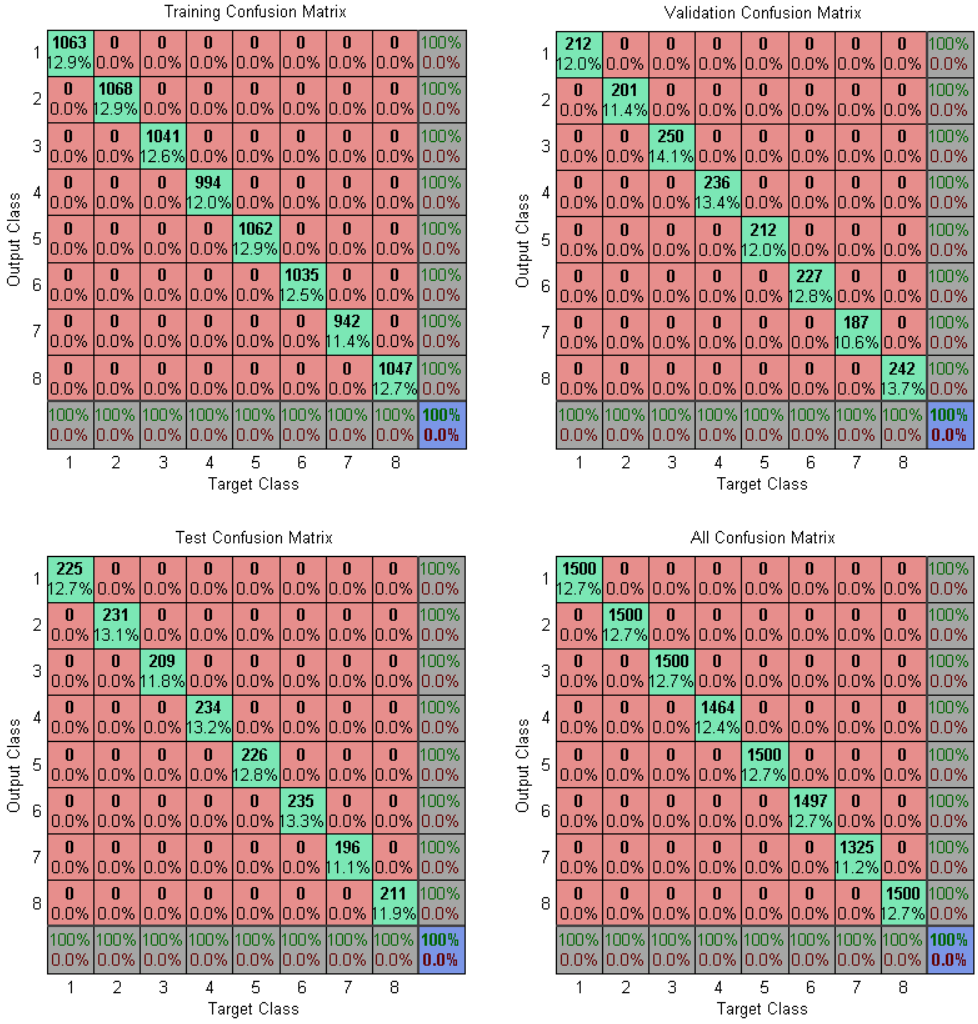

Figure 5.26 – Classification Network Confusion Matrices

Afterwards, eight different identification networks are created according to section 5.1.1, in four of which the hidden and output layers are formed by 142 and 1 neurons respectively since these networks are used to identify the unknown parameter associated with the first four configurations given in Table 5.7. The other four networks are created with 2 neurons in the output layer each corresponding to the unknown parameter associated with 2nd or 3rd degree of freedom's non-linearity since these networks are used to identify the unknown parameters associated with last four configurations given in Table 5.7. Then, the constructed networks are trained with their corresponding data set created beforehand for the classification network, considering its configuration (Table 5.7).

For the six of the identification networks (which correspond to the first six configurations), training, validation and test set regressions between actual value and network output are 1, which imply that the networks are able to identify unknown cubic stiffness constant and/or macro-slip normal force exactly. However, the regression between actual parameter value and network output for the 7th and 8th networks are as given in Table 5.8.

Table 5.8 – Regression between Actual Parameter Value and Network Output for 7th and 8th Configurations

	Training Set	**Validation Set**	**Test Set**
Configuration 7	0.917	0.912	0.920
Configuration 8	0.951	0.949	0.948

Considering the network performances for the 7th and 8th networks, optimization identification is formulated according to Figure 5.19 with a genetic algorithm. To demonstrate the capabilities, only the results for the 7th configuration, whose network performance is lower from the 8th, are presented here.

Bounds of the two unknown parameters, namely stiffness constant of the cubic stiffness element connected to the second degree of freedom and the normal force of the macro-slip element connected to the third degree of freedom are determined from the cumulative distributions of corresponding absolute errors resulting from the network outputs (Figure 5.27 and Figure 5.28).

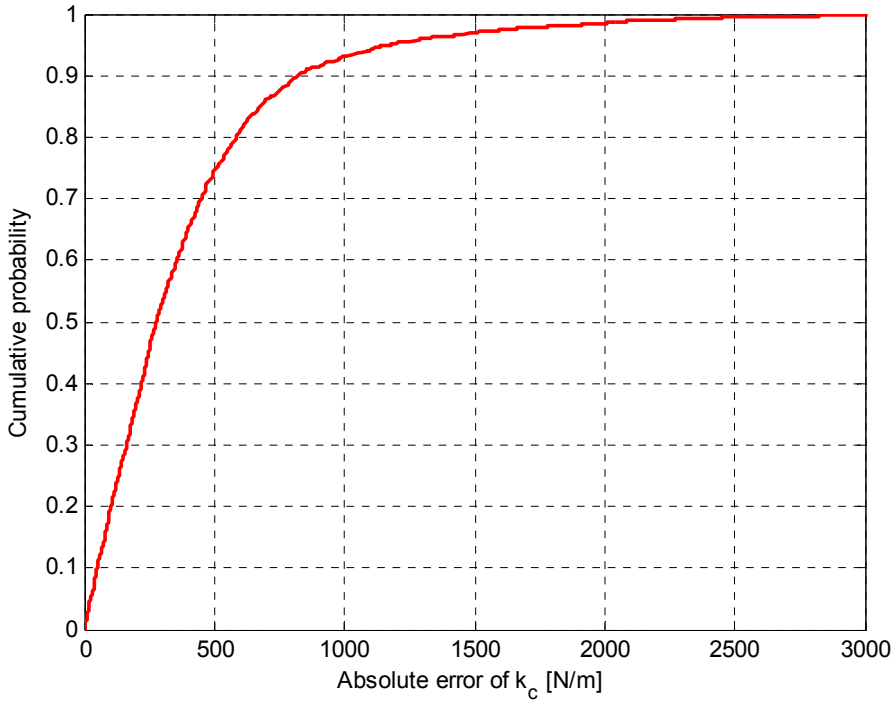

Figure 5.27 – Absolute Error Cumulative Probability of k_c

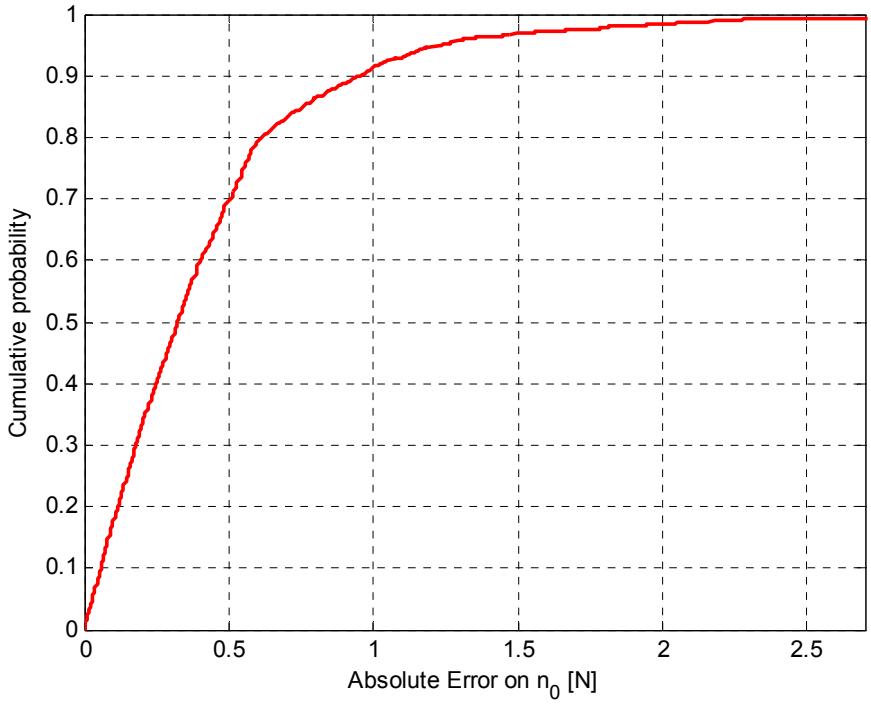

Figure 5.28 – Absolute Error Cumulative Probability of n_0

For retaining at least a 90% probability to have the actual solution within the optimization bounds, kc is limited to ± 1000 N/m and n0 is limited to ± 1 N. The initial point of the optimization routine is set to the network identified parameters, and after 120 runs the optimization is stopped because of the fulfillment relative error tolerance. The frequency response of the optimization identified system together with the network identified and actual systems is given in Figure 5.29 for the 1st degree of freedom. From this result, it is concluded that the proposed approach successfully identifies the parameters of the non-linearities, which are also located and classified beforehand.

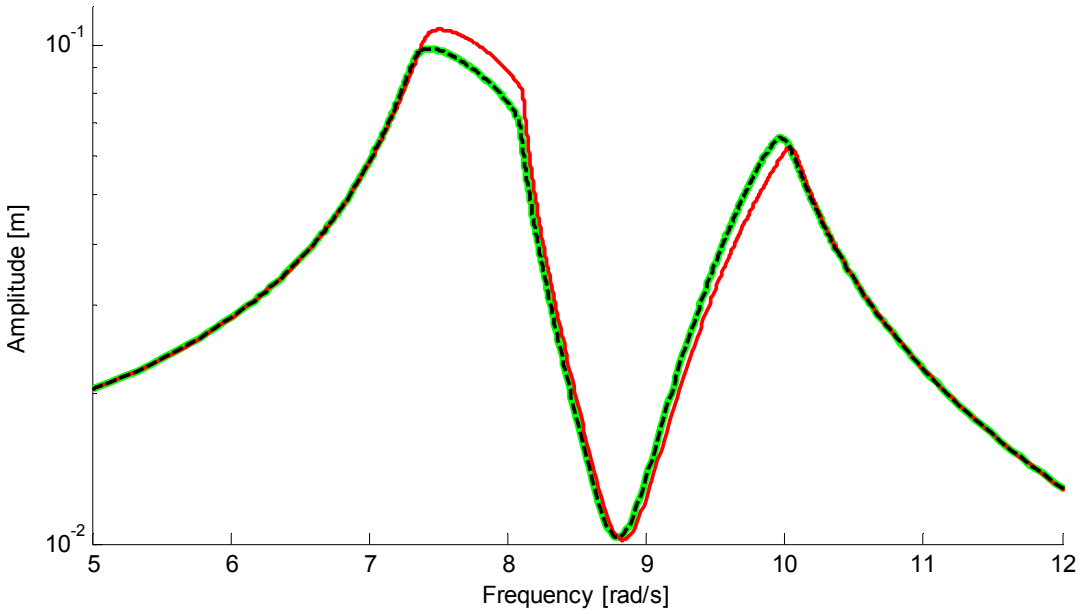

Figure 5.29 – Actual (——), Network Identified (——), and Optimization Identified (– – – –) MDOF System Response

CHAPTER 6

ROBUSTNESS OF MISTUNING

As stated previously, mistuning causes forced response amplification in bladed disks and it cannot be avoided since it is resulting from manufacturing tolerances and operational wear. At this stage, industry has been looking for answers, mainly to two different questions:

- What are the reliable techniques to assess the robustness of any bladed disk design?
- Are there any approaches that can be used to leverage the robustness of a particular bladed disk?

To address the first question, a new stochastic frequency response function (SFRF) is developed in this thesis. The SFRF employed in this study enables interpretation of the forced response of a randomly distorted structure, such as a mistuned bladed disk, in a qualitative and quantitative way. The approach is explicated in section 6.1.

The second question stated above is addressed by many researchers using different techniques such as finding the best order for pre-manufactured blades to be mounted on disks, and intentional mistuning.

The first one works only for assembly type designs, in which case it is possible to mount the blades after all of them are produced. However, with this type of approach, the design space is limited with the readily manufactured and tested blades which significantly reduce the efficiency and reproducibility of the design. Moreover, for integrally bladed disks (blisks) this method is not applicable.

On the other hand intentional mistuning can be applied both to assembly type and integral type bladed disk designs. Nevertheless, intentional mistuning has also some drawbacks. First of all, rather than designing one blade for a disk, several slightly different blades has to be produced. Secondly, not all of the intentional mistuning patterns developed so far work well with every bladed disk design efficiently. There are several parameters including but not limited to manufacturing tolerances, disk design, blade design, and assembling method. Section 6.2 is dedicated to the investigation of several intentional mistuning patterns with the aim of assessing robustness of these patterns.

6.1 A New Stochastic Frequency Response Function

In normal cases, a frequency response function (FRF) of a dynamic system under certain loading conditions is enough to comment on the response of that system. However, for systems which enclose small or large uncertain deviations, a specific FRF will not be sufficient to analyze the system. For example, bladed disk assemblies, whose nominal design is cyclically symmetric, undergo a considerable amount of forced response amplification and mode localization because of the mistuning phenomenon

as described earlier. Moreover, depending on the mistuning pattern associated with a particular disk coming out of the manufacturing line, its response will not match any other disk of the same design since mistuning of the second will be different.

Therefore, to enable a reliable analysis of a bladed disk design, a relatively more data-enclosing frequency response function is needed. The methodology to construct one, which is called SFRF is explained in section 6.1.1 and exemplified in section 6.1.2.

6.1.1 Methodology

To construct a Stochastic Frequency Response Function (SFRF), the problem has to be defined in a probabilistic approach. First, the parameter, whose deviation's effect on the response of the system is sought, is assigned a random distribution. It is important to decide on this random distribution considering the nature of the problem, so that the results are compatible with actual conditions. Afterwards, a dataset of systems is constructed with the defined distribution. Then, a Monte-Carlo simulation is performed where each element of the dataset is solved for the forced response in the desired frequency range of interest. Last but not least, for each frequency step in the solution, the distribution of the amplitudes is calculated.

This procedure is illustrated with a single degree of freedom system whose system parameters are given in Table 6.1.

Table 6.1 – SDOF System Parameters

Parameter	Factor
K [N/m]	25
M [kg]	1
C [Ns/m]	3
Loss factor	0.1

A random deviation with zero mean and a standard deviation of 3 (Figure 6.1) is applied to stiffness, K, of the SDOF system.

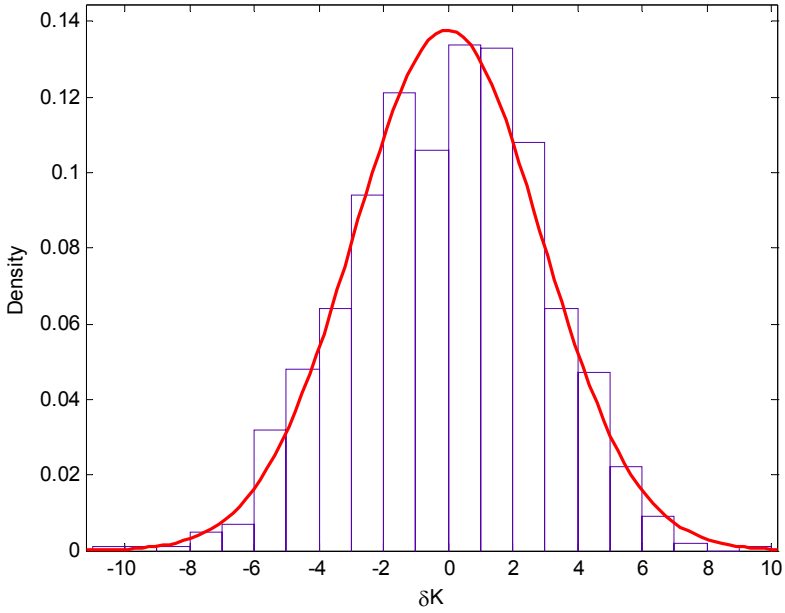

Figure 6.1 – Probability Distribution of δK

A Monte-Carlo simulation of 1000 solutions is carried out which resulted in the FRFs plotted in Figure 6.2. The corresponding SFRF is given in Figure 6.3.

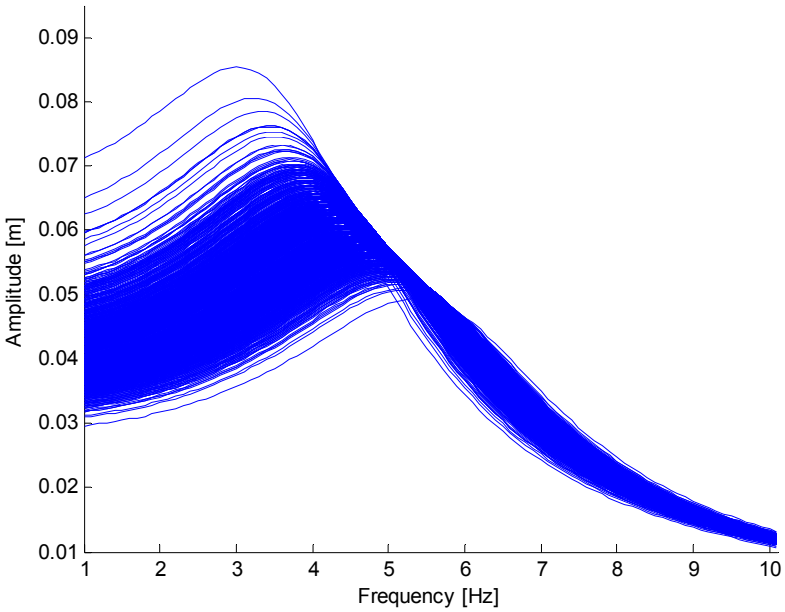

Figure 6.2 – FRFs of 1000 Simulations

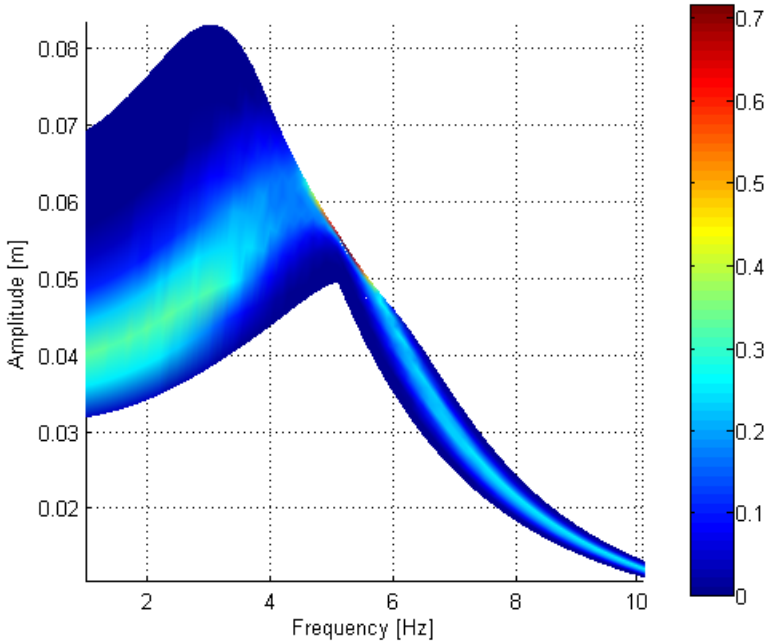

Figure 6.3 – SFRF of 1000 Simulations (Color Scale: Probability)

Note that plotting all of the FRFs in the same plot gives only the boundaries but calculating and plotting an SFRF enables interpretation of the probability of amplitudes related with each frequency step. For example, at 3.2 Hz in Figure 6.3, the amplitude distribution is as depicted in Figure 6.4.

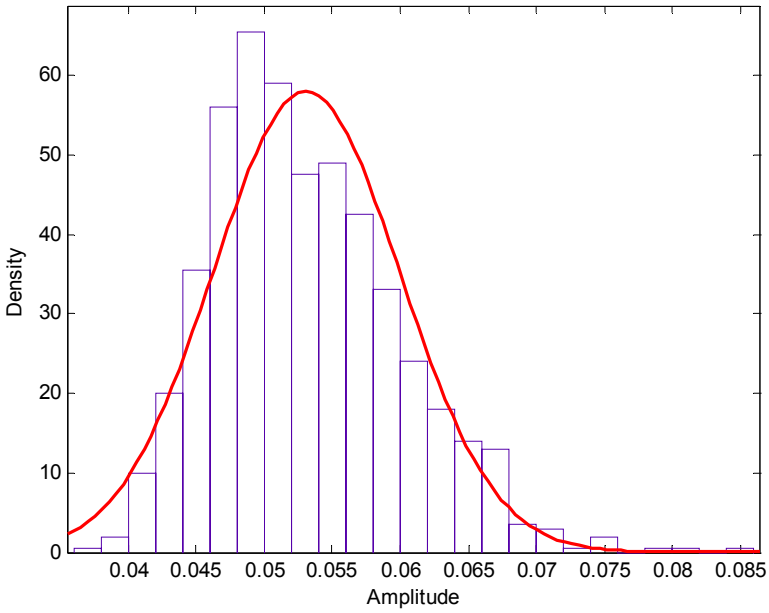

Figure 6.4 – Probability Distribution of Amplitude at 3.2 Hz

6.1.2 Case Study

A 12-bladed lumped parameter model constructed according to section 3.1.2 whose mistuning is defined with a zero mean and 2% random mistuning. A Monte-Carlo simulation with 20000 samples is performed.

The resulting stochastic frequency responses of blades 1 to 4 are given in Figure 6.5 to Figure 6.8, respectively.

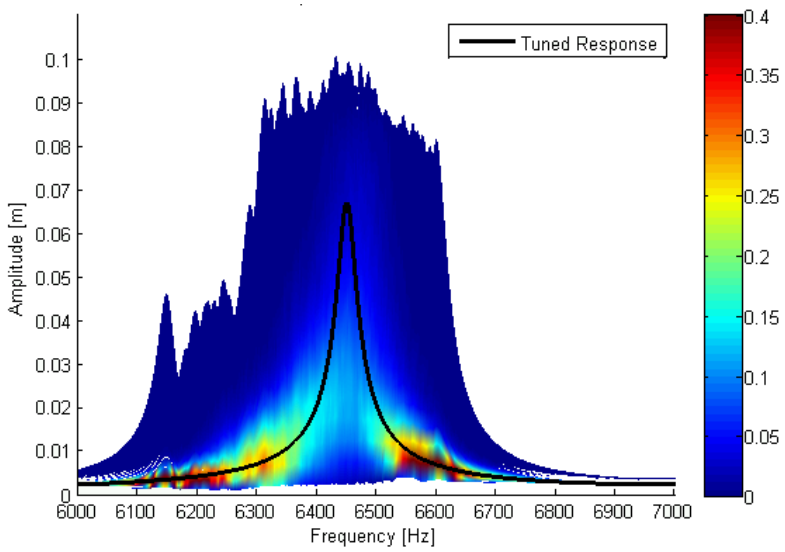

Figure 6.5 – Stochastic Forced Response of Blade 1

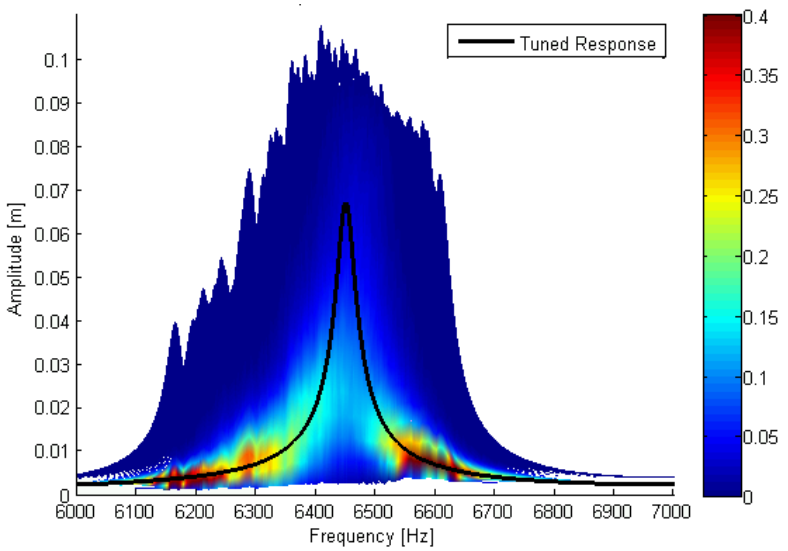

Figure 6.6 – Stochastic Forced Response of Blade 2

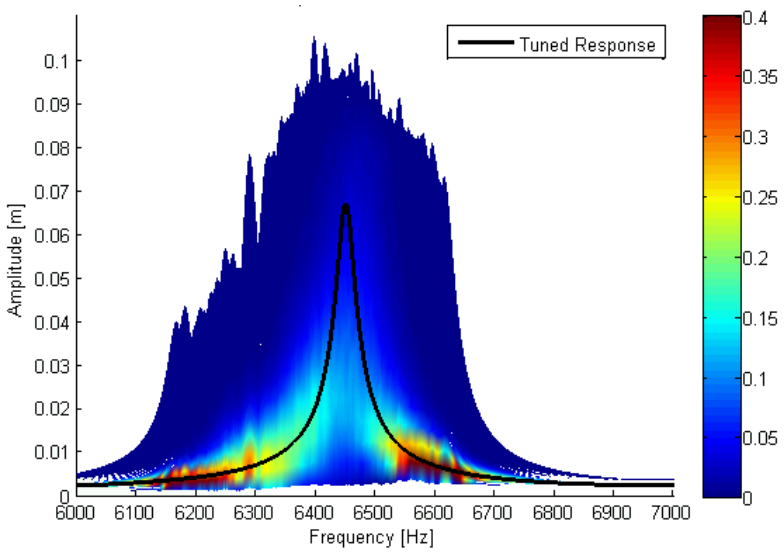

Figure 6.7 – Stochastic Forced Response of Blade 3

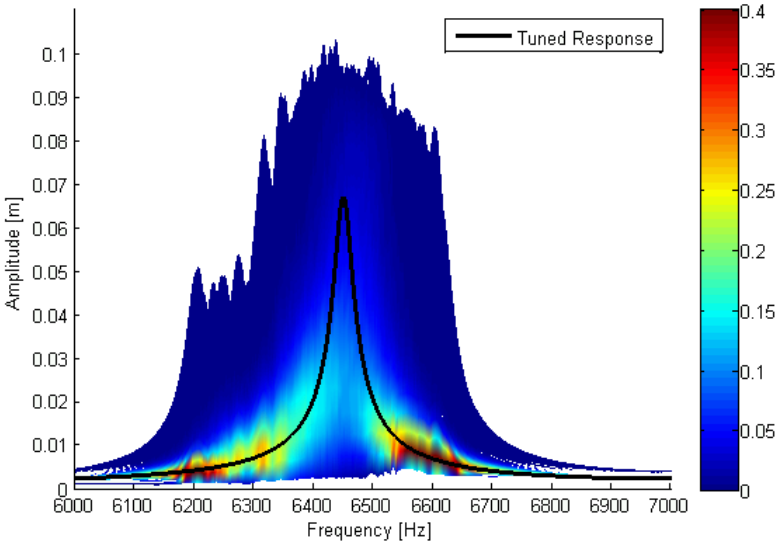

Figure 6.8 – Stochastic Forced Response of Blade 4

As it is clear from Figure 6.5 to Figure 6.8, the stochastic forced response of every blade is the same with small differences, which in turn would mean

that one SFRF for a bladed disk assembly is sufficient to analyze a bladed disk design.

6.2 Investigation of Intentional Mistuning Patterns

'Intentional Mistuning' is to mistune a cyclically symmetric bladed disk with a pre-defined pattern. However, because of the fact that some uncontrolled variation is still unavoidable, it is vital to evaluate any intentional mistuning pattern together with a certain amount of random mistuning.

In this section it is aimed to statistically compare the robustness of intentional mistuning patterns such as harmonic, linear and pseudo harmonic, with different levels of random mistuning applied on top, so that, intentional mistuning patterns will be evaluated without omitting the effect of uncertainties already present in the system.

Two sample bladed disks are used to gather information on disk dependence. Reduced order models of the sample bladed disks are built for this study to reduce computation time.

Monte Carlo simulations with selected intentional and random mistuning pairs are then performed under different engine order excitations to compare the performance of the intentional mistuning patterns applied.

6.2.1 Intentional Mistuning Patterns Applied

The three intentional mistuning patterns used in this study namely; linear, harmonic, and pseudo harmonic patterns can be formulated as follows respectively:

$$\Delta_{Linear} = A_0\left(\frac{2(n-1)}{N}-1\right) \tag{6.1}$$

$$\Delta_{Harmonic} = A_0 \sin\left(\frac{2\pi h(n-1)}{N}\right) \tag{6.2}$$

$$\Delta_{Pseudo-Harmonic} = \begin{cases} A_0 & if \quad n \le N/2 \\ -A_0 & if \quad n > N/2 \end{cases} \tag{6.3}$$

where A_0 is the maximum amplitude of intentional mistuning, n is the current blade, N is the number of blades in the assembly and h is harmonic number.

The graphical representations of linear, harmonic and pseudo-harmonic patterns are given in Figure 6.9, Figure 6.10, and Figure 6.11 respectively for a 12-bladed disk. Note that in the aforementioned figures, maximum amplitude, A_0, is selected as 10%. Moreover, the harmonic number, h, is equal to 1 for the harmonic pattern depicted in Figure 6.10.

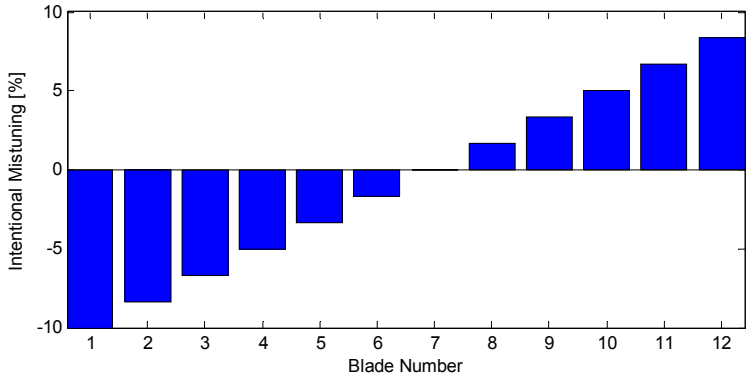

Figure 6.9 – Linear Intentional Mistuning Pattern

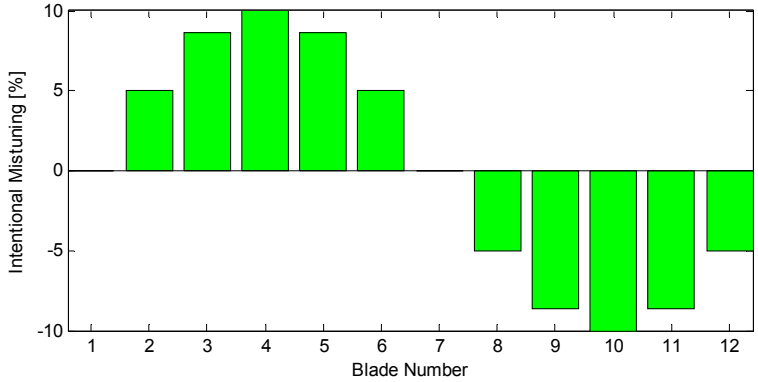

Figure 6.10 – Harmonic Intentional Mistuning Pattern

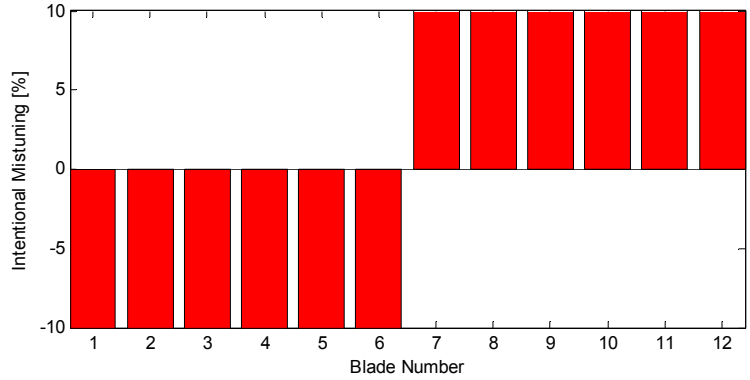

Figure 6.11 – Pseudo Harmonic Intentional Mistuning Pattern

6.2.2 Case Studies

Two case studies are presented here for which, the above described intentional mistuning patterns are applied together with three different random mistuning sets of Gaussian distribution with zero mean and 2%, 5% and 8% standard deviations. For each of these random mistuning patterns four different data sets each containing 2000 bladed disk assemblies are created which correspond to pure random, linear intentional mistuning with random mistuning, harmonic intentional mistuning with random mistuning, and pseudo-random intentional mistuning with random mistuning. Intentional mistuning patterns are applied with maximum amplitude of 10%.

For decreasing the computation time, reduced order modeling, which is presented in section 3.1.2, is employed.

6.2.2.1 Case Study I – 12-Bladed Disk

The finite element model of a sector of the 12-bladed disk used in this study is given in Figure 6.12. Finite element analysis is carried out in ANSYS, and 8-noded brick elements are used, which resulted in 216 nodes, to model the sector. To increase computation speed, reduced order modeling described in section 3.2 is utilized. To construct the reduced order model, 70 modes (10 modes for each nodal diameter) for the disk and 10 modes for each blade are used. The frequency range of interest, where the amplification factors are calculated, is selected according to the excited modes with the 3rd engine order forcing applied.

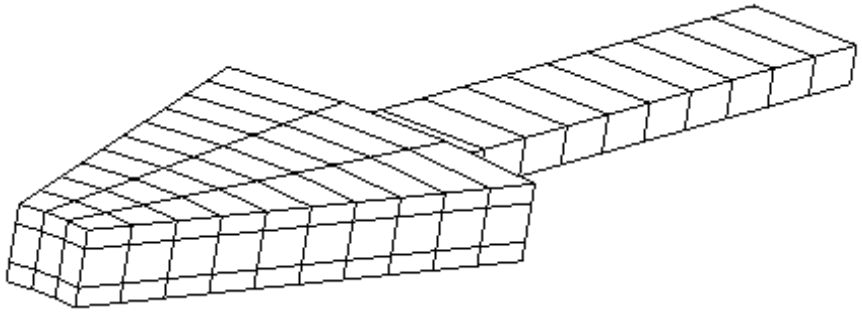

Figure 6.12 – 12-Bladed Disk Sector

The results for 2%, 5% and 8% random mistuning patterns are given in Figure 6.13, Figure 6.14, and Figure 6.15, respectively, via cumulative probability plots of amplification factor. Note that the amplification factor is calculated with respect to the tuned assembly.

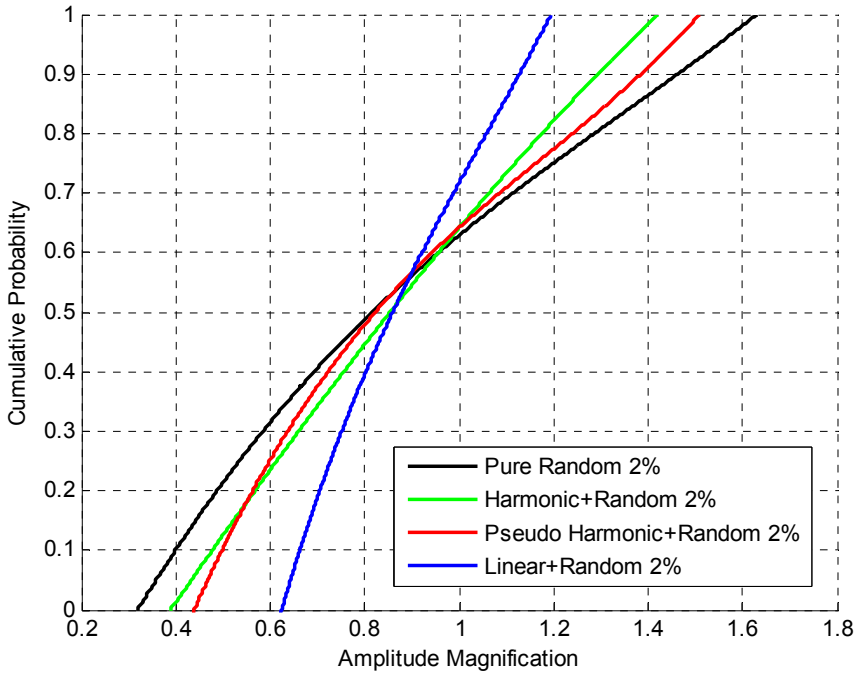

Figure 6.13 – Cumulative Probability of Amplification Factor for All Blades in 2000 Bladed Disk Assemblies with 2% Random Mistuning

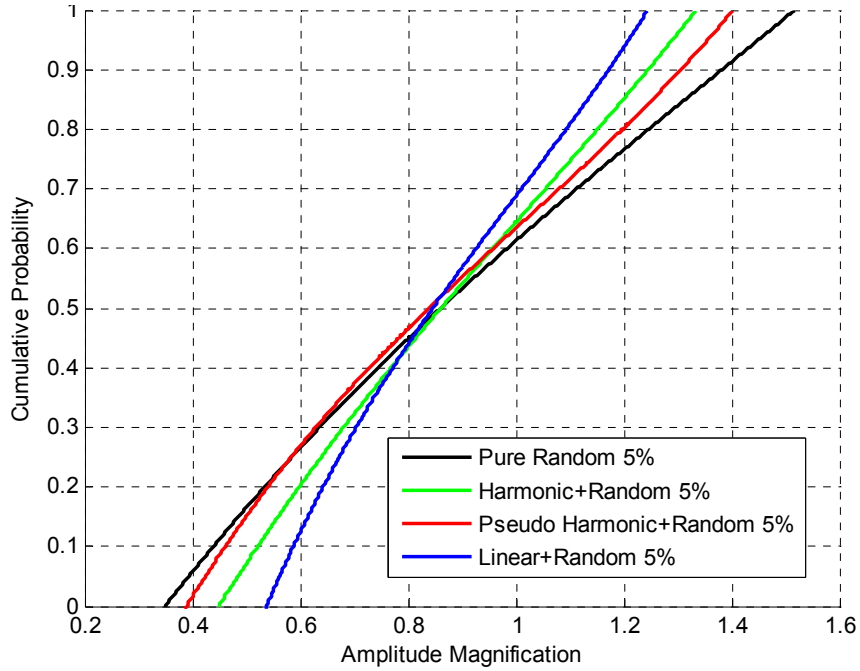

Figure 6.14 – Cumulative Probability of Amplification Factor for All Blades in 2000 Bladed Disk Assemblies with 5% Random Mistuning

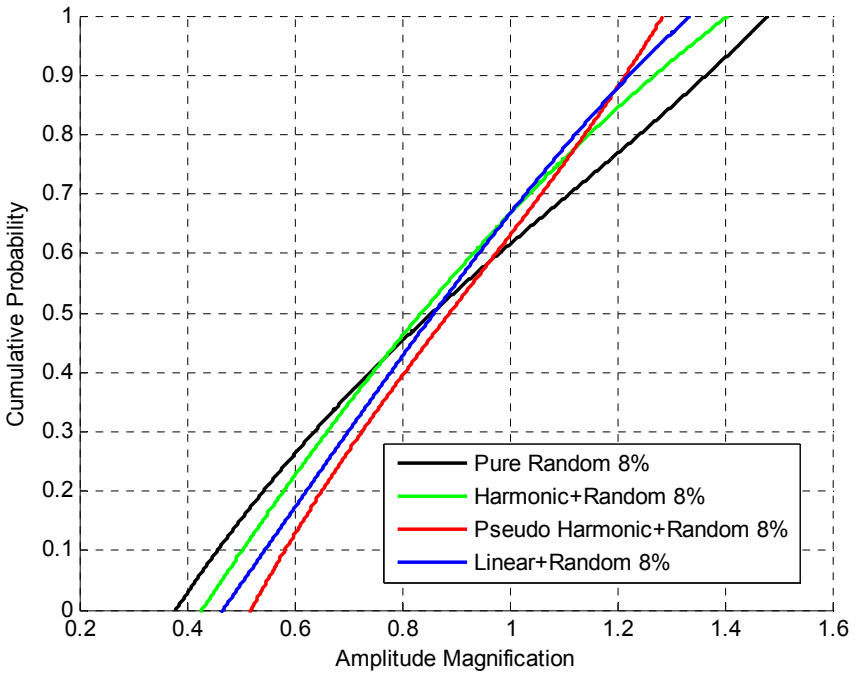

Figure 6.15 – Cumulative Probability of Amplification Factor for All Blades in 2000 Bladed Disk Assemblies with 8% Random Mistuning

From Figure 6.13 and Figure 6.14, it is clearly seen that linear intentional mistuning pattern works better than the others for relatively low random mistuning cases. However it is obvious from Figure 6.15 that, pseudo-harmonic intentional mistuning pattern performed as good as the linear one in terms of the maximum amplification seen among the 2000 bladed disk forced response solutions for relatively high random mistuning. Also, it should be noted that with increasing random mistuning the performance of intentional mistuning patterns decrease with respect to the pure random mistuning case.

6.2.2.2 Case Study II – 17-Bladed Disk

The finite element model of a sector of the 17-bladed disk used in this study is given in Figure 6.16. Finite element work is carried out in ANSYS, and 8-noded brick elements are used, which resulted in 304 nodes, to model the sector. To increase computation speed, reduced order modeling described in section 3.2 as it's done with the 12-bladed disk in case study I. To construct the reduced order model, 100 modes for the disk and 10 modes for each blade are used.

The frequency range of interest, where the amplification factors are calculated, is selected according to the excited modes with the 4^{th} engine order forcing applied.

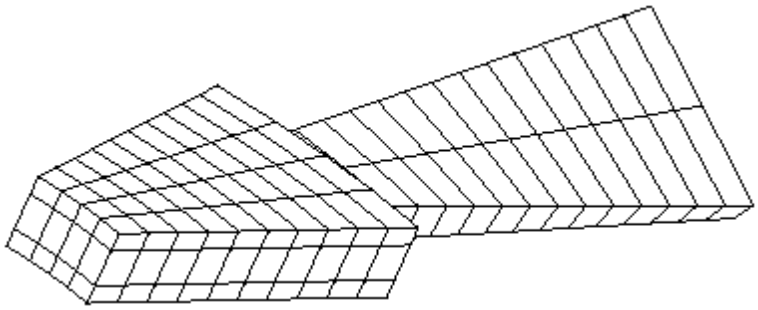

Figure 6.16 – 17-Bladed Disk Sector

The results for 2%, 5% and 8% random mistuning patterns are given in Figure 6.17, Figure 6.18, and Figure 6.19, respectively, via cumulative probability plots of amplification factor. Note that the amplification factor is calculated with respect to the tuned assembly.

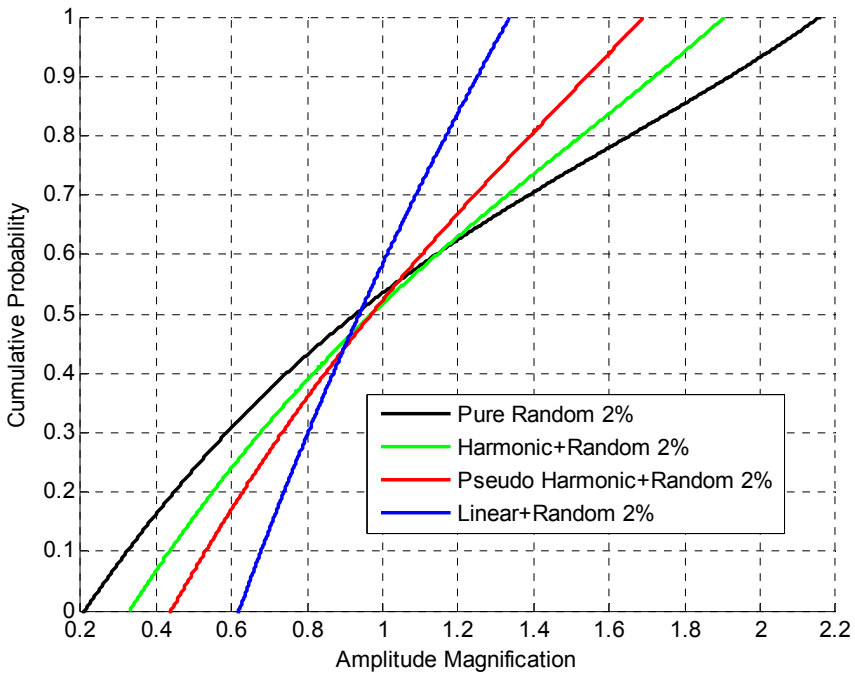

Figure 6.17 – Cumulative Probability of Amplification Factor for All Blades in 2000 Bladed Disk Assemblies with 2% Random Mistuning

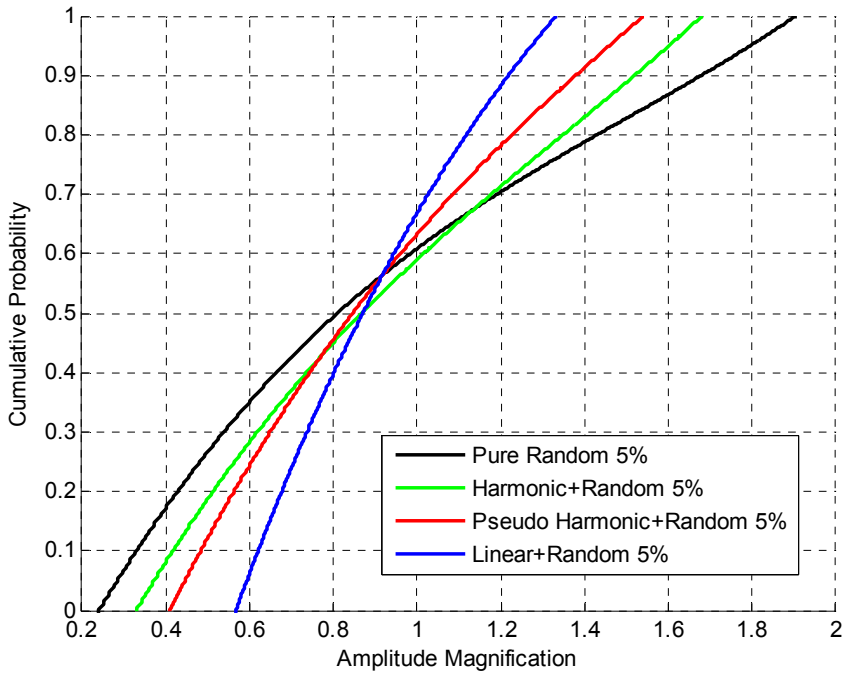

Figure 6.18 – Cumulative Probability of Amplification Factor for All Blades in 2000 Bladed Disk Assemblies with 5% Random Mistuning

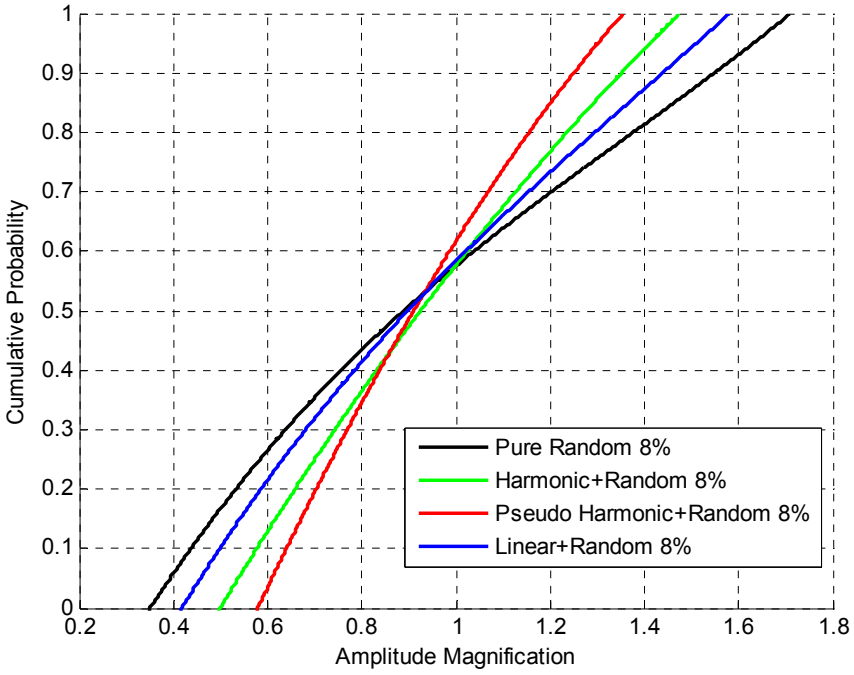

Figure 6.19 – Cumulative Probability of Amplification Factor for All Blades in 2000 Bladed Disk Assemblies with 8% Random Mistuning

For the 17-bladed disk, as it was for the 12-bladed one, linear intentional mistuning pattern works better than the others for relatively low random mistuning cases. However Figure 6.19 shows that, pseudo-harmonic intentional mistuning pattern is much better for high random mistuning cases than the linear one for the 17-bladed disk. Also, it is clear that with increasing number of blades maximum amplitude magnification increases as expected.

CHAPTER 7

CONCLUSIONS AND DISCUSSION

In this chapter, concluding remarks on the subjects included in the research, are presented in the order they appear in this thesis. Then, contributions to the literature are discussed, and some comments are made for the future studies.

7.1 Non-Linear Forced Response Analysis

In this thesis a new approach is introduced to predict forced response of mistuned bladed disk assemblies with non-linearities. The proposed approach eliminates the direct dependency of the number of non-linear equations to be solved to the number of degrees of freedom related with non-linear elements. This is especially important for the analysis of mistuned bladed disk systems, where a small increase in the number of nonlinear elements between adjacent blades results in a considerable increase in the number of degrees of freedom related with non-linear elements in the whole assembly. However in the method suggested, even if large number of nonlinear elements is used in the model, it is possible to keep the number of unknowns significantly low.

Three case studies are presented to demonstrate the application of the approach proposed for the non-linear forced response analysis of mistuned

bladed disks. In the first case study, the methodology is verified with a time-domain solution comparison, whereas in the second one a lumped parameter model is used to represent a 12-bladed mistuned bladed disk assembly and analysis of the system with different contact normal loads are carried out. Lastly, a realistic finite element model is constructed and the modes extracted from the finite element analysis are used to solve the nonlinear system with the proposed approach.

In addition to the new solution methodology proposed for mistuned assembly non-linear analysis, a new adaptive harmonic balance method is developed. The method, via adaptively changing the number of harmonics used in each solution step, enables non-linear analysis to be carried out much faster without decreasing the accuracy.

The methodology proposed is based on continuously monitoring the non-linear forcing vector and including the harmonics which contribute significantly to the non-linear forcing.

7.2 Mistuning Identification

In this thesis, two new tools are provided for mistuning identification where neural networks are utilized; NetID and OptID. NetID is the pure neural network approach to the mistuning identification problem, whereas OptID combines NetID with an optimization routine to further enhance the capabilities.

Two case studies are presented herein to demonstrate the performance of NetID, one of which employs noise injection training procedure to increase the robustness of the proposed method under noisy input. The second case study proves the effectiveness of OptID where a fully featured disk design is identified through utilization of a component mode synthesis based ROM. Moreover, it also shows that OptID and NetID are capable of identifying mistuning even if only incomplete and noisy data is available.

OptID is also applied to a model updating problem where real test data taken from a GARTEUR test bed is employed. It is verified that OptID is efficiently able to update a finite element model based on the modal test results taken from the real structure.

With regard to the utilization of neural networks and optimization in structural dynamics, the last contribution of this thesis is a methodology for non-linearity identification. Using pattern recognition capabilities of neural networks, an approach is developed to identify the location and type of non-linearities in a given structure without restricting the measurements to be taken from non-linear degrees of freedom. Afterwards, another neural network is employed for identifying the recognized non-linearity parametrically. Lastly, with the aid of optimization algorithms the performance of the procedure is increased.

The proposed method is superior to most of the alternatives presented in the literature, since it does not require the test data taken from the points in the structure where non-linearities are assumed to be.

7.3 Robustness of Mistuning

Because of the random nature of the mistuning phenomena, it is possible to encounter dynamically very different bladed disk assemblies in terms of forced response. In this thesis, a new stochastic frequency response function representation is developed in order to enable a single plot contain the information of a structure which has one or more parameters represented by a random distribution. With the aid of this stochastic frequency response function, it is shown that the response of a bladed disk can be represented by only the response of one of its blades.

Intentional mistuning patterns, which are used for suppressing the amplitude magnification resulting from random mistuning, are investigated in a probabilistic study in this thesis via Monte Carlo simulations. From the results of two case studies it is clear that linear intentional mistuning pattern is better than the other two patterns employed in the case studies for relatively low random mistuning. However, it should be noted that applying linear intentional mistuning pattern to a rotor design has some drawbacks. The most important one is that there has to be different blade designs equal to the number of blades in the assembly, which brings additional cost and engineering effort in the design step. Another drawback of this pattern is the spreading of resonant frequencies to a wider span compared to a purely random mistuned assembly. This will bring a wider speed avoidance span when operational speed of the engine is being determined. To avoid the burden of additional design effort and cost, one can choose the pseudo-harmonic intentional mistuning pattern. For implementing this type of intentional mistuning,

there will be only two different blades in the assembly, and the operational speed zones will not be affected as they will be in the case of linear intentional mistuning.

7.4 Contributions to the Literature

The aim of this thesis has always been focused in two main topics:

- Bringing new solutions to dynamics related problems in bladed disk design,
- Contributing to the structural dynamics community via introducing new tools.

In the view of the first, the most important achievements have been the new non-linear modal domain forced response solution procedure developed for mistuned bladed disks, and two new mistuning identification methods [89].

For structural dynamics related research carried out around the world, it is believed that, the new adaptive harmonics balance method will be quite useful in lieu of the classical harmonic balance method since it enables faster solution of non-linear systems with a comparable accuracy.

Moreover, the new non-linearity identification method developed will find a broad application area, since it encapsulates a long desired property: locating, classifying and identifying non-linearities without taking measurements from the non-linear degrees of freedom.

Lastly, the new stochastic frequency response representation is believed to be another useful tool for analyzing dynamic systems which entail uncertain parameters, for example in gear dynamics to model the random deviations caused by the teeth of the same gear.

7.5 Future Work

It should be noted that there are still several aspects of bladed disk dynamics that need further improvement and investigation.

One of these potential areas is mistuning modeling. In section 6, a new stochastic frequency response function is developed and introduced for the analysis of imprecisely-defined structures. The uncertain parameters are modeled with classical random distributions. However, in author's opinion, 'Fuzzy Sets' [90] can also be utilized for mistuning modeling. There are recent studies carried out on vibration and finite element analysis of structures [91-92] which are based on fuzzy modeling. In the light of these publications it is believed that the analysis time associated with mistuned bladed disk design can be improved.

Secondly, sub-structuring techniques can be applied for altering the mistuning associated with a nominal bladed disk design in order to improve computation time in a Monte Carlo simulation of non-linear analysis series. Note that in order to apply the approach proposed in Chapter 4, modal analysis of a full dimensioned mistuned bladed disk model is required. The approach, as it is, is appropriate for analyzing a

particular design and also can be used for Monte Carlo analysis with the increasing computational power available in the industry. However, implementing sub-structuring techniques will increase the computation time for such probabilistic approaches that require rigorous computation since the modal analysis of the full structure will be eliminated.

REFERENCES

[1] D. J. Ewins, "The Effects of Blade Mistuning on Vibration Response – A Survey", *IFToMM 4th International Conference on Rotordynamics*, Prague, Czechoslovakia, 1991.

[2] S.A. Tobias, and R. N. Arnold, "The Influence of Dynamical Imperfections on the Vibration of Rotating Disks", *Proceedings of the Institution of Mechanical Engineers*, IMechE, vol. 171, no. 2, pp. 669-690, 1957.

[3] D. S. Whitehead, "Effect of Mistuning on the Vibration of Turbomachinery Blades Induced by Wakes", *Journal of Mechanical Engineering Science*, vol. 8, no. 1, pp. 15-21, 1966.

[4] D. J. Ewins, "The Effect of Detuning Upon the Forced Vibration of Bladed Disks", *Journal of Sound and Vibration*, vol. 9, no. 1, pp. 65-79, 1969.

[5] Srinivasan, A.V., 1997, "Flutter and Resonant Vibration Characteristics of Engine Blades", *Journal of Engineering for Gas Turbines and Power*, vol. 119, no. 4, pp. 742-775.

[6] J. H., Griffin, "Friction Damping of Resonant Stresses in Gas Turbine Engine Airfoils", *Transactions of ASME, Journal of Engineering Power*, vol. 102, pp. 329–333, 1980.

[7] C. H. Menq, J. H. Griffin, and J. Bielak, "The Forced Response of Shrouded Fan Stages", *ASME Transactions, Journal of Vibration, Acoustics and Stress Reliability Design*, vol. 108, pp. 50-55, 1986.

[8] C. H. Menq, J. H. Griffin, and J. Bielak, "The Influence of a Variable Normal Load on the Forced Vibration of a Frictionally Damped

Structure", *Journal of Engineering for Gas Turbines and Power*, vol. 108, pp. 300–305, 1986.

[9] C. H. Menq, J. Bielak, and J. H. Griffin, "The Influence of Microslip on Vibratory Response, Part I: A new Microslip Model", *Journal of Sound and Vibration*, vol. 107, pp. 279–293, 1986.

[10] C. H. Menq, J. Bielak, and J. H. Griffin, "The Influence of Microslip on Vibratory Response, Part II: A Comparison with Experimental Results", *Journal of Sound and Vibration*, vol. 107, pp. 295-307, 1986.

[11] T. M. Cameron, J. H. Griffin, R. E. Kielb, and T. M. Hoosac, "An Integrated Approach for Friction Damper Design", *ASME Transactions, Journal of Vibration, Acoustics and Stress Reliability Design*, vol. 112, pp. 175-182, 1990.

[12] B. D. Yang, M. L. Chu, and C. H. Menq, "Stick-Slip-Separation Analysis and Non-linear Stiffness and Damping Characterization of Friction Contacts Having Variable Normal Load", *Journal of Sound and Vibration*, vol. 210, pp. 461-481, 1998.

[13] B. D. Yang, and C. H. Menq, "Characterization of 3D Contact Kinematics and Prediction of Resonant Response of Structures Having 3D Frictional Constraint", *Journal of Sound and Vibration*, vol. 217, pp. 909-925, 1998.

[14] B. D. Yang, and C. H. Menq, "Characterization of Contact Kinematics and Application to the Design of Wedge Dampers in Turbomachinery Blading: part I: Stick-Slip Contact Kinematics", *Transactions of ASME, Journal of Engineering Power*, vol. 120, no. 2, pp. 410-417, 1998.

[15] G. Csaba, "Forced Response Analysis in Time and Frequency Domains of a Tuned Bladed Disk with Friction Dampers", *Journal of Sound and Vibration*, vol. 214, pp. 395–412, 1998.

[16] J. J. Chen, and C. H. Menq, "Periodic Response of Blades Having Three-Dimensional Nonlinear Shroud Constraints", *Journal of Engineering for Gas Turbines and Power*, vol. 123, pp. 901–909, 2001.

[17] E. P. Petrov, and D. J. Ewins, "Analytical Formulation of Friction Interface Elements for Analysis of Nonlinear Multi-harmonic Vibrations of Bladed Disks" *Journal of Turbomachinery*, vol. 125, pp. 364–371, 2003.

[18] E. P. Petrov, and D. J. Ewins, "Generic Friction Models for Time-Domain Vibration Analysis of Bladed Disks", *Journal of Turbomachinery*, vol. 126, pp. 184-192, 2004.

[19] K. H. Koh, S. Filippi, J. H. Griffin, and A. Akay, "Characterization of Turbine Blade Friction Dampers", *Journal of Engineering for Gas Turbines and Power*, vol. 127, pp. 856–862, 2005.

[20] E. Ciğeroğlu, and H. N. Özgüven, "Nonlinear Vibration Analysis of Bladed Disks with Dry Friction Dampers", *Journal of Sound and Vibration*, vol. 295, pp. 1028–1043, 2006.

[21] E. Ciğeroğlu, W. Lu, and C. H. Menq, "One-Dimensional Dynamic Microslip Friction Model", *Journal of Sound and Vibration*, vol. 292, pp. 881–898, 2006.

[22] E. Ciğeroğlu, N. An, and C. H. Menq, "A microslip friction model with normal load variation induced by normal motion", *Nonlinear Dynamics*, vol. 50, pp. 609-626, 2007.

[23] E. Ciğeroğlu, N. An, and C. H. Menq, "Wedge Damper Modeling and Forced Response Prediction of Frictionally Constrained Blades", *Proceedings of ASME Turbo Expo 2007*, Montréal, Canada, pp. 519-528, 2007.

[24] E. Ciğeroğlu, N. An, and C. H. Menq, "Forced Response Prediction of Constraint and Unconstraint Structures Coupled Through Frictional Constants", *Journal of Engineering for Gas Turbines and Power*, vol. 131, pp. 022505, 2009.

[25] E. Budak, and H. N. Özgüven, "A Method for Harmonic Response of Structures with Symmetric Non-linearities", *Proceedings of the 15th International Seminar on Modal Analysis*, Leuven, pp. 901-915, 1990.

[26] Ö. Tanrıkulu, B. Kuran, H. N. Özgüven, and M. İmregün, "Forced Harmonic Response Analysis of Nonlinear Structures using Describing Functions", *AIAA Journal*, vol. 31, pp. 1313–1320, 1993.

[27] B. Kuran, and H. N. Özgüven, "A Modal Superposition Method for Non-linear Structures", *Journal of Sound and Vibration,* vol. 189, pp. 315-339, 1996.

[28] G. Orbay, and H. N. Özgüven, "Non-linear Periodic Response Analysis of Mistuned Bladed Disk Assemblies in Modal Domain", *Proceedings of 9th International Conference on Vibrations in Rotating Machinery*, v. 1, pp. 159-170, IMechE, University of Exeter, UK, 2008.

[29] W. Sextro, L. Panning, F. Götting, and K. Popp, "Fast Calculation of the Statistics of the Forced Response of Mistuned Bladed Disk Assemblies with Friction Contacts", *Proceedings of ASME Turbo Expo 2002*, Amsterdam, Netherlands, 2002.

[30] E. P. Petrov, and D. J. Ewins, "Method for Analysis of Nonlinear Multiharmonic Vibrations of Mistuned Bladed Disks with Scatter of Contact Interface Characteristics", *Journal of Turbomachinery*, vol. 127, pp. 128-136, 2005.

[31] M. Kruse, and C. Pierre, "Forced Response of Mistuned Bladed Disks Using Reduced-Order Modeling", *37th AIAA/ASME/ASCE/AHS/ASC*

Structures, Structural Dynamics and Materials Conference and Exhibit, Salt Lake City, UT, pp. 1938-1950, 1996.

[32] M. P. Mignolet, and A. Rivas-Guerra, "Identification of Mistuning Characteristics of Bladed Disks from Free Response Data, Part I", *Journal of Engineering for Gas Turbines and Power*, vol. 123, no. 2, pp. 395-403, 2001.

[33] M. P. Mignolet, and A. Rivas-Guerra, "Identification of Mistuning Characteristics of Bladed Disks from Free Response Data, Part II", *Journal of Engineering for Gas Turbines and Power*, vol. 123, no. 2, pp. 404-411, 2001.

[34] J. A. Judge, C. Pierre, and S. L. Ceccio, "Experimental Identification of Mistuning in Bladed Disks", *Proceedings of the 6th National Turbine Engine High Cycle Fatigue Conference*, Universal Technology Corp., Dayton, OH, 2002.

[35] J. Judge, C. Pierre, and S. L. Ceccio, "Experimental Validation of Mistuning Identification Techniques and Vibration Predictions in Bladed Disks", *Proceedings of the 2001 CEAS/AAIA/AIAE International Forum on Aeroelasticity and Structural Dynamics*, vol. 2, AlfaSur, Madrid, pp. 89-98, 2001.

[36] J. Judge, C. Pierre, and S. L. Ceccio, "Mistuning Identification in Bladed Disks", *Proceedings of the International Conference on Structural Dynamics Modelling*, Madeira Island, Portugal, 2002.

[37] F. Pichot, F. Thouverez, L. Jezequel, and E. Seinturier, "Mistuning Parameters Identification of a Bladed Disk", *Key Engineering Materials: Damage Assessment of Structures*, Vols. 204-205, TransTech Publ., Switzerland, pp. 123-132, 2001.

[38] M. P. Mignolet, and C. C. Lin, "Identification of Structural Parameters in Mistuned Bladed Disks", *Journal of Vibration and Acoustics*, vol. 119, no. 3, pp. 428-438, 1997.

[39] D. M. Feiner, and J. H. Griffin, "Mistuning Identification of Bladed Disks Using a Fundamental Mistuning Model, Part I: Theory", *Journal of Turbomachinery*, vol. 126, no. 1, pp. 150-158, 2004.

[40] D. M. Feiner, and J. H. Griffin, "Mistuning Identification of Bladed Disks Using a Fundamental Mistuning Model, Part II: Application," *Journal of Turbomachinery*, vol. 126, no. 1, pp. 159-165, 2004.

[41] D. M. Feiner, and J. H. Griffin, "A Completely Experimental Method of Mistuning Identification in Integrally Bladed Rotors", *Proceedings of the 8th National Turbine Engine High Cycle Fatigue Conference*, Universal Technology Corp., Dayton, OH, pp. 1.1-1.13, 2003.

[42] N. E. Kim, and J. H. Griffin, "System Identification in Higher Modal Density Regions of Bladed Disks", *Proceedings of the 8th National Turbine Engine High Cycle Fatigue Conference*, Universal Technology Corp., Dayton, OH, pp. 1.68-1.82, 2003.

[43] S. H. Lim, C. Pierre, and M. P. Castanier, "System Identification in Higher Modal Density Regions of Bladed Disks", *Proceedings of the 9th National Turbine Engine High Cycle Fatigue Conference*, Universal Technology Corp., Dayton, OH, 2004.

[44] J. Li, C. Pierre, and S. L. Ceccio, "Validation of a New Technique for Mistuning Identification and Model Updating Based on Experimental Results for an Advanced Bladed Disk Prototype", *Evaluation, Control and Prevention of High Cycle Fatigue in Gas Turbine Engines for Land, Sea and Air Vehicles*, NATO Research and Technology Organization RTO-MP-AVT-121, pp. 36-1-36-16, 2005.

[45] F. Pichot, D. Laxalde, J. J. Sinou, F. Thouverez, and J. P. Lombard, "Mistuning Identification for Industrial Blisks Based on the Best Achievable Eigenvector", *Computers & Structures*, vol. 84, Nos. 29-30, pp. 2033-2049, 2006.

[46] D. Laxalde, F. Thouverez, J. J. Sinou, J. P. Lombard, and S. Baumhauer, "Mistuning Identification and Model Updating of an Industrial Blisk", *International Journal of Rotating Machinery*, vol. 2007, no. 1, pp. 17289, 2007.

[47] A. C. Madden, M. P. Castanier, and B. I. Epureanu, "Reduced-Order Model Construction Procedure for Robust Mistuning Identification of Blisks", *Proceedings of the 49th AIAA/ASME/ASCE/AHS/ASC Structures, Structural Dynamics, and Materials Conference*, AIAA, Reston, VA, 2008.

[48] J. A. Judge, C. Pierre, and S. L. Ceccio, "Experimental Mistuning Identification in Bladed Disks Using a Component-Mode-Based Reduced-Order Model", *AIAA Journal*, vol. 47, no. 5, pp. 1277-1287, 2009.

[49] R. I. Levin, and N. A. J. Lieven, "Dynamic Finite Element Model Updating Using Neural Networks", *Journal of Sound and Vibration*, vol. 210, no. 5, pp. 593-607, 1998.

[50] C. C. Chang, T. Y. P. Chang, and Y. G. Xu, "Adaptive neural networks for model Updating of Structures", *Smart Materials and Structures*, vol. 9, pp. 59-68, 2000.

[51] C. C. Chang, T. Y. P. Chang, and Y. G. Xu, "Selection of Training Samples for Model Updating Using Neural Networks", *Journal of Sound and Vibration*, vol. 249, pp. 867-883, 2002.

[52] Y. Lu, and Z. Tu, "A two-level neural network approach for dynamic FE model updating including damping", *Journal of Sound and Vibration*, vol. 275, pp. 931-952, 2004.

[53] J. L. Zapico, A. Gonzalez-Buelga, M. P. Gonzalez, and R. Alonso, "Finite Element Model Updating of a Small Steel Frame Using Neural Networks", *Smart Materials and Structures*, vol. 17, pp. 045016, 2008.

[54] S. Chen, and A. Billings, "Neural Networks for Nonlinear System Modeling and Identification", *International Journal of Control*, vol. 56, no. 2, pp. 319-346, 1992.

[55] S. F. Masri, A. G. Chassiakos, and T. K. Caughey, "Identification of Nonlinear Dynamic Systems Using Neural Networks", *Journal of Applied Mechanics*, vol. 60, pp. 123-133, 1993.

[56] A. C. Gondhalekar, E. P. Petrov, and M. Imregun, "Parameters Identification for Nonlinear Dynamic Systems via Genetic Algorithm Optimization", *Journal of Computational and Nonlinear Dynamics*, vol. 4, pp.041002, 2009.

[57] M. B. Özer, H. N. Özgüven, and T. J. Royston, "Identification of Structural Non-linearities Using Describing Functions and Sherman-Morrison Method", *Proceedings of the 23rd International Modal Analysis Conference*, pp.199-212, Orlando, Florida, January 30 - February 3, 2005.

[58] M. B. Özer, H. N. Özgüven, and T. J. Royston, "Identification of Structural Non-Linearities Using Describing Functions and the Sherman– Morrison Method", *Mechanical Systems and Signal Processing*, vol. **23**, pp. 30–44, 2009.

[59] D. J. Ewins, "The Effect of Detuning Upon the Forced Vibration of Bladed Disks", *Journal of Sound and Vibration*, vol. 9, pp. 65-79, 1969.

[60] D. J. Ewins, "Further Studies of Bladed Disk Vibration: Effects of Packeting", *Proceedings of ImechE Conference on Vibrations in Rotating Machinery 1980*, pp. 97-102, 1980.

[61] J. H. Griffin, and T. M. Hoosac, "Model Development and Statistical Investigation of Turbine Mistuning", *ASME Journal of Vibration, Acoustics, Stress and Reliability in Design*, vol. 106, pp. 204-210, 1984.

[62] M. P. Castanier, and C. Pierre, "Consideration on the Benefits of Intentional Mistuning for the Forced Response of Turbomachinery Rotors", *Proceedings of ASME International Mechanical Engineering Congress and Exposition 1997*, Dallas, TX, 1997.

[63] M. P. Castanier, and C. Pierre, "Investigation of Combined Effects of Intentional and Random Mistuning on the Forced Response of Bladed Disks", *Proceedings of 34th AIAA/ASME/SAE/ASEE Joint Propulsion Conference and Exhibit*, Cleaveland, OH, 1998.

[64] J. P. Ayers, D. M. Feiner, and J. H. Griffin, "Reducing Mistuning Effects by Optimally Switching Blades", *Proceedings of 10th National Turbine Engine High Cycle Fatigue Conference*, 2005.

[65] M. Nicolic, E. Petrov, and D. J. Ewins, "Robust Strategies for Forced Response Reduction of Bladed Disks Based on Large Mistuning Concept", *Proceedings of ASME Turbo Expo 2007, Power for Land, Sea and Air*, Montreal, Canada, 2007.

[66] M. P. Castanier, and C. Pierre, "Modelling and Analysis of Mistuned Bladed Disk Vibration: Status and Emerging Directions", *Journal of Propulsion and Power*, vol. 22, no. 2, pp. 384-396, 2006.

[67] R. R. Jr. Craig, and M. C. C. Bampton, "Coupling of Substructures for Dynamic Analysis", *AIAA Journal*, vol. 6, no. 7, pp. 1313-1319, 1968.

[68] R. C. F. Dye, and T. A. Henry, "Vibration Amplitudes of Compressor Blades Resulting from Scatter in the Blade Natural Frequencies", *Transactions of ASME, Journal of Engineering and Power,* July 1969, pp. 182-188, 1969.

[69] R. Bladh, M. P. Castanier, and C. Pierre, "Component-Mode-Based Reduced Order Modelling Techniques for Mistuned Bladed Disks - Part I: Theoretical Models", *Journal of Engineering for Gas Turbines and Power,* vol. 123, pp. 89-99, 2001.

[70] H. N. Özgüven, "Structural Modifications Using Frequency Response Functions", *Mechanical Systems and Signal Processing*, vol. 4, no. 1, pp.53-63, 1990.

[71] W. Romberg, "Vereinfachte Numerische Integration", *Det Kongelige Norske Videnskabers Selskab Forhandlinger,* vol. 28, no. 7, pp. 30-36, 1955.

[72] L. F. Richardson, "The Approximate Solution by Finite Differences of Physical Problems Involving Differential Equations, with an Application to the Stresses in a Masonry Dam", *Philosophical Transactions of the Royal Society of London. Series A*, vol. 210, pp. 307-357, 1911.

[73] F. L. Bauer, H. Rutishauser, and E. Stiefel, "New Aspects in Numerical Quadrature", *Experimental Arithmetic, High-Speed Computing and Mathematics, Proceedings of Symposium of Applied Mathematics*, vol. 15, pp. 199-218, 1963.

[74] I. P. Mysovskikh, "Romberg Method", *Encyclopedia of Mathematics*, Springer-Verlag, 2002.

[75] M. A. Crisfield, "A Fast Incremental/Iterative Solution Procedure that Handles Snap-through", *Computers and Structures*, vol. 13, pp. 55-62, 1981.

[76] R. C. Maple, P. I. King, P. D. Orkwis, and J. M. Wolff, "Adaptive Harmonic Balance Method for Nonlinear Time-periodic Flows", *Journal of Computational Physics*, vol. 193, pp. 620-641, 2004.

[77] L. Zhu, and C. E. Christoffersen, "Adaptive Harmonic Balance Analysis of Oscillators Using Multiple Time Scales", *3rd International IEEE Northeast Workshop on Circuits and Systems Digest*, pp. 187-190, 2005.

[78] G. Orbay, "Nonlinear Vibration of Mistuned Bladed Disk Assemblies", MSc Thesis, Middle East Technical University, 2008.

[79] C. M. Bishop, "Neural Networks for Pattern Recognition", *Oxford university Press*, Oxford, UK, 1998.

[80] G. Casella, and E. L. Lehmann, "Theory of Point Estimation", *Springer*, New York, USA, 1999.

[81] R. J. Allemang, and D. L. Brown, "A Correlation Coefficient for Modal Vector Analysis", *Proceedings of 1st International Modal Analysis Conference*, pp. 110-116, 1982.

[82] C. M. Fonseca, and P. J. Fleming, "An Overview of Evolutionary Algorithms in Multiobjective Optimization", *Evolutionary Computing*, vol. 3, no. 1, pp. 1-16, 1995.

[83] C. M. Fonseca, and P. J. Fleming, "Genetic Algorithms for Multiobjective Optimization: Formulation, Discussion, and Generalization", *Proceedings of 5th International Conference on Genetic Algorithms*, Sam Mateo, CA, 1993.

[84] The MathWorks, Inc., "Optimization Toolbox User's Guide, Version 4", Natick, MA, 2009.

[85] M. Link, M. Friswell, "Working Group 1: Generation of Validated Structural Dynamic Models – Results of a Benchmark Study Utilizing

the GARTEUR SM-AG19 Test-bed", *Mechanical Systems and Signal Processing*, vol. 17, no. 1, pp. 9-20, 2003.

[86] D. Göge, M. Link, "Results Obtained by Minimizing Natural Frequency and Mode Shape Errors of a Beam Model", *Mechanical Systems and Signal Processing*, vol. 17, no. 1, pp. 21-27, 2003.

[87] C. Thonon, J. C. Golinval, "Results Obtained by Minimizing Natural Frequency and MAC-value Errors of a Beam Model", *Mechanical Systems and Signal Processing*, vol. 17, no. 1, pp. 65-72, 2003.

[88] M. T. Kozak, M. Öztürk, H. N. Özgüven, "A Method in Model Updating Using Miscorrelation Index Sensitivity", *Mechanical Systems and Signal Processing*, vol. 23, pp. 1747-1758, 2009.

[89] M. E. Yümer, E. Ciğeroğlu, H. N. Özgüven, "Mistuning Identification of Bladed Disks Utilizing Neural Networks", *Proceedings of ASME Turbo Expo 2010*, Glasgow, United Kingdom, 2010.

[90] L. A. Zadeh, "Fuzzy Sets", *Information and Control*, vol. 8, pp. 338-353, 1965.

[91] G. Maglaras, E. Nikolaidis, R. T. Haftka, and H. H. Cudley, "Analytical-Experimental Comparison of Probabilistic Methods and Fuzzy Set Based Methods for Designing under Uncertainty", *Structural Optimization*, vol. 13, pp. 69-80, 1997.

[92] L. Chen, and S. S. Rao, "Fuzzy Finite-Element Approach for the Vibration Analysis of Imprecisely-Defined Systems", *Finite Elements in Analysis and Design*, vol. 27, pp. 69-83, 1997.

APPENDIX A. RICHARDSON – ROMBERG EXTRAPOLATION

Richardson-Romberg extrapolation enables calculating high accuracy function estimates through employing multiple low-accuracy evaluations by eliminating error modes on a function F with an estimation of that depends on a positive step size h, that can be defined as $F(h)$. We require that the error for this estimation be as follows;

$$F - F(h) = f_0 h^{k_0} + f_1 h^{k_1} + f_2 h^{k_2} + \cdots \tag{A.1}$$

where f_i are unknown, and k_i are known constants such that $h^{k_i} > h^{k_{i+1}}$. So that the exact value of F is given as

$$F = F(h) + f_0 h^{k_0} + f_1 h^{k_1} + f_2 h^{k_2} + \cdots \tag{A.2}$$

which can simply be represented by

$$F = F(h) + f_0 h^{k_0} + O\left(h^{k_1}\right). \tag{A.3}$$

By employing equation (A.3), following two are the representation of the same F' with different step sizes, namely h and h/t for an arbitrary t.

$$F' = F'(h) + f_0' h^{k_0} + O\left(h^{k_1}\right) \tag{A.4}$$

$$F' = F'\left(\frac{h}{t}\right) + f_0'\left(\frac{h}{t}\right)^{k_0} + O\left(h^{k_1}\right) \tag{A.5}$$

Subtracting (A.4) from t^{k_0} times (A.5) and solving for *F*' gives

$$F' = \frac{t^{k_0} F'\left(\frac{h}{t}\right) - F'(h)}{t^{k_0} - 1} + O\left(h^{k_1}\right) \tag{A.6}$$

As it is clear from (A.6), a better estimation of *F*' is achieved since the largest error term, $O\left(h^{k_0}\right)$, is eliminated. To increase the accuracy, one can simply repeat this process to eliminate more error terms.